STRUCTURE AND PHYSIOLOGY OF MITOCHONDRIAL REPLICATIVE DNA HELICASES

By

Minyoung So

A DISSERTATION

Submitted to
Michigan State University
in partial fulfillment of the requirements
for the degree of

Biochemistry and Molecular Biology – Doctor of Philosophy

2017

ABSTRACT

STRUCTURE AND PHYSIOLOGY OF
MITOCHONDRIAL REPLICATIVE DNA HELICASES

By

Minyoung So

The mitochondrial replicative DNA helicase (mtDNA helicase) unwinds double-stranded mitochondrial DNA (mtDNA) by using NTP hydrolysis at the mtDNA replication fork. Moreover, single-stranded DNA annealing activity and branch migration are identified in human mtDNA helicase, expanding its roles in mtDNA repair or recombination. The mtDNA helicase is also proposed to tether mitochondrial nucleoid to the mitochondrial inner membrane or to load itself on the closed DNA. Consequently, defects in the mtDNA helicase gene cause several mitochondrial diseases. I have pursued a comprehensive understanding of the structural and functional roles for both human and *Drosophila* mtDNA helicases and *Drosophila* Ind1, a putative interacting partner of the *Drosophila* mtDNA helicase, in mitochondrial DNA maintenance. In particular, research in this dissertation has focused mainly on the N-terminal primase-like domains, which have no primase activity in metazoan mtDNA helicases and contain a species-specific iron-sulfur cluster in *Drosophila* mtDNA helicase.

Structural studies of human mtDNA helicase present several different oligomeric states and structural dynamicity of its full-length form and demonstrate that the zinc binding-like domain imparts the structural flexibility to the helicase. In addition, open-ring structures and one-arm extended structures are observed, supporting a self-loading mechanism (Chapter 2).

Functional studies in chapter 3 suggest that the N-terminal domains of the mtDNA helicases function as a binding module that interacts with a metal cofactor, lipid, and single-stranded DNA. I confirm the presence of the iron-sulfur cluster in the N-terminal domain of

Drosophila mtDNA helicase and also show that the N-terminal domain serves a role in membrane binding through electrostatic interactions with cardiolipin. In addition, the positively-charged region where pathogenic mutants are clustered in the RNA polymerase-like domain of human mtDNA helicase contributes to single-stranded DNA binding that is likely required to mtDNA helicase self-loading, translocation, and annealing (Chapter 3).

Drosophila Ind1, as a putative iron-sulfur donor to *Drosophila* mtDNA helicase, has been characterized. Its mitochondrial localization, dimerization, and the membrane binding property driven by electrostatic and hydrophobic interactions were demonstrated. In particular, the membrane binding property of *Drosophila* Ind1 may facilitate the transfer of an iron-sulfur cluster to membrane-bound recipients: complex I and possibly *Drosophila* mtDNA helicase (Chapter 4).

Although the putative interaction between the mtDNA helicase and the Ind1 was not detected under given conditions in this research, I hypothesize that the expected protein-protein interactions may occur under optimized conditions with an appropriate cofactor (ATP) and chaperone proteins, based on experimental results and comparison with other protein in its Mrp/MinD family in chapter 4. Including the experimental plans to test this hypothesis, I designed the detailed plans that expand studies in this dissertation. The proposal is categorized into three unsolved questions: biological roles of the iron-sulfur cluster in *Drosophila* mtDNA helicase, effects of *Dm* Ind1 on oxidative phosphorylation and mtDNA replication, and new binding partners of the mtDNA helicase (Chapter 5). These approaches will contribute to the better understanding of the mtDNA helicase in various mechanisms to maintain mtDNA stability.

ACKNOWLEDGEMENTS

A few days ago, I saw a figure of the metamorphosis of *Drosophila melanogaster* by chance, and I thought my life is somewhat similar to it. I have been in a pupa for several years in Michigan state university. During achieving Ph. D, I have been changed intellectually, mentally, emotionally and behaviorally. Being a voracious larva, I did not want to get helped. I wanted to be independent, but I also wanted to get all glory alone. However, now I know that any change cannot be made without other's help. Although it seems to be impossible that I repay all the helps I got, I want, at least, to send my thanks to all the people who helped me in my pupa stage.

First, I need to thank my mentor, Dr. Laurie Kaguni. She has been a role model for me, showing a successful woman scientist. Without her guidance and support, I couldn't complete Ph. D. program. She has been helped me to be a professional scientist with honest opinions and encouragements. Whenever I suffered from my challenging projects, she supported for me to be perseverant. Besides academic supports, she always cared about my well-being as American Mom. I have never forgotten the care packages she gave me for several Thanksgiving days. I am grateful that I got her mentorship.

Second, I would like to thank my committee members, Dr. John LaPres, Dr. Bill Henry, Dr. Min-Hao Kuo and Dr. Kathleen Gallo. Whenever I visited them, they always welcome me and gave me helpful feedbacks. In committee meetings, they always discussed my challenging projects with me sincerely without testing or judging me. I thanked them for their sweet support and valuable scientific advice.

I thank all the current and previous people in Dr. Kaguni's research group both in MSU and FinMIT. In particular, I send special thanks to Dr. Stacy Hovde, Dr. Grzegorz Ciesielski and

Dr. Johnny Stiban. They gave me tremendous helps, while I conducted experiments, analyzed data and wrote this dissertation. They were always there for me as friends, too. I send my true thank to them. I also have two special undergraduates, Megan Hawley and Yukei Wan, whom I have to send my thanks. They were powerful helpers and sweet young friends.

I would also like to thank people in the biochemistry department: professors, post-doctors and graduate students. I specially thank Dr. Jon Kaguni and Dr. Shelagh Ferguson-Miller for their kind supports and my good neighbors, Dr. Magdalena Felczak and Dr. Sundari Chodavarapu, who gave me a lot of advice for both science and life.

My beloved friends who studied together and lived in this tough graduate life together would never be forgotten. I send my special thanks to Dr. Hang Nguyen, Dr. Jeongwoon Kim, Dr. Zhenzhen Wang, and Dr. Hyejin Hwang. They always helped me to put myself together when I was low.

I thank God who gives His love and leads me to a right way. Without God, I am nothing. I also thank my fiancé, God's biggest gift, Dr. Lars Junghans. My tough graduate years are blessed because of him. My beloved family in Korea: Dad, Mom, my sister, my brother, and their families. I love them so much. They are my rock. Wherever I live, I belong to them. I dedicate this dissertation to Mom and Dad.

Thank all, you gave me wings. Now, I am ready to fly to the sky.

TABLE OF CONTENTS

LIST OF FIGURES

KEY TO ABBREVIATIONS

2D-NS-EM	two-dimensional negative stain-EM
2D-AGE	two-dimensional agarose gel electrophoresis
adPEO	autosomal dominant progressive external ophthalmoplegia
AP-MS	coaffinity purification coupled with mass spectrometry
ATP	adenosine triphosphate
BDGP DGC	Berkeley Drosophila Genome Project *Drosophila* Gene Collection
bp	base pairs
BrdU	Bromodeoxyuridine
BSA	bovine serum albumin
CD	circular dichroism
CIA	cytosolic iron-sulfur cluster assembly
CIA	cytosolic iron-sulfur cluster assembly
CL2D	two-dimensional reference free class average classification
CLSM	confocal laser scanning microscope
CSB	conserved sequence block
CTD	C-terminal helicase domain
CV	column volume
DBR	double-stand break repair
DGRC	*Drosophila* Genomics Resource Center
D-loop	displacement loop
Dm	*Drosophila melanogaster*
DNA	deoxyribonucleic acid

DNA-CT	DNA-mediated charge transfer
DoDM	*n*-dodecyl-β-D-maltopyranoside
dsDNA	double-stranded DNA
DTBP	dimethyl 3,3’ dithiobispropionimidate-2HCl
EDTA	ethylenediaminetetraacetic acid
EGFP	enhanced green fluorescent protein
EM	electron microscopy
ER	endoplasmic reticulum
ESP	electrostatic surface potential
GA	Glutaraldehyde
GraFix	glycerol gradient sedimentation combined with chemical crosslinking
HA	Hemagglutinin
IPTG	isopropyl β-D-1-thiogalactopyranoside
KD	knock-down
kDa	Kilodalton
mtDNA	mitochondrial DNA
mtDNA helicase	mitochondrial replicative DNA helicase
MTS	mitochondrial targeting sequence
mtSSB	mitochondrial single-stranded DNA binding protein
NCR	non-cording region
NTD	N-terminal primase-like domain
NTP	nucleoside triphosphate
OD	optical density
ORF	open reading frame

PA	phosphatidic acid
PC	Phosphatidylcholine
PE	Phosphatidylethanolamine
PG	Phosphatidylglycerol
PI	Phosphatidylinositol
PMSF	phenylmethylsulfonyl fluoride
PNK	polynucleotide kinase
pol γ	DNA polymerase γ
PS	Phosphatidylserine
RITOLS	RNA Incorporated Throughout Lagging Strand
RNA	ribonucleic acid
ROS	reactive oxygen species
RPD	RNA polymerase-like domain
SDS-PAGE	sodium dodecyl sulfate polyacrylamide gel electrophoresis
SF4	superfamily 4
ssDNA	single-stranded DNA
T7gp4	bacteriophage T7 gene 4 protein
TAS	termination associated sequence
TBST	Tris-buffered saline, 0.1% Tween 20
TCA	trichloroacetic acid
TLC	thin layer chromatography
TWINKLE	T7 gp4-like protein with intramitochondrial nucleoid localization
ZBD	zinc binding-like domain
ΔCTD	C-terminal helicase domain-truncated variant

ΔNTD	N-terminal primase-like domain-truncated variant
ΔZBD	ZBD-truncated variant

CHAPTER 1
Introduction and background

The mitochondrial replicative DNA helicase (mtDNA helicase) is one of the essential components in mitochondrial DNA (mtDNA) replication. The replication is an important mechanism to maintain the mitochondrial genomic stability that affects directly on cellular energy production and ultimately on the health of the cell and the organism. In this chapter, for the better understanding of the mtDNA helicase and the mtDNA replication mechanism, roles of mitochondria in cells, mitochondrial genomes, and mechanisms to maintain the genome such as mtDNA replication and repair will be reviewed. In particular, mtDNA replication will be discussed, focused on mitochondrial genome structures, replication models, and protein components. In addition, iron-sulfur cluster proteins in DNA-processing mechanisms will be introduced to give background knowledge for the iron-sulfur cluster containing *Dm* mtDNA helicase.

*General mitochondrial roles in cell*s

A mitochondrion is the only organelle that has its own genome in the animal cell. Although mitochondrial proteomes vary depending on cell types and the surroundings (1), ~1500 mitochondrial proteins are involved in several important metabolism (2); mitochondrial proteins produce primarily cellular ATP by oxidative phosphorylation, regulate redox states, maintain the cellular Ca^{2+} level, and relay apoptotic signals to decide life and death of a cell. Most of these mitochondrial mechanisms are related to electron transport chain complexes and the ATP synthase, directly or indirectly (3,4). Among these oxidative phosphorylation complexes, 13 polypeptides are encoded by mtDNA, indicating that stability of mitochondrial genome affects metabolic functions of mitochondria through oxidative phosphorylation.

Communication between mitochondria and other organelles have been hypothesized

since the late 1980s (5). Currently, the mitochondrial communication with the nucleus (5,6), the endoplasmic reticulum (ER) (7), and peroxisomes (8) has been identified, although the mitochondrial-mediated peroxisome biogenesis is under the debate (9). In particular, functional contributions of contacts between the ER and mitochondria are detected in apoptotic pathway, mitochondrial fission, and cristae remodeling (10). Related to the ER-mitochondrial communication, a recent report shows that a spatial relationship between mtDNA replication and ER-mitochondrial contacts is demonstrated by using a live-cell microscopy imaging (11). In human cultured cells, the proximity of nucleoids to ER tubules is required for mtDNA synthesis, although it is unclear whether the contact is mediated directly by protein(s) or indirectly by signaling molecule(s) (12). This putative regulation of mtDNA replication through the ER contact is supported by a previous study (13) in which membrane attachment of mtDNA replicative protein complex is detected at the cholesterol-rich ER-mitochondrial junction. In addition, the proposed membrane-tethering property of the mtDNA helicase in a mitochondrial nucleoid (14) is also likely to be related to the mtDNA replication controlled by the ER contact. Thus, I hypothesized that the mtDNA helicase might bind to the membrane via cholesterol to tether nucleoids at ER-mitochondrial junctions. The proposed membrane binding property of the mtDNA helicase was tested directly with asolectin liposomes in the presence or absence of cholesterol or cardiolipin. This will be discussed in chapter 3.

mtDNA genome

In a mammalian somatic cell, hundreds to thousands of mitochondria are observed, and one mitochondrion has two to tens of mtDNA copies. Sizes and structures in eukaryotic mtDNA vary prodigiously across species; they range 10-1000 kbp and exist as circular or linear DNA

(15). Generally, mtDNA in most metazoan cells is a double-stranded circular DNA of 14-20 kbp and encodes the same essential subunits of electron transport chain complexes for the oxidative phosphorylation regardless of species. In humans, 37 genes are tightly packed in 16,569 bp DNA, including genes for 13 proteins in electron transport chain complexes I, III, IV and V, 22 transfer RNAs, and 2 ribosomal RNAs (Fig. 1)(16). *Drosophila* mtDNA has 19,517 bp DNA that encodes the same genes but presents a different gene organization, comparing to human mtDNA (17).

Two strands in mammalian mtDNA have different buoyancies caused by biased distribution of G+T in one strand (18). Thus, the G+T rich strand is denoted as the heavy (H) chain and its complementary strand is called as the light (L) chain. Each strand has one promoter for transcription denoted by HSP and LSP, respectively, producing polycistronic mRNA. Each strand also has one origin of replication (for the H-strand, O_H, and for the L-strand, O_L).

The non-cording region (NCR) shows the most sequence variation in animal mtDNA (16). NCR in mammalian mtDNA span through ~1 kb and has three conserved sequence blocks (CSB) and one termination associated sequence (TAS) (Fig. 1). NCR serves important roles in initiations of both replication and transcription, containing an $O_{H,}$ and two transcriptional promoters, HSP and LSP. In the mammalian NCR, a stable displacement loop (D-loop) structure is often observed. The third strand that separates the parental strands of mtDNA is called 7S DNA due to its sedimentation property (19). 7S DNA is a prematurely terminated heavy strand. The length of 7S DNA varies and decides the size of D-loop. In humans, it stretches generally from near O_H to the TAS, a termination site for both RNA and DNA synthesis (20,21). 7S DNA has been hypothesized as a primer for H-strand replication because the 5' end starts from O_H and 7S DNA is able to be a primer for polymerase β *in vitro* (22). In addition, loss of 7S DNA has been reported in mtDNA helicase-(23) and mitochondrial single-stranded DNA-binding protein

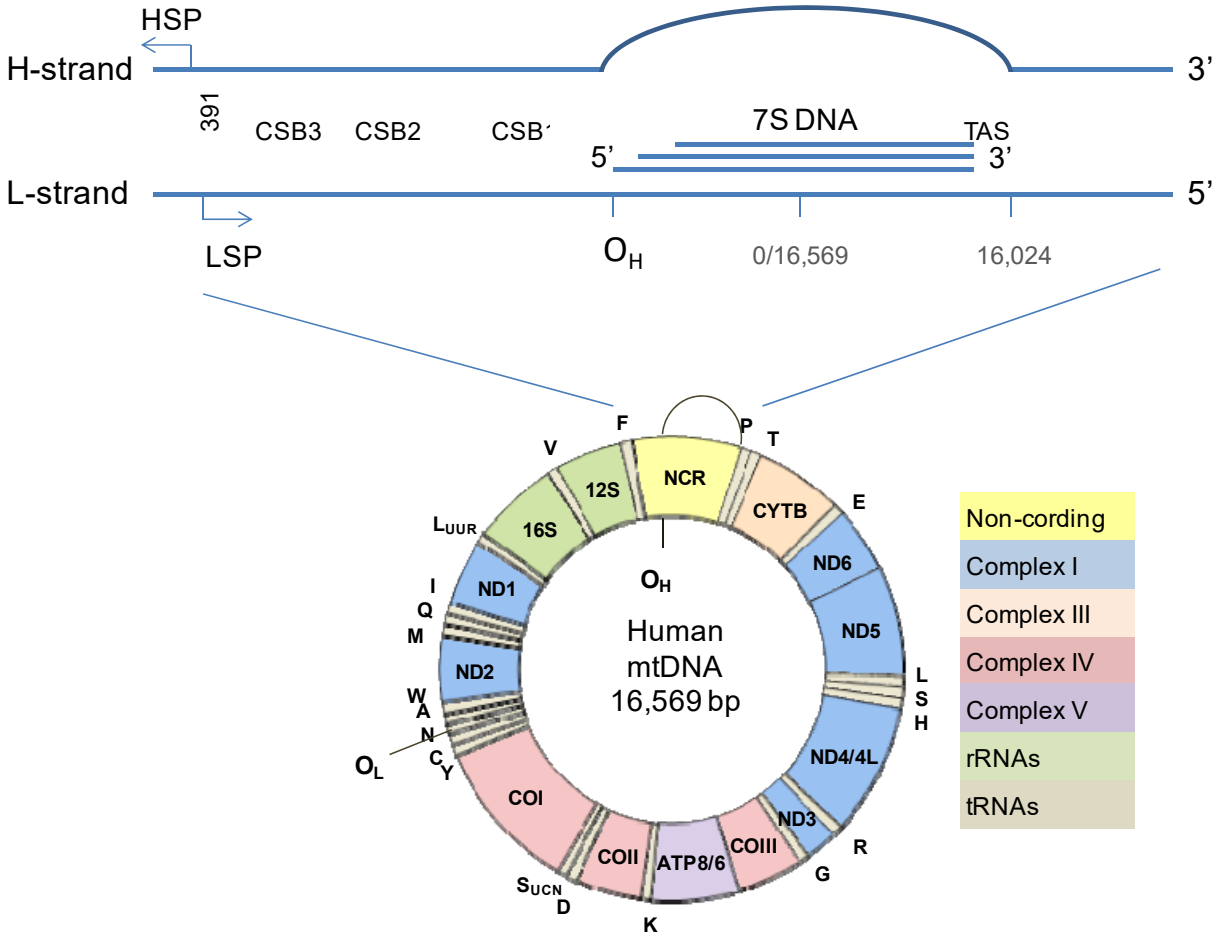

Figure 1. **Human mtDNA** (Top) Schematic diagram of non-cloning region (NCR) and 7S DNA. NCR contains CSB (conserved sequence block), TAS (termination-associated sequences), O_H (origin of replication for the heavy strand), HSP (heavy strand promoter) and LSP (light strand promoter). (Bottom) Schematic diagram of the human mitochondrial genome. Human mtDNA has 37 genes tightly packed in 16,569 bp DNA, including genes for 13 proteins in electron transport chain complexes I, III, IV and V, 22 transfer RNAs and 2 ribosomal RNAs. Modified from *Nicholls, T. J., and Minczuk, M. (2014) In D-loop: 40 years of mitochondrial 7S DNA. Experimental gerontology* ***56****, 175-181.*

(mtSSB)-(24) depleted cells, implying a relationship between 7S DNA and these replicative proteins. Contrarily, the relatively rapid turnover rate of 7S DNA entails a doubt why those futile productions are used for replication of such a genetically efficiently-designed molecule like mtDNA, weakening the hypothesis of 7S DNA as a primer (16). Thus, it is believed that the relationship between 7S DNA and mtDNA replication could be more complicated. Another proposed role for 7S DNA is related in recombination because recombination breakpoint hotspots are found in the termini of 7S DNA (25). The mtDNA helicase may serve a role in branch migration or annealing (26) during the D-loop related recombination; however, because human mtDNA helicase is not enriched at the 3' end of the 7S DNA under normal conditions (21), more investigation will be warranted for the relationship between the mtDNA helicase and 7S DNA in recombination.

In *Drosophila,* the non-cording region is denoted by A+T region, due to the high content of A+T (27). The A+T region contains the origin of mtDNA replication and consists of two sub-regions, which have own tandem repeats (28). A recent report shows that lower copies of the repeat I element in the A+T region are associated with low mtDNA copy numbers, proposing to the reduction of repeat I element could impede the mtDNA replication initiation (29).

It is likely that clarifying functions of D-loop and relationships between the non-cording region and mtDNA replication would expedite the complete understanding of the mtDNA replication mechanism including its initiation and termination steps.

mtDNA replication modes

Several mtDNA replication models have been proposed for mtDNA synthesis. It is likely that the replication mode of mtDNA has been evolved in the several ways. For example, rolling-

circle replication is detected in the mtDNA replication of *C. elegans* (30). Using two-dimensional agarose gel electrophoresis (2D-AGE), they found cruciform structures and multimers of its mtDNA. In addition, the concatemeric tail was also identified by transmission electron microscopy, supporting a rolling-circle mechanism for the mtDNA synthesis of *C. elegans*. In *Drosophila*, asynchronous, asymmetrical and unidirectional mtDNA replication was found in partially replicated mtDNA molecules by electron microscopy (EM) in the 1970s (31). However, they also observed that the subset of mtDNA shows a strand-coupled replication. In contrast, a recent 2D-AGE study shows that mtDNA replication in *Drosophila* is unidirectional and mainly strand-coupled replication, although mtDNA was synthesized partially in an asynchronous manner in a limited region near downstream of the NCR (28). Taking together, *Drosophila* mtDNA replication is likely to have both a strand-coupled unidirectional mode and a strand-uncoupled unidirectional mode, depending on regions within the mtDNA. The discrepancies in regions between old and recent studies remain to be clarified.

In human, three models have been proposed: a strand-displacement model, a strand-coupled model, and RITOLS (**R**NA **I**ncorporated **T**hrough**o**ut **L**agging **S**trand) (32). Although the exact model for the mammalian mtDNA replication is currently under the debate, a concurrence of the models in replication of the heavy strand (leading strand) is likely to be found; DNA synthesis is primed by an RNA primer that is transcribed from LSP, starts at the O_H in the NCR, and is elongated in a continuous and unidirectional fashion (33,34).

The strand-displacement model was proposed firstly in 1972 by EM study (35,36). During the asynchronous, unidirectional synthesis of H-strand originated from O_H, the remaining, parental, single-stranded H-strand is protected by mtSSB (37). When it completes two-thirds of the nascent H-strand, the O_L is exposed and forms a stem-loop structure (38),

where mitochondrial RNA polymerase synthesizes a primer (39), and synthesis of nascent L-strand is started synchronously by DNA polyerase γ in the opposite direction of the continuous replication of H-strand (33).

In 2000, a single-strand nuclease-resistant Y arc, which represents symmetric and synchronous replication, was detected in isolated mitochondrial DNA from both mouse and human cultured cells by 2D-AGE (40). According to this result, a strand-coupled model, which is symmetric and synchronous and unidirectional replication, was proposed. However, a small subset of the Y arc was single-strand-specific nuclease-sensitive, indicating the presence of single-stranded DNA. The following experiment, which used the highly purified mtDNA to remove the single-stranded DNA, detected RNA:DNA hybrids, which are resistant to restriction endonucleases but sensitive to RNase H. Because this suggests incorporation of ribonucleotides into the parental H-strand (41), RITOLS model was proposed to explain this result (35,42). The RNA:DNA hybrids were detected indeed in *vivo* by interstrand cross-linking and *in organello* labeling (43). The same study showed that the incorporated RNA is not synthesized concomitantly with the nascent H-strand synthesis but derived from pre-existing mature RNA. By taking this result, the RITOLS model was revised to the bootlace model, in which processed RNA transcripts are incorporated into the displaced, parental strand at the replication fork (43,44). However, the removal of incorporated RNA is unclear in the bootlace mechanism. The preparation of mtDNA was the main issue between the strand-displacement model and the strand-coupled model in the past. The similar issue has not been resolved clearly even with current advanced technology. Recently, mtSSB was found on the parental H-strand by ChIP-Seq and its *in vivo* occupancy pattern showed a gradual reduction of mtSSB concentration from the D-loop region to the O_L (37), supporting the strand-displacement model. In contrast, as

mentioned above, RNA:DNA hybrids were detected *in vivo* by interstrand cross-linking and *in organello* labeling, corroborating RNA incorporation in the RITOLS (bootlace) model (43). Further studies are required to finish this debate.

Mitochondrial replisome

The stability of mtDNA is mainly maintained by replication and repair mechanisms. mtDNA is replicated by a unique machinery, the mitochondrial replisome. The minimal mitochondrial replisome is considered to consist of DNA polymerase γ (pol γ), mtSSB and mtDNA helicase (45). These key mitochondrial replicative proteins have been identified and well-documented in human and *Drosophila* systems by our group and others.

Pol γ has been believed to be the only DNA polymerase in animal mitochondria. Currently, PrimPol (primase-polymerase) is identified to be imported to mitochondria, but it is unlikely to be involved essentially in mtDNA replication. It is thought to have a limited role under abnormal conditions such as replication stalling (reviewed in (46)). In vertebrate mtDNA polymerase, pol γ forms heterotrimer, consisting of one pol γ-α, and two pol γ-β subunits. The catalytic subunit of pol γ, pol γ-α, has 5' to 3' DNA polymerase activity, 3' to 5' exonuclease activity, and 5' deoxyribose phosphate lyase activity, and the accessory subunit, pol γ-β, is required for processivity of DNA synthesis, and DNA and nucleotide binding activity (32,33,47). Pol γ has a high fidelity; its *in vitro* error rate is only about once over half million bases polymerized. Pol γ is thought to serve roles in all mitochondrial DNA processes unlike nuclear polymerases that are highly specified. Mutations in human pol γ have been studied extensively, related to mitochondrial diseases. Severe forms of POLG syndrome is mostly involved in recessive mutations of the POLG1 gene, which are clustering at five distinct modules in pol γ-α

(48). The cluster prediction was used to develop a web-based server that helps diagnosis of etiology of a new pol γ pathogenic mutant (49).

mtSSB binds to single-stranded mtDNA in order to protect it against damage during replication, repair, and recombination. mtSSB also stimulates both DNA polymerase activity of pol γ and unwinding activity of the mtDNA helicase (50,51). Recently, biochemical and EM studies demonstrated that the elevated level of mtSSB proteins in both humans and *Drosophila* causes opening of the template DNA, and it shows a correlation with stimulation of pol γ by mtSSB, presenting how mtSSB stimulates pol γ (52). Disruption of the mtSSB gene results in lethality of *D. melanogaster* (53), and mtSSB protein knockdown shows a reduced mtDNA levels in cultured *D. melanogaster* cells (54), suggesting mtSSB is essential for mtDNA replication.

The mtDNA helicase, known as TWINKLE (**T**7 gp4-like protein **w**ith **i**ntramitochondrial **n**u**c**leoid **l**ocalization), is a replicative DNA helicase that unwinds mtDNA duplex with a 5' to 3' polarity by using NTP hydrolysis (55). It binds to both single-stranded DNA (ssDNA) and double-stranded DNA (dsDNA) (56,57) and loads itself to closed ssDNA circles or dsDNA bubbles (58). In addition, annealing activity (56) and weak activity to resolve G-quadruplex DNA structures (26) are also identified, implying a possibility for the mtDNA helicase to participate in mtDNA repair mechanisms; however, the clear biological roles for these activities of the mtDNA helicase remain uncertain (See more in a paragraph of mtDNA repair and recombination.)

The mtDNA helicase has a sequence homology with bacteriophage T7 gene 4 protein (T7gp4), a bi-functional primase-helicase (59). The mtDNA helicase and T7 gp4 share five conserved motifs in the C-terminal helicase domain, and seven motifs in the N-terminal primase-

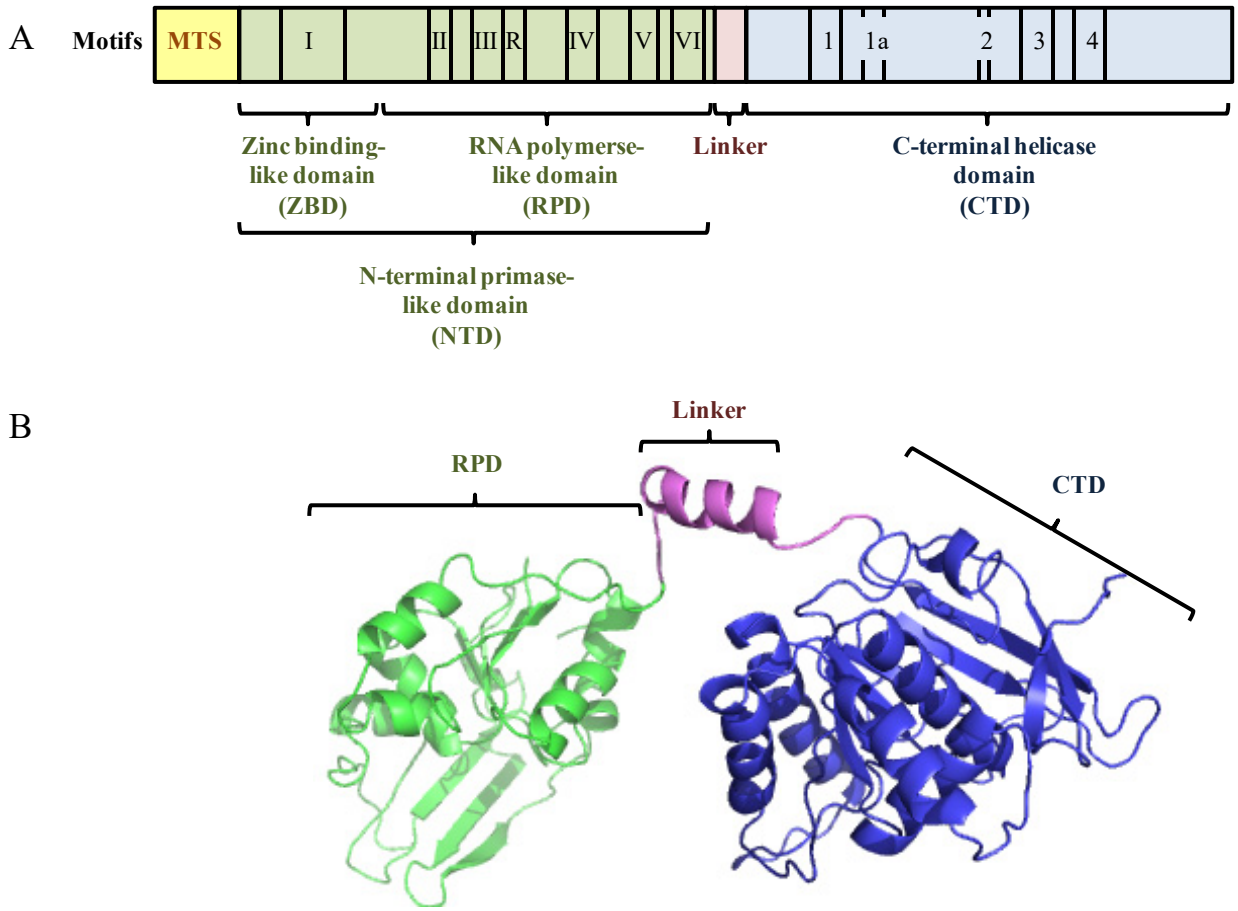

Figure 2. **Schematic representation of the domains and the conserved motifs in *Drosophila* mtDNA helicase (A) and a homology model of *Drosophila* mtDNA helicase monomer (B) A.** The N-terminal primase-like domain (NTD) has seven conserved amino acids motifs (motifs I-VI and RNAP basic motif (R)) and the C-terminal helicase domain (CTD) has five conserved amino acids motifs (motifs 1, 1a, 2, 3, and 4). The linker connects between the NTD and the CTD. MTS represents mitochondrial targeting sequence. **B.** A homology model of a monomer of *Drosophila* mtDNA helicase was generated by Phyre2 using bacteriophage T7 primase-helicase as a template (PDB #: 1NUI) (60). The ZBD is not generated. The RPD (green), which is faded out in this monomer, aligns with the neighboring CTD (not shown) at the back side in a hexameric form. The CTD (blue) in this monomer aligns with the other neighboring RPD (not shown) at the front side.

like domain (61) (Fig. 2). However, most metazoan mtDNA helicases lack the primase activity because some essential acidic amino acids are missing in motifs IV-VI (topoisomerase-primase fold) of the N-terminal primase-like domain (NTD). In addition, most metazoan mtDNA helicases, including human mtDNA helicase, do not possess all of the four highly conserved cysteine residues in a zinc binding-like domain (ZBD) (motif I). Interestingly, mtDNA helicases of insects, however, have all four cysteine residues in their ZBD (61), and *D. melanogaster* coordinates iron-sulfur cluster with the cysteine residues (57). Instead of the primase activity, the NTD may be used as a binding module in the mtDNA helicase (Chapter 3). Moreover, biological roles for metal cofactors including an iron-sulfur cluster in species-specific mtDNA processes are needed to be understood (See more in a paragraph of iron-sulfur cluster proteins in DNA processing mechanisms and Chapter 5.)

Recently the structure of human mtDNA helicase was reported as an atomic model based on EM images and small angle X-ray scattering (62). Similar to structures of T7 gp4 (60,63), it has a two-layered ring, in which RPDs and highly flexible ZBDs form a one-layered open-ring on the top of a ring-shaped hexameric C-terminal domains (CTD) with interactions between one CTD and the neighboring RPD. Due to its low resolution (12 Å) of EM images, the structure interpretation of the full-length human mtDNA helicase depends on the EM model. An advanced structure with better quality may be necessary to understand the molecular details of the mtDNA helicase in mtDNA processes. Investigations of partial protein structures such as domain- or subdomain-truncated structures may produce better images or crystals with higher resolutions. In this dissertation, the structure of the zinc binding domain-deleted human mtDNA helicase was investigated by negative stain electron microscopy as an example (Chapter 2).

mtDNA repair and recombination

In addition to mtDNA replication, several repair and recombination mechanisms maintain mtDNA integrity. mtDNA is more vulnerable to DNA damages than nuclear DNA because of its proximity to electron transport chain complexes that produce reactive oxygen species (ROS), and the lack of protection by histone proteins (64). Although it had been believed that there was a lack of repair mechanisms in mitochondria, since Clayton and coworkers reported that UV-induced thymidine dimers remains unrepaired in mtDNA (65). Indeed, nucleotide excision repair by which bulky DNA lesions can be fixed, is thought not to exist in animal mitochondria (66), but several other repair proteins have been identified in animal mitochondria, including enzymes involved in base excision repair, mismatch repair, and homologous repair (66).

Recent reports show evidences that the mtDNA helicase may serve role(s) in mtDNA repair (56,67,68). Strand annealing activity is identified in human mtDNA helicase, like many RecQ helicases working in double-stand break repair (DBR), implying its involvement in DBR (56,67,68). In addition, branch migration activity is observed in D-loop-like substrates *in vitro* (26,67), corresponding to the previous *in vivo* research with the overexpressed mtDNA helicase, which causes the increase Holliday junction (69) and suppresses ROS-induced replication stalling (70). These data suggests that the mtDNA helicase is likely to serve roles in homologous recombination and/ or recombination-mediated replication initiation.

Mitochondrial DNA stability maintained by replication and repair mechanisms is important for mitochondrial diseases. In addition to mitochondrial diseases such as mtDNA depletion syndrome, progressive external ophthalmoplegia, and ataxia-neuropathy (71), mtDNA defects are thought to be also related to neurodegenerative diseases, aging, and cancers (3,72), which are so-called “complex” diseases (4). Thus, a new paradigm to explain the etiology of

complex diseases with mitochondrial biogenesis has been rising (4,73).

Iron-sulfur cluster proteins in DNA processing mechanisms

Iron-sulfur clusters are ancient cofactors thought to be involved in the emergence of the origin of life (74). Iron-sulfur clusters are now found in a wide range of enzymes as prosthetic groups, and fulfill multifaceted roles in cellular metabolism (75). During the last decade, iron-sulfur clusters have been identified in diverse nucleic acid processing enzymes such as primases (76,77), polymerases (78), helicases (57,79,80), nucleases (81-83), glycosylases (84), and transcription factors (85). Iron-sulfur clusters in DNA processing enzymes are primarily essential for structural stability, and only a few proteins such as glycosylases (84) and some DNA repair helicases (80) are known to contain iron-sulfur clusters that modulate enzymatic activity (86). A novel role for iron-sulfur clusters in DNA processing enzymes, named DNA-mediated charge transfer (DNA-CT), has been demonstrated in nuclear DNA repair (in endonuclease III, MutY, DinG, and XPD) and transcription (in SoxR) (87-89). However, a clear role for iron-sulfur clusters in DNA replication has not been described until recently, although iron-sulfur clusters have been detected in many nuclear replicative proteins such as DNA polymerases α, δ, and ε (78), and primases (90,91). Barton and collaborators demonstrated that DNA binding by human primase is regulated by the oxidation state of its iron-sulfur cluster, and electron transport by DNA-CT leads to reduction of the ISC and subsequent primase handoff, such that DNA polymerase α serves as a putative electron transfer partner at the replication fork (92).

Mitochondria are essential for iron-sulfur cluster biogenesis in animal cells (93). Whereas a considerable number of DNA processing proteins in the nucleus have been found to have iron-sulfur clusters, iron-sulfur clusters in mitochondrial DNA metabolism have only recently been

explored. Dna2 helicase-nuclease (81,94) and exonuclease 5 (95) have been reported as iron-sulfur cluster-containing DNA processing proteins that function in mitochondria (75). Dna2 serves roles in maintaining both nuclear and mitochondrial genomes (96). The iron-sulfur cluster in Dna2 is suggested to provide a functional link between its nuclease and helicase domains because mutagenesis in the iron-sulfur cluster-coordinating cysteine residues reduces both nuclease and ATPase activities (81). In human mitochondria, Dna2 stimulates mtDNA polymerase activity and removes RNA primers in replication, and processes 5'-flap intermediates in long-patch base excision repair (97). Yeast exonuclease 5, which is essential in mitochondrial DNA replication and recombination, contains conserved cysteine residues to coordinate an iron-sulfur cluster (95). Its human homolog has been demonstrated to contain an iron-sulfur cluster that is critical for its nuclease activity, although human exonuclease 5 lacks a mitochondrial leader sequence (83). Additionally, the mtDNA helicase from *D. melanogaster* contains a 2Fe-2S cluster in its N-terminal, primase-like domain; the iron-sulfur cluster plays roles in mtDNA binding and protein stability (57). The homologous T7gp4 coordinates a zinc ion by the homologous cysteines in its N-terminal primase domain, and human mtDNA helicase does not bind either metal because the cysteine residues are not conserved (98). This evolutionary change from a zinc ion to an iron-sulfur cluster and to the absence of a metal is intriguing, because the function of the N-terminal primase-like domains of animal mtDNA helicases has not yet been established clearly. Functions for the N-terminal primase-like domains in humans and *Drosophila* were researched (Chapter 3), and the putative iron-sulfur cluster donor, *Dm* Ind1, was characterized (Chapter 4) with an ultimate goal to understand the delivery and functions of the species-specific iron-sulfur cluster in *Dm* mtDNA helicase. The specific experimental plans to investigate the biological functions of the cluster will be discussed in chapter 5.

BIBLIOGRAPHY

BIBLIOGRAPHY

1. Shokolenko, I. N., Alexeyev, M. F., LeDoux, S. P., and Wilson, G. L. (2010) The approaches for manipulating mitochondrial proteome. *Environmental and molecular mutagenesis* **51**, 451-461

2. Taylor, S. W., Fahy, E., Zhang, B., Glenn, G. M., Warnock, D. E., Wiley, S., Murphy, A. N., Gaucher, S. P., Capaldi, R. A., Gibson, B. W., and Ghosh, S. S. (2003) Characterization of the human heart mitochondrial proteome. *Nature biotechnology* **21**, 281-286

3. Wallace, D. C. (2012) Mitochondria and cancer. *Nature reviews. Cancer* **12**, 685-698

4. Wallace, D. C. (2011) Bioenergetic origins of complexity and disease. *Cold Spring Harbor symposia on quantitative biology* **76**, 1-16

5. Cagin, U., and Enriquez, J. A. (2015) The complex crosstalk between mitochondria and the nucleus: What goes in between? *The international journal of biochemistry & cell biology* **63**, 10-15

6. Quiros, P. M., Mottis, A., and Auwerx, J. (2016) Mitonuclear communication in homeostasis and stress. *Nature reviews. Molecular cell biology* **17**, 213-226

7. Marchi, S., Patergnani, S., and Pinton, P. (2014) The endoplasmic reticulum-mitochondria connection: one touch, multiple functions. *Biochimica et biophysica acta* **1837**, 461-469

8. Sugiura, A., Mattie, S., Prudent, J., and McBride, H. M. (2017) Newly born peroxisomes are a hybrid of mitochondrial and ER-derived pre-peroxisomes. *Nature* **542**, 251-254

9. Schrader, M., and Pellegrini, L. (2017) The making of a mammalian peroxisome, version 2.0: mitochondria get into the mix. *Cell death and differentiation*

10. Prudent, J., and McBride, H. M. (2017) The mitochondria-endoplasmic reticulum contact sites: a signalling platform for cell death. *Current opinion in cell biology* **47**, 52-63

11. Lewis, S. C., Uchiyama, L. F., and Nunnari, J. (2016) ER-mitochondria contacts couple mtDNA synthesis with mitochondrial division in human cells. *Science* **353**, aaf5549

12. Ziviani, E., and Scorrano, L. (2016) Cell biology: The organelle replication connection. *Nature* **538**, 326-327

13. Gerhold, J. M., Cansiz-Arda, S., Lohmus, M., Engberg, O., Reyes, A., van Rennes, H., Sanz, A., Holt, I. J., Cooper, H. M., and Spelbrink, J. N. (2015) Human Mitochondrial DNA-Protein Complexes Attach to a Cholesterol-Rich Membrane Structure. *Scientific reports* **5**, 15292

14. Rajala, N., Gerhold, J. M., Martinsson, P., Klymov, A., and Spelbrink, J. N. (2014) Replication factors transiently associate with mtDNA at the mitochondrial inner membrane to facilitate replication. *Nucleic acids research* **42**, 952-967

15. Kolesnikov, A. A., and Gerasimov, E. S. (2012) Diversity of mitochondrial genome organization. *Biochemistry. Biokhimiia* **77**, 1424-1435

16. Nicholls, T. J., and Minczuk, M. (2014) In D-loop: 40 years of mitochondrial 7S DNA. *Experimental gerontology* **56**, 175-181

17. Oliveira, M. T., Garesse, R., and Kaguni, L. S. (2010) Animal models of mitochondrial DNA transactions in disease and ageing. *Experimental gerontology* **45**, 489-502

18. Taanman, J.-W. (1999) The mitochondrial genome: structure, transcription, translation and replication. *Biochimica et Biophysica Acta (BBA) - Bioenergetics* **1410**, 103-123

19. Kasamatsu, H., Robberson, D. L., and Vinograd, J. (1971) A novel closed-circular mitochondrial DNA with properties of a replicating intermediate. *Proceedings of the National Academy of Sciences of the United States of America* **68**, 2252-2257

20. Doda, J. N., Wright, C. T., and Clayton, D. A. (1981) Elongation of displacement-loop strands in human and mouse mitochondrial DNA is arrested near specific template sequences. *Proceedings of the National Academy of Sciences of the United States of America* **78**, 6116-6120

21. Jemt, E., Persson, O., Shi, Y., Mehmedovic, M., Uhler, J. P., Davila Lopez, M., Freyer, C., Gustafsson, C. M., Samuelsson, T., and Falkenberg, M. (2015) Regulation of DNA replication at the end of the mitochondrial D-loop involves the helicase TWINKLE and a conserved sequence element. *Nucleic acids research* **43**, 9262-9275

22. Eichler, D. C., Wang, T. S., Clayton, D. A., and Korn, D. (1977) In vitro replication of mitochondrial DNA. Elongation of the endogenous primer sequence in D loop mitochondrial DNA by human DNA polymerase beta. *The Journal of biological chemistry* **252**, 7888-7893

23. Milenkovic, D., Matic, S., Kuhl, I., Ruzzenente, B., Freyer, C., Jemt, E., Park, C. B., Falkenberg, M., and Larsson, N. G. (2013) TWINKLE is an essential mitochondrial helicase required for synthesis of nascent D-loop strands and complete mtDNA replication. *Human molecular genetics* **22**, 1983-1993

24. Ruhanen, H., Borrie, S., Szabadkai, G., Tyynismaa, H., Jones, A. W., Kang, D., Taanman, J. W., and Yasukawa, T. (2010) Mitochondrial single-stranded DNA binding protein is required for maintenance of mitochondrial DNA and 7S DNA but is not required for mitochondrial nucleoid organisation. *Biochimica et biophysica acta* **1803**, 931-939

25. Kraytsberg, Y., Schwartz, M., Brown, T. A., Ebralidse, K., Kunz, W. S., Clayton, D. A., Vissing, J., and Khrapko, K. (2004) Recombination of human mitochondrial DNA. *Science* **304**, 981

26. Khan, I., Crouch, J. D., Bharti, S. K., Sommers, J. A., Carney, S. M., Yakubovskaya, E., Garcia-Diaz, M., Trakselis, M. A., and Brosh, R. M., Jr. (2016) Biochemical Characterization of the Human Mitochondrial Replicative Twinkle Helicase: SUBSTRATE SPECIFICITY, DNA BRANCH MIGRATION, AND ABILITY TO OVERCOME BLOCKADES TO DNA UNWINDING. *The Journal of biological chemistry* **291**, 14324-14339

27. Fauron, C. M., and Wolstenholme, D. R. (1976) Structural heterogeneity of mitochondrial DNA molecules within the genus Drosophila. *Proceedings of the National Academy of Sciences of the United States of America* **73**, 3623-3627

28. Joers, P., and Jacobs, H. T. (2013) Analysis of replication intermediates indicates that Drosophila melanogaster mitochondrial DNA replicates by a strand-coupled theta mechanism. *PloS one* **8**, e53249

29. Salminen, T. S., Oliveira, M. T., Cannino, G., Lillsunde, P., Jacobs, H. T., and Kaguni, L. S. (2017) Mitochondrial genotype modulates mtDNA copy number and organismal phenotype in Drosophila. *Mitochondrion*

30. Lewis, S. C., Joers, P., Willcox, S., Griffith, J. D., Jacobs, H. T., and Hyman, B. C. (2015) A rolling circle replication mechanism produces multimeric lariats of mitochondrial DNA in Caenorhabditis elegans. *PLoS genetics* **11**, e1004985

31. Goddard, J. M., and Wolstenholme, D. R. (1978) Origin and direction of replication in mitochondrial DNA molecules from Drosophila melanogaster. *Proceedings of the National Academy of Sciences of the United States of America* **75**, 3886-3890

32. Kasiviswanathan, R., Collins, T. R., and Copeland, W. C. (2012) The interface of transcription and DNA replication in the mitochondria. *Biochimica et biophysica acta* **1819**, 970-978

33. Ciesielski, G. L., Oliveira, M. T., and Kaguni, L. S. (2016) Animal Mitochondrial DNA Replication. *The Enzymes* **39**, 255-292

34. Uhler, J. P., and Falkenberg, M. (2015) Primer removal during mammalian mitochondrial DNA replication. *DNA repair* **34**, 28-38

35. Holt, I. J. (2009) Mitochondrial DNA replication and repair: all a flap. *Trends in biochemical sciences* **34**, 358-365

36. Clayton, D. A. (1982) Replication of animal mitochondrial DNA. *Cell* **28**, 693-705

37. Miralles Fuste, J., Shi, Y., Wanrooij, S., Zhu, X., Jemt, E., Persson, O., Sabouri, N., Gustafsson, C. M., and Falkenberg, M. (2014) In vivo occupancy of mitochondrial single-stranded DNA binding protein supports the strand displacement mode of DNA replication. *PLoS genetics* **10**, e1004832

38. Hixson, J. E., Wong, T. W., and Clayton, D. A. (1986) Both the conserved stem-loop and divergent 5'-flanking sequences are required for initiation at the human mitochondrial origin of light-strand DNA replication. *The Journal of biological chemistry* **261**, 2384-2390

39. Fuste, J. M., Wanrooij, S., Jemt, E., Granycome, C. E., Cluett, T. J., Shi, Y., Atanassova, N., Holt, I. J., Gustafsson, C. M., and Falkenberg, M. (2010) Mitochondrial RNA polymerase is needed for activation of the origin of light-strand DNA replication. *Molecular cell* **37**, 67-78

40. Holt, I. J., Lorimer, H. E., and Jacobs, H. T. (2000) Coupled leading- and lagging-strand synthesis of mammalian mitochondrial DNA. *Cell* **100**, 515-524

41. Yang, M. Y., Bowmaker, M., Reyes, A., Vergani, L., Angeli, P., Gringeri, E., Jacobs, H. T., and Holt, I. J. (2002) Biased incorporation of ribonucleotides on the mitochondrial L-strand accounts for apparent strand-asymmetric DNA replication. *Cell* **111**, 495-505

42. Holt, I. J., and Reyes, A. (2012) Human mitochondrial DNA replication. *Cold Spring Harbor perspectives in biology* **4**

43. Reyes, A., Kazak, L., Wood, S. R., Yasukawa, T., Jacobs, H. T., and Holt, I. J. (2013) Mitochondrial DNA replication proceeds via a 'bootlace' mechanism involving the incorporation of processed transcripts. *Nucleic acids research* **41**, 5837-5850

44. Holt, I. J., and Jacobs, H. T. (2014) Unique features of DNA replication in mitochondria: a functional and evolutionary perspective. *BioEssays : news and reviews in molecular, cellular and developmental biology* **36**, 1024-1031

45. Korhonen, J. A., Pham, X. H., Pellegrini, M., and Falkenberg, M. (2004) Reconstitution of a minimal mtDNA replisome in vitro. *The EMBO journal* **23**, 2423-2429

46. Bailey, L. J., and Doherty, A. J. (2017) Mitochondrial DNA replication: a PrimPol perspective. *Biochemical Society transactions* **45**, 513-529

47. Kaguni, L. S. (2004) DNA polymerase gamma, the mitochondrial replicase. *Annual review of biochemistry* **73**, 293-320

48. Euro, L., Farnum, G. A., Palin, E., Suomalainen, A., and Kaguni, L. S. (2011) Clustering of Alpers disease mutations and catalytic defects in biochemical variants reveal new features of molecular mechanism of the human mitochondrial replicase, Pol gamma. *Nucleic acids research* **39**, 9072-9084

49. Farnum, G. A., Nurminen, A., and Kaguni, L. S. (2014) Mapping 136 pathogenic mutations into functional modules in human DNA polymerase gamma establishes predictive genotype-phenotype correlations for the complete spectrum of POLG syndromes. *Biochimica et biophysica acta* **1837**, 1113-1121

50. Oliveira, M. T., and Kaguni, L. S. (2010) Functional roles of the N- and C-terminal regions of the human mitochondrial single-stranded DNA-binding protein. *PloS one* **5**, e15379

51. Oliveira, M. T., and Kaguni, L. S. (2011) Reduced stimulation of recombinant DNA polymerase gamma and mitochondrial DNA (mtDNA) helicase by variants of mitochondrial single-stranded DNA-binding protein (mtSSB) correlates with defects in mtDNA replication in animal cells. *The Journal of biological chemistry* **286**, 40649-40658

52. Ciesielski, G. L., Bermek, O., Rosado-Ruiz, F. A., Hovde, S. L., Neitzke, O. J., Griffith, J. D., and Kaguni, L. S. (2015) Mitochondrial Single-stranded DNA-binding Proteins Stimulate the Activity of DNA Polymerase gamma by Organization of the Template DNA. *The Journal of biological chemistry* **290**, 28697-28707

53. Maier, D., Farr, C. L., Poeck, B., Alahari, A., Vogel, M., Fischer, S., Kaguni, L. S., and Schneuwly, S. (2001) Mitochondrial single-stranded DNA-binding protein is required for mitochondrial DNA replication and development in Drosophila melanogaster. *Molecular*

biology of the cell **12**, 821-830

54. Farr, C. L., Matsushima, Y., Lagina, A. T., 3rd, Luo, N., and Kaguni, L. S. (2004) Physiological and biochemical defects in functional interactions of mitochondrial DNA polymerase and DNA-binding mutants of single-stranded DNA-binding protein. *The Journal of biological chemistry* **279**, 17047-17053

55. Korhonen, J. A., Gaspari, M., and Falkenberg, M. (2003) TWINKLE Has 5' -> 3' DNA helicase activity and is specifically stimulated by mitochondrial single-stranded DNA-binding protein. *The Journal of biological chemistry* **278**, 48627-48632

56. Sen, D., Nandakumar, D., Tang, G. Q., and Patel, S. S. (2012) Human mitochondrial DNA helicase TWINKLE is both an unwinding and annealing helicase. *The Journal of biological chemistry* **287**, 14545-14556

57. Stiban, J., Farnum, G. A., Hovde, S. L., and Kaguni, L. S. (2014) The N-terminal domain of the Drosophila mitochondrial replicative DNA helicase contains an iron-sulfur cluster and binds DNA. *The Journal of biological chemistry* **289**, 24032-24042

58. Jemt, E., Farge, G., Backstrom, S., Holmlund, T., Gustafsson, C. M., and Falkenberg, M. (2011) The mitochondrial DNA helicase TWINKLE can assemble on a closed circular template and support initiation of DNA synthesis. *Nucleic acids research* **39**, 9238-9249

59. Spelbrink, J. N., Li, F. Y., Tiranti, V., Nikali, K., Yuan, Q. P., Tariq, M., Wanrooij, S., Garrido, N., Comi, G., Morandi, L., Santoro, L., Toscano, A., Fabrizi, G. M., Somer, H., Croxen, R., Beeson, D., Poulton, J., Suomalainen, A., Jacobs, H. T., Zeviani, M., and Larsson, C. (2001) Human mitochondrial DNA deletions associated with mutations in the gene encoding Twinkle, a phage T7 gene 4-like protein localized in mitochondria. *Nature genetics* **28**, 223-231

60. Kato, M., Ito, T., Wagner, G., Richardson, C. C., and Ellenberger, T. (2003) Modular architecture of the bacteriophage T7 primase couples RNA primer synthesis to DNA synthesis. *Molecular cell* **11**, 1349-1360

61. Shutt, T. E., and Gray, M. W. (2006) Twinkle, the mitochondrial replicative DNA helicase, is widespread in the eukaryotic radiation and may also be the mitochondrial DNA primase in most eukaryotes. *Journal of molecular evolution* **62**, 588-599

62. Fernandez-Millan, P., Lazaro, M., Cansiz-Arda, S., Gerhold, J. M., Rajala, N., Schmitz, C. A., Silva-Espina, C., Gil, D., Bernado, P., Valle, M., Spelbrink, J. N., and Sola, M. (2015) The hexameric structure of the human mitochondrial replicative helicase Twinkle. *Nucleic acids research* **43**, 4284-4295

63. Toth, E. A., Li, Y., Sawaya, M. R., Cheng, Y., and Ellenberger, T. (2003) The crystal structure of the bifunctional primase-helicase of bacteriophage T7. *Molecular cell* **12**, 1113-1123

64. Achanta, G., Sasaki, R., Feng, L., Carew, J. S., Lu, W., Pelicano, H., Keating, M. J., and Huang, P. (2005) Novel role of p53 in maintaining mitochondrial genetic stability through interaction with DNA Pol gamma. *The EMBO journal* **24**, 3482-3492

65. Clayton, D. A., Doda, J. N., and Friedberg, E. C. (1974) The absence of a pyrimidine

dimer repair mechanism in mammalian mitochondria. *Proceedings of the National Academy of Sciences of the United States of America* **71**, 2777-2781

66. Larsen, N. B., Rasmussen, M., and Rasmussen, L. J. (2005) Nuclear and mitochondrial DNA repair: similar pathways? *Mitochondrion* **5**, 89-108

67. Sen, D., Patel, G., and Patel, S. S. (2016) Homologous DNA strand exchange activity of the human mitochondrial DNA helicase TWINKLE. *Nucleic acids research* **44**, 4200-4210

68. Suhasini, A. N., and Brosh, R. M., Jr. (2013) Disease-causing missense mutations in human DNA helicase disorders. *Mutation research* **752**, 138-152

69. Pohjoismaki, J. L., Goffart, S., and Spelbrink, J. N. (2011) Replication stalling by catalytically impaired Twinkle induces mitochondrial DNA rearrangements in cultured cells. *Mitochondrion* **11**, 630-634

70. Pohjoismaki, J. L., Williams, S. L., Boettger, T., Goffart, S., Kim, J., Suomalainen, A., Moraes, C. T., and Braun, T. (2013) Overexpression of Twinkle-helicase protects cardiomyocytes from genotoxic stress caused by reactive oxygen species. *Proceedings of the National Academy of Sciences of the United States of America* **110**, 19408-19413

71. Copeland, W. C. (2008) Inherited mitochondrial diseases of DNA replication. *Annual review of medicine* **59**, 131-146

72. Wallace, D. C. (2005) Mitochondria and cancer: Warburg addressed. *Cold Spring Harbor symposia on quantitative biology* **70**, 363-374

73. Picard, M., Wallace, D. C., and Burelle, Y. (2016) The rise of mitochondria in medicine. *Mitochondrion* **30**, 105-116

74. Koonin, E. V., and Martin, W. (2005) On the origin of genomes and cells within inorganic compartments. *Trends in genetics : TIG* **21**, 647-654

75. Stiban, J., So, M., and Kaguni, L. S. (2016) Iron-sulfur clusters in mitochondrial metabolism: Multifaceted roles of a simple cofactor. *Biochemistry (Moscow)* **81**, 1066-1080

76. O'Brien, E., and Holt, M. E. (2017) The [4Fe4S] cluster of human DNA primase functions as a redox switch using DNA charge transport. **355**

77. Weiner, B. E., Huang, H., Dattilo, B. M., Nilges, M. J., Fanning, E., and Chazin, W. J. (2007) An iron-sulfur cluster in the C-terminal domain of the p58 subunit of human DNA primase. *The Journal of biological chemistry* **282**, 33444-33451

78. Netz, D. J., Stith, C. M., Stumpfig, M., Kopf, G., Vogel, D., Genau, H. M., Stodola, J. L., Lill, R., Burgers, P. M., and Pierik, A. J. (2012) Eukaryotic DNA polymerases require an iron-sulfur cluster for the formation of active complexes. *Nature chemical biology* **8**, 125-132

79. Fan, L., Fuss, J. O., Cheng, Q. J., Arvai, A. S., Hammel, M., Roberts, V. A., Cooper, P. K., and Tainer, J. A. (2008) XPD helicase structures and activities: insights into the cancer

and aging phenotypes from XPD mutations. *Cell* **133**, 789-800

80. Rudolf, J., Makrantoni, V., Ingledew, W. J., Stark, M. J., and White, M. F. (2006) The DNA repair helicases XPD and FancJ have essential iron-sulfur domains. *Molecular cell* **23**, 801-808

81. Pokharel, S., and Campbell, J. L. (2012) Cross talk between the nuclease and helicase activities of Dna2: role of an essential iron-sulfur cluster domain. *Nucleic acids research* **40**, 7821-7830

82. Yeeles, J. T., Cammack, R., and Dillingham, M. S. (2009) An iron-sulfur cluster is essential for the binding of broken DNA by AddAB-type helicase-nucleases. *The Journal of biological chemistry* **284**, 7746-7755

83. Sparks, J. L., Kumar, R., Singh, M., Wold, M. S., Pandita, T. K., and Burgers, P. M. (2012) Human exonuclease 5 is a novel sliding exonuclease required for genome stability. *The Journal of biological chemistry* **287**, 42773-42783

84. Boal, A. K., Genereux, J. C., Sontz, P. A., Gralnick, J. A., Newman, D. K., and Barton, J. K. (2009) Redox signaling between DNA repair proteins for efficient lesion detection. *Proceedings of the National Academy of Sciences of the United States of America* **106**, 15237-15242

85. Khoroshilova, N., Popescu, C., Munck, E., Beinert, H., and Kiley, P. J. (1997) Iron-sulfur cluster disassembly in the FNR protein of Escherichia coli by O2: [4Fe-4S] to [2Fe-2S] conversion with loss of biological activity. *Proceedings of the National Academy of Sciences of the United States of America* **94**, 6087-6092

86. White, M. F., and Dillingham, M. S. (2012) Iron-sulphur clusters in nucleic acid processing enzymes. *Current opinion in structural biology* **22**, 94-100

87. Arnold, A. R., Grodick, M. A., and Barton, J. K. (2016) DNA Charge Transport: from Chemical Principles to the Cell. *Cell chemical biology* **23**, 183-197

88. Grodick, M. A., Muren, N. B., and Barton, J. K. (2015) DNA charge transport within the cell. *Biochemistry* **54**, 962-973

89. Fuss, J. O., Tsai, C. L., Ishida, J. P., and Tainer, J. A. (2015) Emerging critical roles of Fe-S clusters in DNA replication and repair. *Biochimica et biophysica acta* **1853**, 1253-1271

90. Klinge, S., Hirst, J., Maman, J. D., Krude, T., and Pellegrini, L. (2007) An iron-sulfur domain of the eukaryotic primase is essential for RNA primer synthesis. *Nature structural & molecular biology* **14**, 875-877

91. Vaithiyalingam, S., Warren, E. M., Eichman, B. F., and Chazin, W. J. (2010) Insights into eukaryotic DNA priming from the structure and functional interactions of the 4Fe-4S cluster domain of human DNA primase. *Proceedings of the National Academy of Sciences of the United States of America* **107**, 13684-13689

92. O'Brien, E., Holt, M. E., Thompson, M. K., Salay, L. E., Ehlinger, A. C., Chazin, W. J., and Barton, J. K. (2017) The [4Fe4S] cluster of human DNA primase functions as a redox switch using DNA charge transport. *Science* **355**

93. Maio, N., and Rouault, T. A. (2015) Iron-sulfur cluster biogenesis in mammalian cells: New insights into the molecular mechanisms of cluster delivery. *Biochimica et biophysica acta* **1853**, 1493-1512

94. Budd, M. E., Reis, C. C., Smith, S., Myung, K., and Campbell, J. L. (2006) Evidence suggesting that Pif1 helicase functions in DNA replication with the Dna2 helicase/nuclease and DNA polymerase delta. *Molecular and cellular biology* **26**, 2490-2500

95. Burgers, P. M., Stith, C. M., Yoder, B. L., and Sparks, J. L. (2010) Yeast exonuclease 5 is essential for mitochondrial genome maintenance. *Molecular and cellular biology* **30**, 1457-1466

96. Duxin, J. P., Dao, B., Martinsson, P., Rajala, N., Guittat, L., Campbell, J. L., Spelbrink, J. N., and Stewart, S. A. (2009) Human Dna2 is a nuclear and mitochondrial DNA maintenance protein. *Molecular and cellular biology* **29**, 4274-4282

97. Zheng, L., Zhou, M., Guo, Z., Lu, H., Qian, L., Dai, H., Qiu, J., Yakubovskaya, E., Bogenhagen, D. F., Demple, B., and Shen, B. (2008) Human DNA2 is a mitochondrial nuclease/helicase for efficient processing of DNA replication and repair intermediates. *Molecular cell* **32**, 325-336

98. Kaguni, L. S., and Oliveira, M. T. (2016) Structure, function and evolution of the animal mitochondrial replicative DNA helicase. *Critical reviews in biochemistry and molecular biology* **51**, 53-64

CHAPTER 2
Structural analysis of human mtDNA helicase

ABSTRACT

Mitochondrial replicative DNA helicase (mtDNA helicase) is an essential protein in the mitochondrial DNA replisome. Its flexible structure and insolubility at low ionic strength render its structural study difficult. Recently, an atomic model of human full-length mtDNA helicase was published based on a cryo-electron microscopy structure (12 Å) under high salt conditions (1.5 M NaCl) (1). To pursue a higher resolution structure at physiological ionic strength, human mtDNA helicase was prepared under two different salt conditions (100 mM and 330 mM NaCl) and the oligomeric states were investigated using several approaches, including chemical crosslinking, GraFix (glycerol gradient sedimentation combined with chemical crosslinking), and two-dimensional negative stain electron microscopy (2D-NS-EM). All three approaches showed that the human mtDNA helicase exists in heterogeneous oligomeric states. The full-length mtDNA helicase exists largely as hexamers and heptamers ranging from hexamers to octamers. NS-EM in high salt buffer showed 15% of completely-extended star-shaped particles, but the majority of molecules were contained a mixture of extended and compact arms, indicating its dynamic conformations. Their diversity decreases significantly in a truncated variant lacking the zinc binding-like domain (ZBD), and the variant shows predominantly hexameric, symmetric, and compact particles. This result indicates that the ZBD renders structural flexibility to the human mtDNA helicase. Under low salt conditions, oligomers with compact arms were predominant and multimers of oligomers including dimers of oligomers were observed. This multimer formation was reversible under high salt conditions. In addition to dimers of oligomers, open-ring structures and one-arm-extended structures we observed by NS-EM support a mechanism of self-directed loading to single-stranded DNA. However, further biochemical and physiological experiments will be required to elucidate the mechanisms.

INTRODUCTION

The human mitochondrial replicative DNA helicase (mtDNA helicase), also known as TWINKLE, was identified during research of autosomal dominant progressive external ophthalmoplegia (2), a late-onset human mitochondrial disease involving exercise intolerance, muscle weakness, and progressive weakening of the external eye muscles (3). Since the identification, it has been demonstrated that the human mtDNA helicase is an essential enzyme for mitochondrial DNA (mtDNA) maintenance and regulation of mtDNA copy number (4,5). The mtDNA helicase as a replicative DNA helicase unwinds the mitochondrial DNA duplex in a distinct 5' to 3'direction by using ATP hydrolysis (6). Besides nucleotide-dependent double-stranded DNA (dsDNA) unwinding activity and DNA dependent ATPase activity (6), nucleotide-independent single-stranded DNA (ssDNA) annealing activity has been demonstrated, suggesting a role in recombination-mediated replication initiation in mitochondria (7). As the name TWINKLE (**T**7 gp4-like protein **w**ith **i**ntramitochondrial **n**ucleoid **l**ocalization) implies, the mtDNA helicase has an apparent sequence homology with bacteriophage T7 gene 4 protein (T7gp4), a bi-functional primase-helicase (2), and both are classified as *Escherichia coli* (*E. coli*) DnaB-like replicative helicases, or superfamily 4 (SF4) replicative helicases (8).

The mtDNA helicase and T7gp4 have an N-terminal primase-like domain (NTD) and a C-terminal helicase domain (CTD), and the two domains are connected by a flexible linker (9) (see Fig. 2 in chapter 1). The NTD consists of a zinc binding-like domain (ZBD) and an RNA polymerase-like domain (RPD) (Fig. 1 in Literature review). In T7gp4, the ZBD recognizes the trinucleotide sequence (5'-GTC-3') in a DNA template (10) and delivers a newly synthesized primer to the DNA polymerase, cooperating with the RPD (11). Primer synthesis occurs in the RPD in T7gp4. Although the NTD of the mtDNA helicase has the same structural folds (1), it

has not been reported to have detectable primase activity because it has lost the essential catalytic amino acids required for primer synthesis during the evolutionary process. The C-terminal helicase domain assembles into a ring-shaped structure (1) and catalyzes helicase activity (12). In T7gp4, oligomerization of the CTD results from two main interactions: the main intersubunit interaction between an α-helix (residues 264-284) in the linker region and an adjacent subunit (residues 364-395) (13), and interactions in the nucleotide binding site which is located at the subunit interface (14). Therefore, the stability of oligomeric structure of T7gp4 is increased by the presence of nucleotide in the binding site (15). The human mtDNA helicase lacking its CTD does not form oligomeric structures (12), implying that a similar mechanism would be used for oligomerization of the mtDNA helicase.

Studies of oligomeric states of the human mtDNA helicase and T7 gp4 have suggested that they assemble as both hexamers and heptamers, unlike other helicases in the SF4 family that form ring-shaped hexamers (16-18). The proportion of the heptameric form in T7gp4 is increased in the presence of dTDP, while its hexameric form is dominant in the presence of dTTP. Therefore, mutants that have mutations in the γ-phosphate interacting residues are unable to switch from the heptamer to the hexamer. In addition, the heptamer in T7gp4 cannot bind to either ssDNA or dsDNA, showing it is not a biologically active form (16). However, the presence of ssDNA shifts the equilibrium to the hexamer exclusively. Therefore, Richardson and coworkers have suggested a ring-opening model in which one protomer of a heptamer is released in order to load a hexameric form of T7 DNA helicase onto ssDNA (16). Interestingly, the ratio of heptamers to hexmers in the mitochondrial replicative DNA helicase may be independent of NTP binding and appears to be influenced by ionic strength (17). The human mtDNA helicase exists mostly as a heptameric form in 100 mM NaCl with cofactors such as Mg^{2+} and ATPγS,

and the protein is largely a hexameric form under high salt conditions (330 mM of NaCl) (17).

Three dimensional (3D) structural studies have been pursued for T7gp4, mostly by X-ray crystallography: ΔNTD (residues 241-566: hexamer) (13), ΔZBD (residues 63-566: heptamer) (18), ΔCTD (residues 1-255: monomer) (10). These 3D structures have demonstrated that the CTDs of each protomer form a compact, closed ring and that the NTDs locate on the top of the CTDs of its neighbor protomer, building a two-layer ring. These overall structures including intersubunit contacts do not differ significantly between a hexamer and a heptamer (18). Although a model of the full-length helicase after examination by EM and small angle X-ray scattering has been reported, the ZBD of the model relied largely on homology modeling (1). To investigate a full-length mtDNA helicase, in particular, considering the structure of its ZBD, we first have pursued 2D-NS-EM with the aid of biochemical analyses such as chemical crosslinking with and without affinity chromatography, and GraFix for the full-length mtDNA helicase. Then, a ZBD-lacking mtDNA helicase was prepared and analyzed by 2D-NS-EM. All approaches showed that the human mtDNA helicase and its ZBD-deleted variant exhibit heterogeneity in oligomeric state. Moreover, through the 2D-NS-EM, putative intersubunit interactions between the zinc binding-like domain and the RNA polymerase-like domain in the N-terminal domain were observed, and the 2D-NS-EM images of the ZBD-lacking mtDNA helicase showed that the ZBD imparts structural heterogeneity that may relate to its as-yet undiscovered functionality.

MATERIALS AND METHODS

Overexpression and purification of human mtDNA helicase

N- and C-terminally hexahistidine (His)-tagged human mtDNA helicase was expressed in *Spodoptera frugiperda* cells and purified to near homogeneity, as described in Rosado-Ruiz *et al.* (19). The previous study (17) demonstrated the placement of the tag in N-and C-terminally tagged helicase does not affect the results of stability, oligomerization property, chemical cross-linking, gel filtration and electron microscopy.

Crosslinking analysis of human mtDNA helicase

His-tagged human mtDNA helicase (1 μg, 0.05 μM as hexamer) was preincubated in a reaction buffer (50 mM HEPES, pH 7.5, 100 mM NaCl, 4 mM $MgCl_2$,2 mM ATPγS 5 mM β-mercaptoethanol) for 15 min at 21°C. Then, indicated amount of freshly made crosslinking agents such as dimethyl 3,3' dithiobispropionimidate-2HCl (DTBP) (PIERES) or glutaraldehyde (Sigma) was added for 30 min at 21°C in total 50 μl of reaction mixture in order to crosslink oligomers. The reactions were quenched with 200 μl of 1M Tris-HCl, pH 8.0 and precipitated with trichloroacetic acid using 1μg of cytochrome *c* as a carrier. For *in vitro* column crosslinking, the purified His-tagged human mtDNA helicase (0.5 mg, 2.3 μM as a hexamer) was loaded onto 0.5 ml of Ni-NTA resin which preincubated equilibration buffer (50 mM HEPES, pH 7.5, 500 mM NaCl, 10% glycerol, 5 mM β-mercaptoethanol). After 20 column volume (CV) of washing with wash buffer (50 mM HEPES, pH 7.5, 500 mM NaCl, 50 mM imidazole, 10% glycerol, 5mM β-mercaptoethanol), cross-linking was performed with 3 CV of 9 mM DTBP on the column using gravity flow, followed by 10 CV of 500 mM Tris-HCl, pH 8.0 buffer to quench remaining DTBP. Elution was done with 250 mM imidazole. Cross-linked products were

separated in 3-7% SDS-polyacrylamide gels. Proteins were analyzed by Coomassie staining or immunoblotting.

GraFix analysis of human mtDNA helicase

GraFix was performed based on analytical velocity sedimentation by combining 12-30% glycerol gradient with 0-0.15% glutaraldehyde gradient, as described in Rosado-Ruiz *et al.* (19).Briefly, His-tagged human mtDNA helicase (1 μg, 2.3 nM as a hexamer) was layered onto preformed 12–30% glycerol and 0-0.15% glutaraldehyde gradients (11 ml) containing 50 mM HEPES, pH 8.0, 330 or 100 mM NaCl, 1 mM phenylmethylsulfonyl fluoride, 10 mM sodium metabisulfite, 2 μg/ml leupeptin, and 5 mM β-mercaptoethanol. If helicase is under low ionic strength (100 mM NaCl), preincubation was performed for 15 min at 21°C in the presence of 0.02% (v/v) *n*-dodecyl β-D-maltoside, 4 mM $MgCl_2$ and 2 mM ATPγS. Centrifugation was at 37,000 rpm for 15 h at 4°C in a Beckman SW40 rotor. Fractions were analyzed by SDS-PAGE followed by silver staining or immunoblotting.

Protein immunoblotting

His-tagged human mtDNA helicase was separated by SDS-PAGE and transferred to nitrocellulose membranes (GE healthcare). The membranes were pre-incubated with 5 % w/v skim milk in a TBST buffer (20 mM Tris-HCl, pH 7.5, 150 mM NaCl, and 0.05 % v/v Tween 20), followed by 3 hours incubation with anti-His antibody (1:5000, in TBST with 1% skim milk) (BD Pharmingen) or anti-*Dm* mtDNA helicase antibody (1:500, in TBST with 1 % skim milk) (20). After washing three times for 10 min each, membranes were incubated with horseradish peroxidase-conjugated goat anti-rabbit IgG (1:5000, in TBST with 1 % skim milk) (Bio-Rad), or

alkaline phosphatase-conjugated goat anti-rabbit IgG (1:5000, in TBST with 1 % skim milk) (Bio-Rad), and the probed protein were developed by using ECL Western blotting reagent (Perkin Elmers) or by precipitating nitro blue tetrazolium (330 ug/ml) (Sigma) and 5-bromo-4-chloro-3-indolyl phosphate (165 ug/ml) (Sigma), respectively.

Two-dimensional negative stain electron microscopy and image processing

Electon microscopy and data processing was performed by collaborators Drs. Jose Maria Carazo and Ana Lucia Alvarez in Centro Nacional de Biotecnología Consejo Superior de Investigaciones Cientificas (CSIC) in Spain. Briefly, samples were adsorbed directly onto carbon/collodion-coated copper grids. After negative staining, the samples were observed in a JEOL JEM-1011 electron microscope. Micrographs were taken at a magnification of 50,000X. Image processing analysis was carried by using a two-dimensional reference free class average classification (CL2D) algorithm.

RESULTS

In vitro crosslinking of the human mtDNA helicase shows several different oligomeric forms.

In vitro crosslinking was performed to make oligomers of the human mtDNA helicase stable in unfavorable buffering conditions such as low salt (~100 mM NaCl) and low temperature (~4ºC). In order to crosslink the oligomeric forms of the human mtDNA helicase, I chose DTBP as a chemical crosslinking reagent. Because it is water soluble and membrane permeable, it can be used for *in vivo* crosslinking of intact mitochondria as well as for *in vitro* crosslinking. A purified recombinant human mtDNA helicase showed crosslinked dimer species and oligomeric forms by immunoblot analysis (Fig. 3 A).

On-column crosslinking of a recombinant His-tagged human mtDNA helicase showed several crosslinked oligomeric species ranging from a dimer to a hexamer (Fig. 3 B) although the hexameric form was largely absent. Crosslinked hexamers likely lost protomers during SDS-PAGE because the central disulfide bond of DTBP can be cleaved with reducing agents (21). In this approach, the helicase was bound on Ni-NTA resin stably and tightly during the loading, washing, crosslinking and quenching steps, and eluted as crosslinked forms. This data suggests that the on-column crosslinking method could be used for screening for partner proteins of a His-tagged mtDNA helicase from cell extracts or mitochondrial extracts because the Ni-NTA resin retains stable oligomeric mtDNA helicase and creates space for prey proteins to access the helicase by separating helicase oligomer molecules on the resin.

GraFix shows that the oligomeric states of human mtDNA helicase at high ionic strength (330 mM NaCl) are a mixture of hexamers and heptamers.

To prepare oligomers of a purified human mtDNA helicase for EM, I used the GraFix

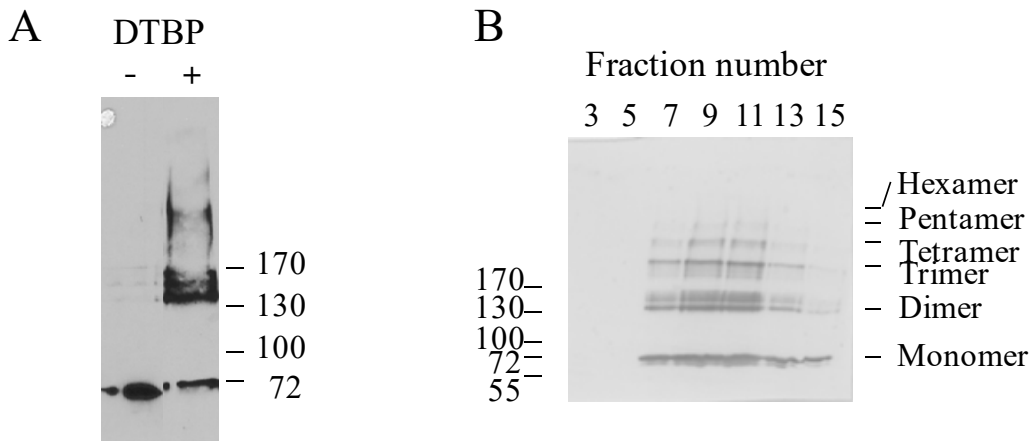

Figure 3. ***In vitro*** **DTBP crosslinking of purified human mtDNA helicase A. DTBP crosslinking B. On-column crosslinking** A His-tagged human mtDNA helicase was crosslinked on a Ni-NTA column. 0.5 mg (2.3 μM as a hexamer) of helicase protein was loaded on 0.5 ml of Ni-NTA resin. After 20 CV of washing, cross-linking was performed with 3 CV of 9 mM DTBP on the column by using gravity flow, followed by 10 CV of 500 mM Tris-HCl, pH 8.0 buffer to quench the remaining DTBP. Elution was done with 250 mM imidazole. Eluted helicase protein exhibited its oligomeric forms in immunoblot after 3-7% SDS-PAGE.

technique (22,23), in which a protein complex is purified by density gradient sedimentation and undergoes a weak chemical crosslinking at the same time. As a crosslinking reagent, a gradient of 0–0.15 % glutaraldehyde was used. The peak fraction of the GraFix of the human mtDNA helicase in high ionic strength (330 mM NaCl) showed apparent hexamer and heptamer bands on a silver-stained 3-7% SDS-polyacrylamide gel (Fig. 4 A). The ratio of the hexamer to the heptamer in the peak fractions (fraction 10-13) was ~ 1:1. The result was not in agreement with the previously published 2D-NS-EM data (17) in which the hexameric form is dominant over the heptameric form under high ionic strength. However, clear images of oligomeric states from the peak fractions (fraction 10-13) of the high salt GraFix of the human mtDNA helicase could not be collected by 2D-NS-EM (Fig. 5) because of protein heterogeneity resulting from protein contaminants of ~70 kDa (Fig. 4 A) and over-crosslinked proteins that were detected on the top of both the silver stained gel (Fig. 4 A) and immunoblot (Fig. 4 B).

Two-dimensional negative stain EM images of the non-crosslinked human mtDNA helicase at high ionic strength (330 mM NaCl) show a mixture of hexamers and heptamers and a few octamers.

To evaluate equilibrium between hexamers and heptamers of the human mtDNA helicase under different ionic strength conditions, experiments were conducted as described in a previous publication (17). Purified full-length human mtDNA helicase was prepared and observed under 2D-NS-EM (Fig. 6 A), and the resulting images were of sufficient resolution to show the elongated flexible arms (Fig. 6 (B-D)) that had not been detected earlier (17). The non-crosslinked human mtDNA helicase at high ionic strength was observed as hexamers, heptamers and a few octamers, corresponding to the high salt GraFix data (Fig. 4). Contrary to the data of

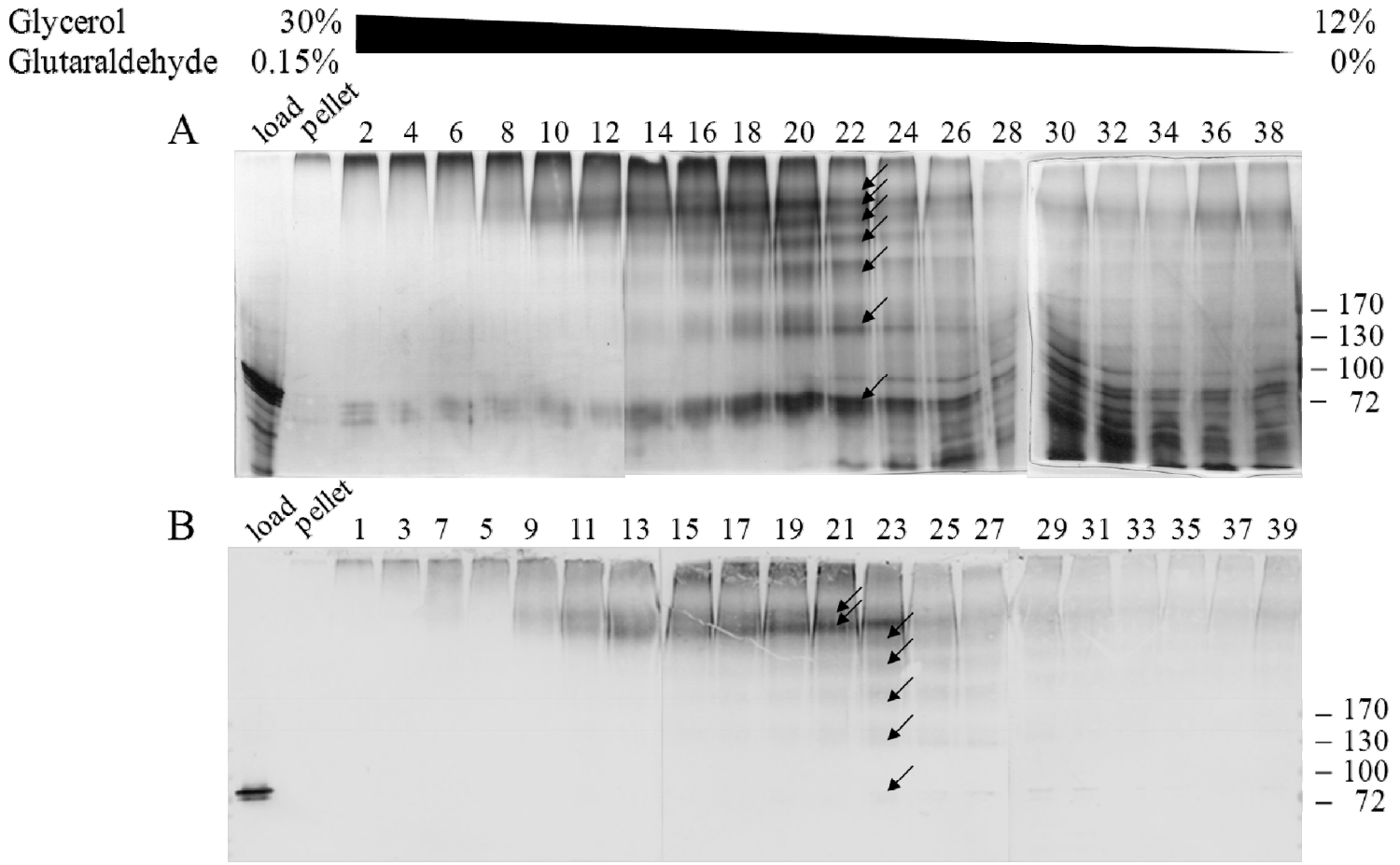

Figure 4. **Fraction analysis of the high salt GraFix of the human mtDNA helicase** The high salt (330 mM NaCl) GraFix of the Ni-NTA purified human mtDNA helicase was performed with 0 - 0.15% glutaraldehyde in a 12~30% glycerol gradient. Fractions were analyzed by 3-7% SDS-PAGE and visualized by silver-stain (A) or immunoblot (B). Hexamers and heptamers were detected in a main peak (fractions 10-13). Arrows indicate all seven oligomeric states. Some species result from incompletely crosslinked proteins under the denaturing condition of SDS-PAGE.

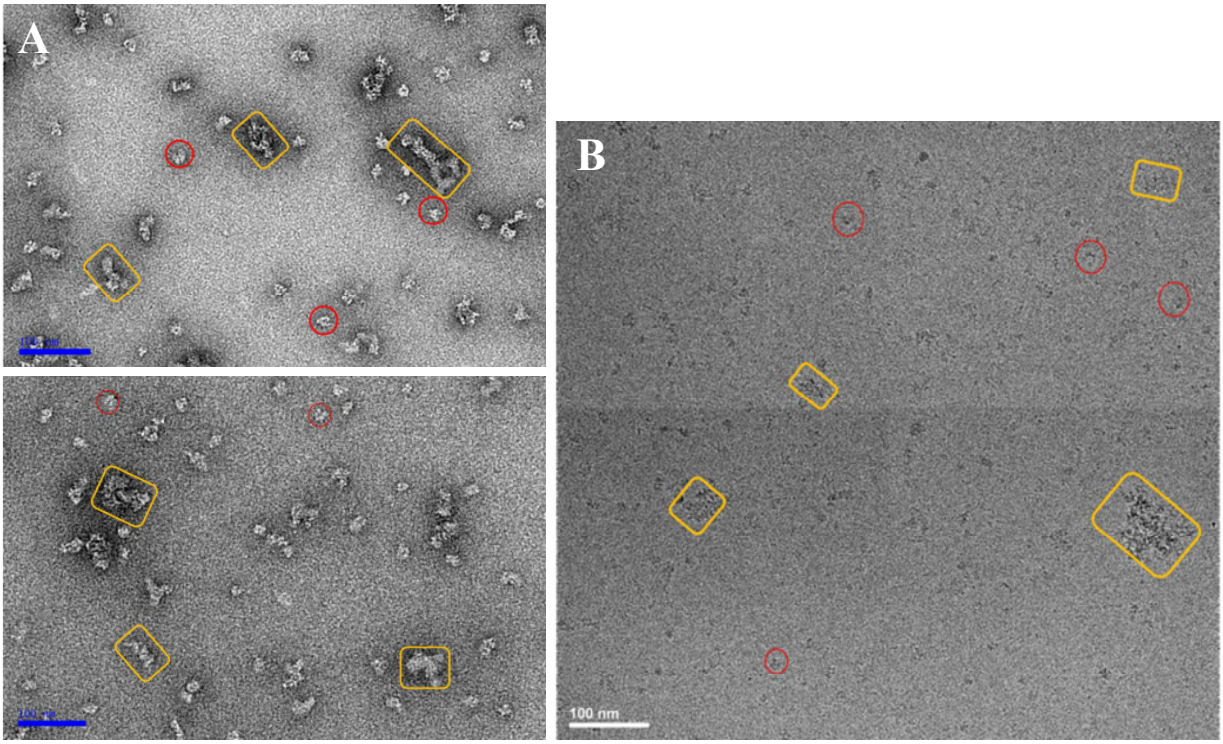

Figure 5. **Electron micrographs of the crosslinked human mtDNA helicase at 330 mM NaCl A.** Micrographs of the negative stained human mtDNA helicase under 8% glycerol (upper panel) and 22% glycerol (lower panel) show mixture of individual oligomers (red circles) and random aggregates (yellow rectangles). **B.** A micrograph of unstained cryo-EM of the human mtDNA helicase. This protein was prepared by the GraFix procedure shown in Figure 3. Fractions 8 and 9 were used for these observations. Data was produced by collaborators, Ana Lucia Alvarez and Jose Maria Carazo.

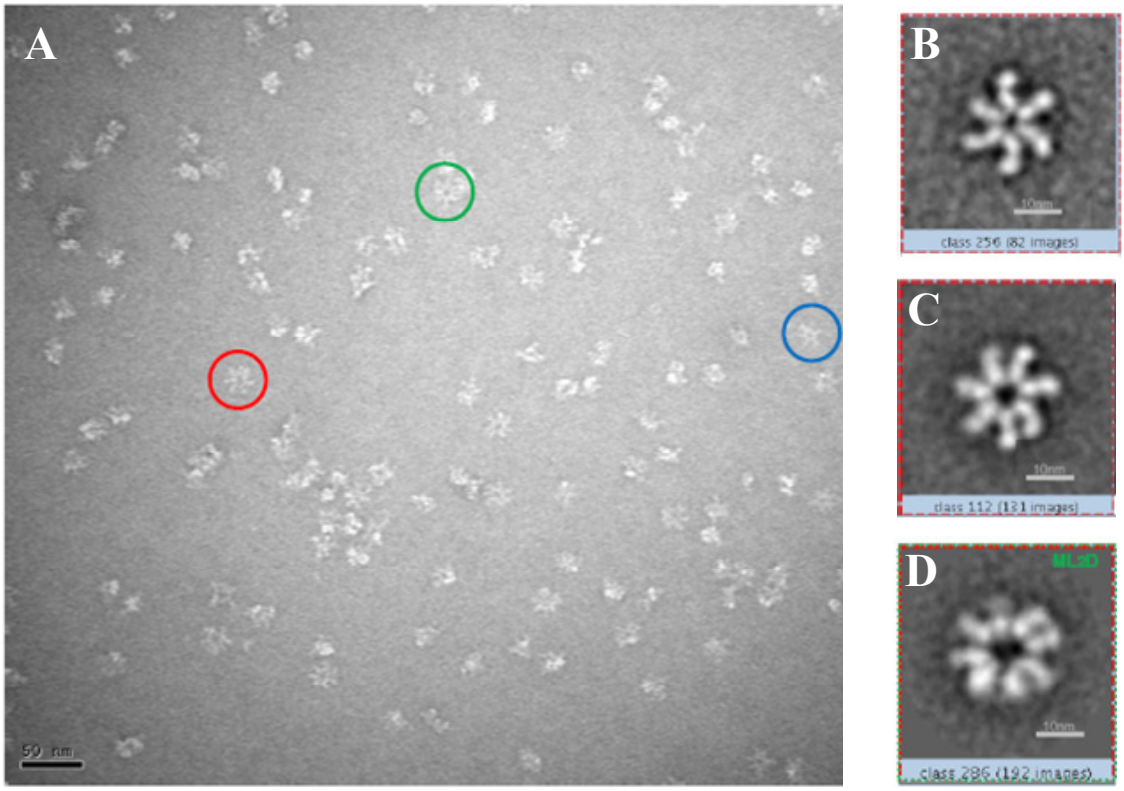

Figure 6. **Electron micrograph and representative average images of the human mtDNA helicase at 330 mM NaCl A.** A micrograph area of the negative stained human mtDNA helicase has hexamers (blue circles), heptamers (red circles) and optamers (green circles). A representative average images of **B.** a hexamer, **C.** a heptamer and **D.** an octamer. Data was produced by collaborators, Ana Lucia Alvarez and Jose Maria Carazo.

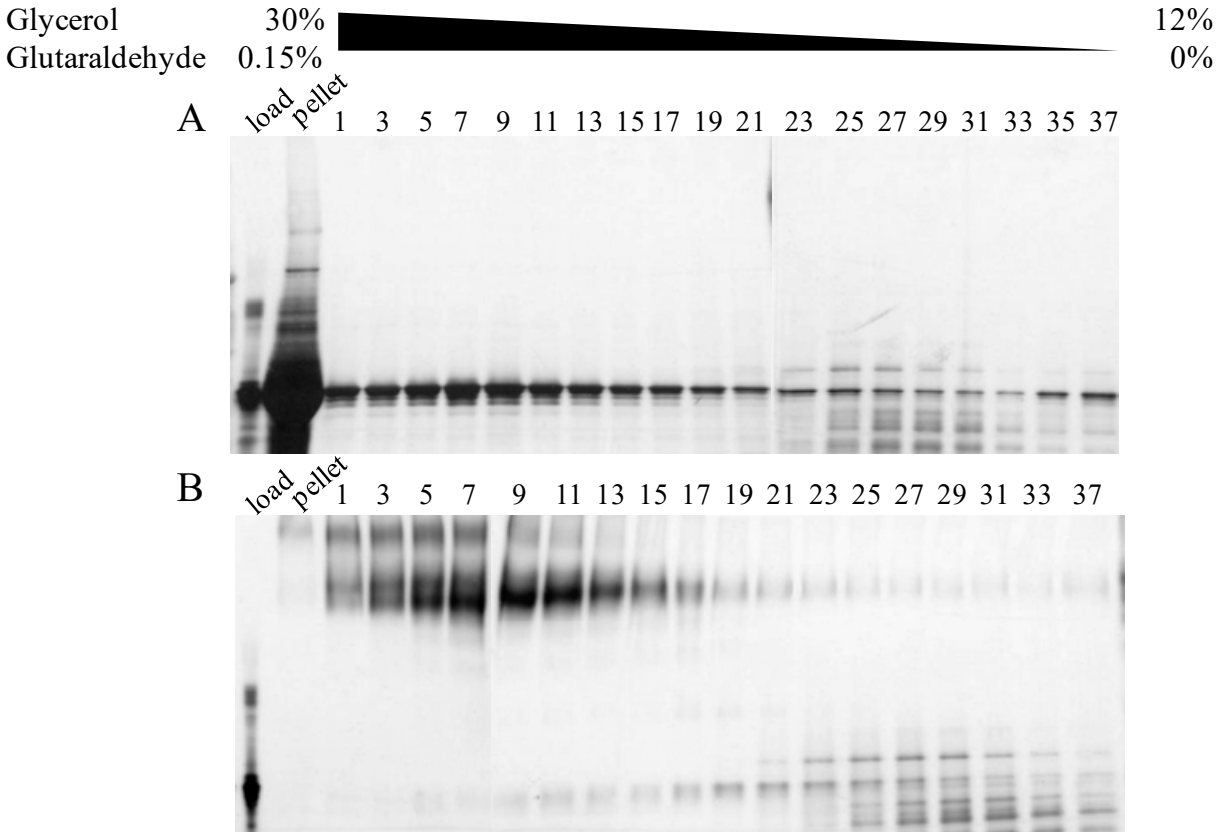

Figure 7. **Fraction analysis of velocity sedimentation (A) and GraFix (B) of the human mtDNA helicase under low salt** A low salt (100 mM NaCl) GraFix of Ni-NTA purified human mtDNA helicase was performed with 0 - 0.15% glutaraldehyde in a 12~30% glycerol gradient, and velocity sedimentation was performed without glutaraldehyde. To prevent aggregation and increase solubility of the human mtDNA helicase under low salt conditions, cofactors (4 mM of Mg^{2+} and 2 mM of ATP γS) and a detergent (0.02 % of n-dodecyl β-D-maltoside) were added, and sedimentation was performed at 17 ºC. Fractions were analyzed by 3-7% SDS-PAGE and visualized by silver staining. Hexamers and heptamers were detected in the main peaks (Fractions 3~11). Dimers of oligomers are detected in the peak fractions of the GraFix. For the 2D-NS-EM, the pooled peaks were concentrated and diluted to reduce glycerol concentration in the EM buffer (50 mM HEPES pH8.0, 100 mM NaCl, 4 mM $MgCl_2$, 2 mM ATP γS, 0.004 % of n-dodecyl β-D-maltoside, 20 mM arginine, 2 mM β-mercaptoethanol, 2 mM sodium metabissulfite, 0.4 ug/ml leupeptin, 0.2 mM PMSF, and residual glyceraldehyde.)

Ziebarth *et al*. (17), the most abundant oligomeric state in 2D-NS-EM images at high ionic strength was a heptamer (50 %), suggesting that ionic strength alone is not a determinant of oligomeric state.

Multimers of oligomers of the human mtDNA helicase are observed under conditions of physiological ionic strength by Grafix and 2D-NS-EM.

To investigate oligomeric states of the human mtDNA helicase under conditions of physiological ionic strength, low salt GraFix and velocity sedimentation were performed at 100 mM NaCl in the presence of cofactors (4 mM $MgCl_2$ and 2 mM ATPγS) and a non-ionic detergent (0.02% n-dodecyl β-D-maltoside). Heptameric and hexameric bands detected in the peak fractions of the low salt GraFix (Fig. 7 B) were similar to those observed in the peak of the high salt GraFix (Fig. 4). Compared to the high salt data, the low salt fractions on the silver-stained SDS-polyacrylamide gel (Fig. 7 B) showed increased levels of the high molecular weight species, which might be any form of dimeric oligomers such as a double hexamer or a double heptamer and/ or a mixture of a hexamer and a heptamer. However, the contaminants near ~70 kDa in the peak fractions were decreased (Fig. 7 B). The non-ionic detergent (n-dodecyl β-D-maltoside) in the low salt GraFix likely inhibits possible non-ionic interactions between helicase oligomers and the ~70 kDa contaminants. The 2D-NS-EM data showed that both crosslinked and non-crosslinked human mtDNA helicases exist predominantly as aggregate-like particles under conditions of low ionic strength (100 mM NaCl). They were also found as hexamer- or heptamer-like particles, but the flexible arms that were observed under high ionic strength were not detected clearly at low ionic strength (Fig. 8 A, B). When the protein was crosslinked by the GraFix, the arms appeared more constricted, making the states of the oligomeric particles

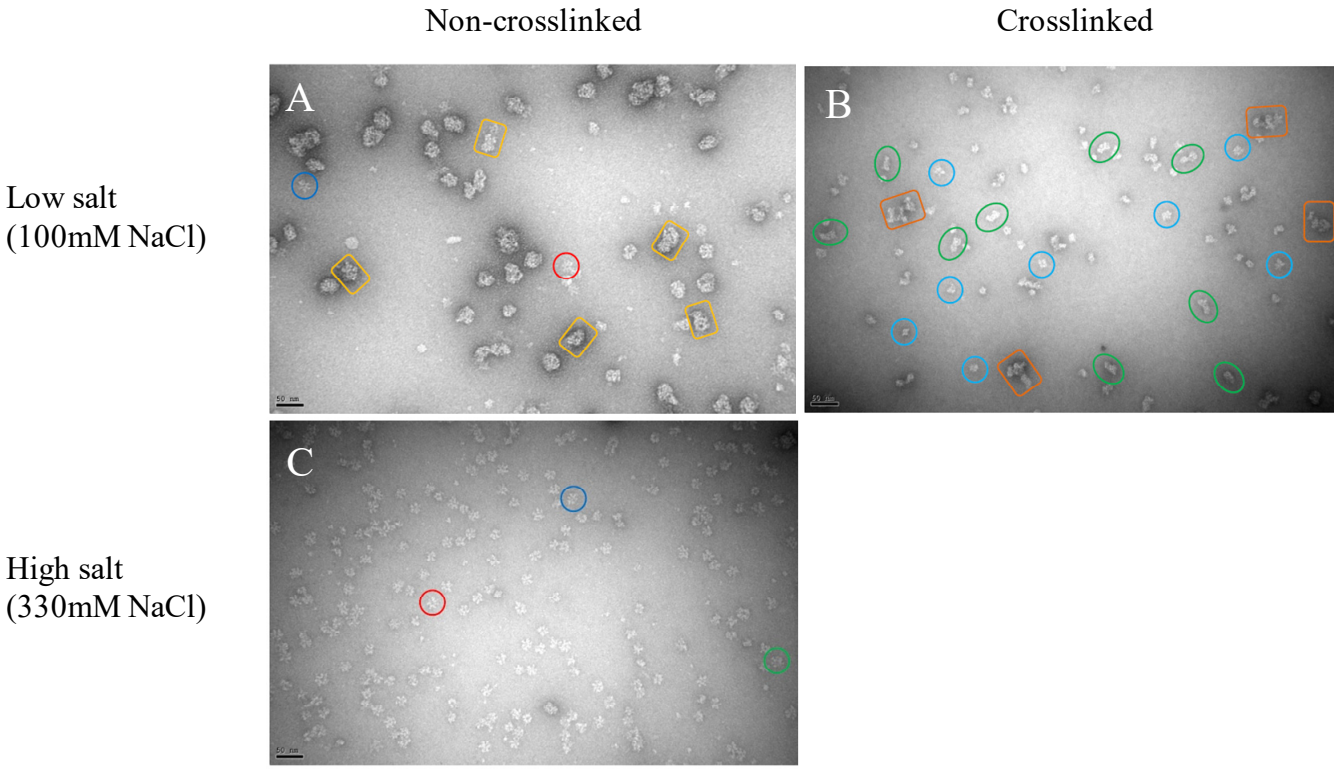

Figure 8. **Electron micrographic images of human mtDNA helicase at 100 mM NaCl** The mtDNA helicase from peak fractions of velocity sedimentation without crosslinking (A) and GraFix with crosslinking (B) was observed by 2D-NS-EM. The electron micrographic image (C) was obtained by three-fold dilution of sample in (A). Particles in blue circles, green ellipses and orange squares are observed by EM as single oligomers, double oligomers and aggregates, respectively. Particles in red circles were seen as heptamers. The bar in each image represents 50 µm. Data was produced by collaborators, Ana Lucia Alvarez and Jose Maria Carazo.

indistinguishable (Fig. 8 B). The aggregate-like particles and dimers of oligomers were observed largely in the crosslinked human mtDNA helicase under low ionic strength (Fig. 8 B); the dimers of oligomers were also found in the low salt GraFix (Fig. 7 B). Interestingly, the aggregate-like particles of the non-crosslinked human mtDNA helicase under low ionic strength were dissociable when they were diluted in high salt buffer (330 mM NaCl), suggesting the aggregate was not in a denatured state (Fig. 8 C). Moreover, the extended arms reappear after the elevation of salt concentration. The finding that multimeric oligomers under physiological ionic strength are converted to single oligomers at higher ionic strength opens the possibility that the human mtDNA helicase might use a double oligomer state to load onto DNA in the absence of a helicase loader.

Reference-free class average classification (CL2D) of the full-length mtDNA helicase shows conformational diversity under high ionic strength.

A total of 14,500 top view particles of the full-length mtDNA helicase were extracted from electron micrographs of 2D-NS-EM under the high ionic strength conditions. To align and classify the images, 2D clustering was used (Fig. 9). CL2D showed structural heterogeneity of different oligomers that consist of particles with 6-, 7-, and 8-fold symmetry in 45%, 50% and 5% of the total images, respectively (Fig. 9 and Fig. 10 A). The diameters of the oligomers were ~12.5 nm, ~13.5 nm, and ~14.5 nm, and the average diameters in these central channels were 3 nm, 4 nm, and 6 nm, respectively. All three channels are large enough to accommodate dsDNA as well as ssDNA. Completely extended particles in which all of the protomers extend out from the center cavity constituted 15% of total images (Fig. 10 A), and compact particles in which all arms were bent toward the center made up 35%. The majority showed particles with a mixture of

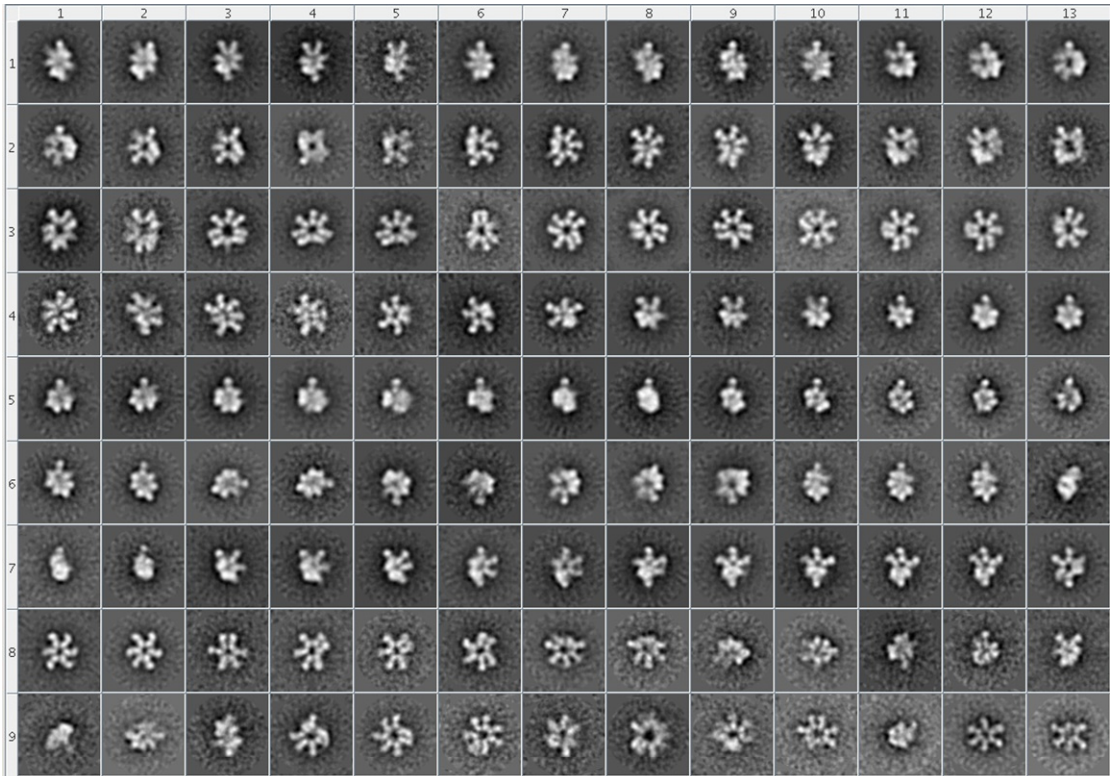

Figure 9. **Reference free class average classification (CL2D) of 14,500 particle images of the full-length mtDNA helicase at 330 mM NaCl** Data was produced by collaborators, Ana Lucia Alvarez and Jose Maria Carazo.

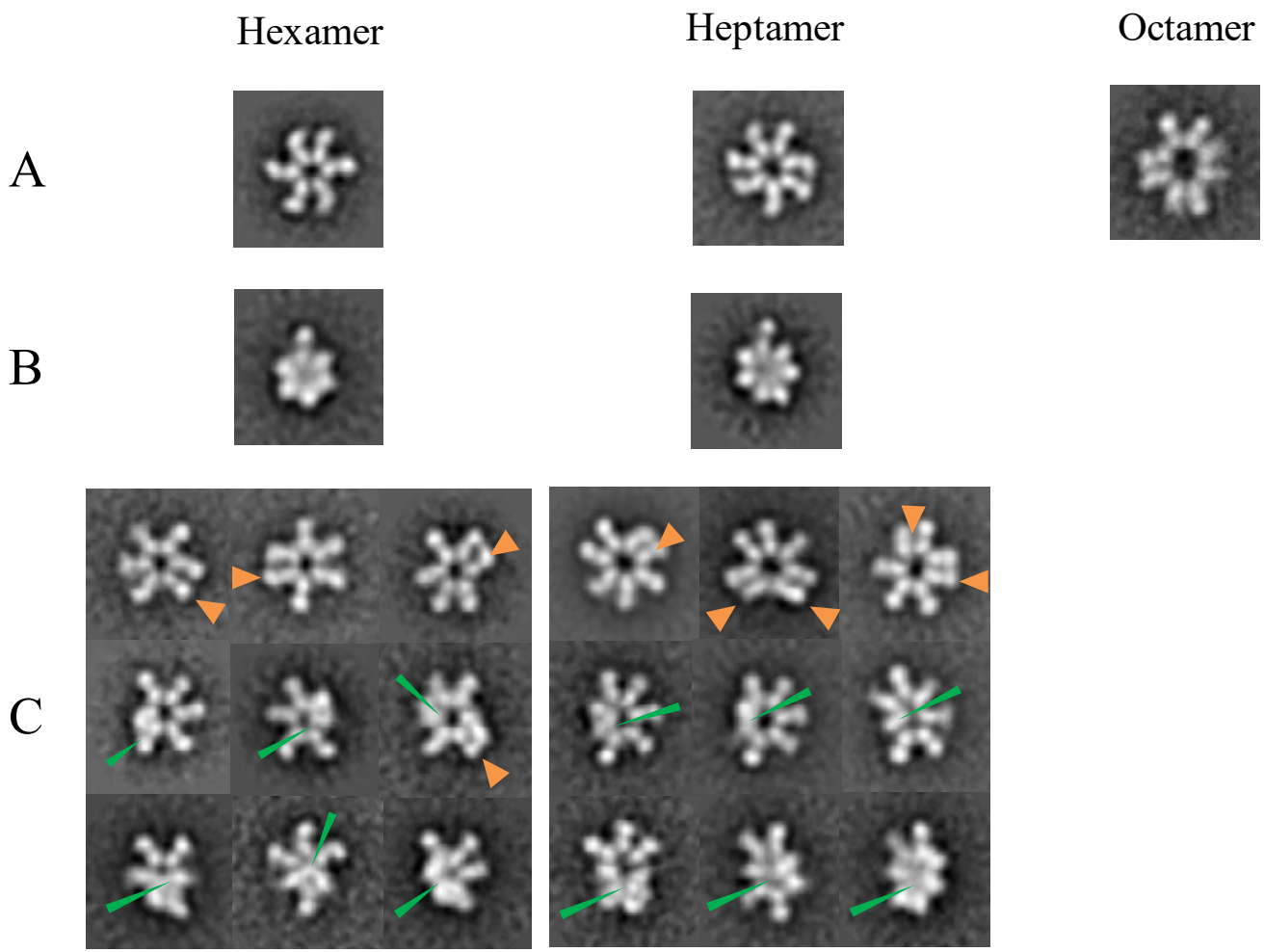

Figure 10. **Representative 2D-NS-EM images of the wild type mtDNA helicase at 330 mM NaCl A.** Representative images of different types of oligomers: a hexamer, a heptamer, and an octamer **B.** One-arm-extended compact particles **C.** Various conformational states in extended particles are caused by "close pairs" that are indicated by orange arrowheads and by "bent arms" that are indicated by green arrowheads. Data was produced by collaborators, Ana Lucia Alvarez and Jose Maria Carazo.

extended and compact protomers, corresponding to 50% of total images. Interestingly, ~ 20% of the particles showed a one-arm-extended conformation in which all other arms were retracted (Fig. 10 B). This structural predisposition to have one flexible arm might be related to the initiation step of a ring-opening mechanism that has been demonstrated with T7gp4 (24). Initiation of ring-opening in this mechanism is facilitated by the binding of DNA to one NTD of T7gp4, resulting in conformational change to open the ring. The one-arm-extended form in the mtDNA helicase (Fig. 10 B) might be the structural conformation to search for DNA before loading on DNA. In addition, open-rings in which a gap was found between two protomers were also detected among the total images (data not shown). These observations support a self-directed ring-opening mechanism for DNA loading by the mtDNA helicase.

Most of 2D class images in the wild type showed asymmetry. These asymmetrical structures were caused by angular movements of extended arms and/ or bending of the arms (Figure 10 C), implying interdomain interactions. The angular movements of the arms formed close pairs of the extended arms, likely resulting from an interaction between the same domains of neighbor protomers such as RPD-RPD and ZBD-ZBD. Bending could result from intrasubunit interactions such as ZBD-RPD or RPD (or ZBD)-CTD interactions within a protomer. Intersubunit interactions may also result from interaction between two domains of different protomers. However, the types of interactions could not be resolved by the 2D image analysis, indicating the need for higher resolution by cryo-electron microscopy.

The zinc binding-like domain enables the human mtDNA helicase to assume diverse conformations.

It is possible that the various conformations observed in the asymmetric images of the

full-length mtDNA helicase are caused by random movements rather than by specific inter- or intra-subunit interactions. To evaluate this possibility, we prepared a truncated variant of mtDNA helicase lacking the ZBD (ΔZBD: E147 - K684). A total of 9,991 particles from a negative stained ΔZBD sample were used for reference-free 2D image classification (Fig. 11). Overall features were similar to the features of a full-length helicase including a mixture of several oligomers (Fig. 12 A), presence of compact and extended particles (Fig. 11 and Fig. 12), and a one-arm-extended conformation (Fig. 12 B). However, in images of the ΔZBD the asymmetric conformational variety as compared to the full-length helicase was significantly reduced and the RPDs in each particle were isolated from one another, suggesting it is the ZBD that enables the mtDNA helicase to acquire a wide range of conformations. The presence of pentamers is also an interesting difference from the full-length sample. Pentamers of mtDNA helicase have not been reported to date including in the full-length sample in our study. The composition of oligomers in the ΔZBD was 10% pentamers, 50% hexamers, 30% heptamers and 10% octamers. The percentage of hexamers did not change significantly, but the percentage of heptamers decreased considerably, resulting in increase of the percentages of pentamers and octamers, as compared to percentages of oligomers in the full-length mtDNA helicase. In addition, the percentage of compact particles also increased to ~70% in ΔZBD from 35% in the full-length helicase. In summary, the loss of ZBD tends to render the human mtDNA helicase predominantly hexameric, symmetric and compact, suggesting that the ZBD imparts the structural flexibility in the human mtDNA helicase.

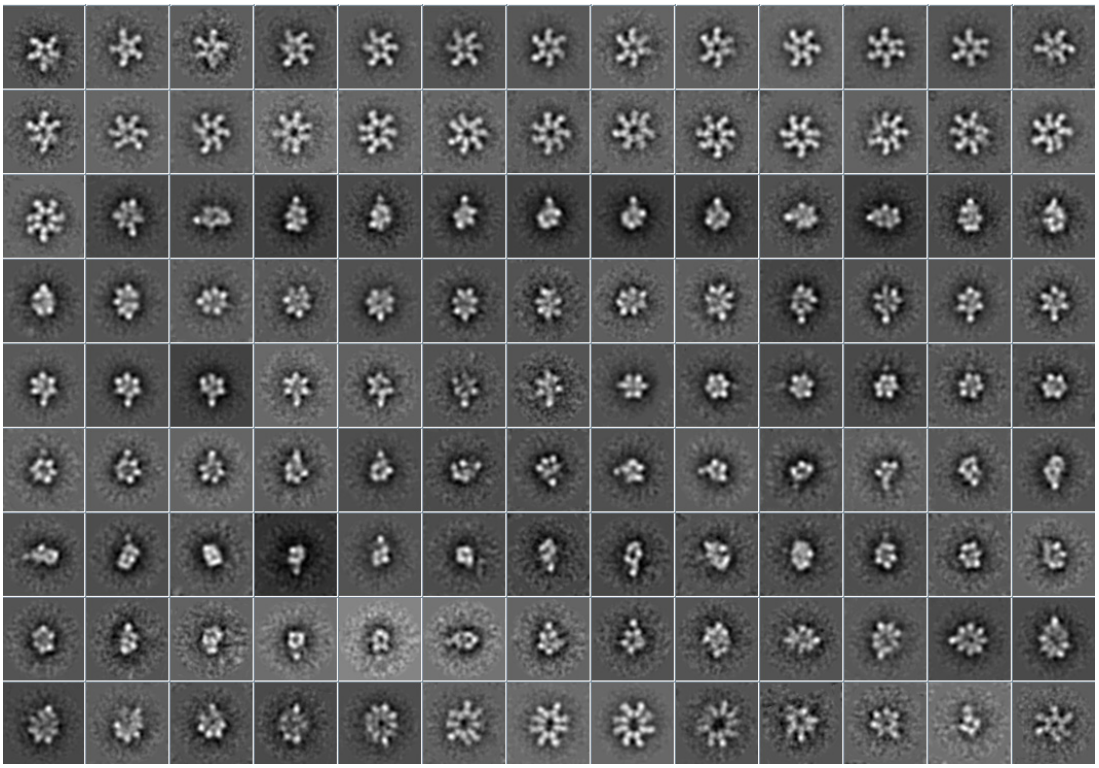

Figure 11. **Reference free class average classification (CL2D) of 9,991 particle images of the ZBD-lacking mtDNA helicase (ΔZBD) at 330 mM NaCl** Data was produced by collaborators, Ana Lucia Alvarez and Jose Maria Carazo.

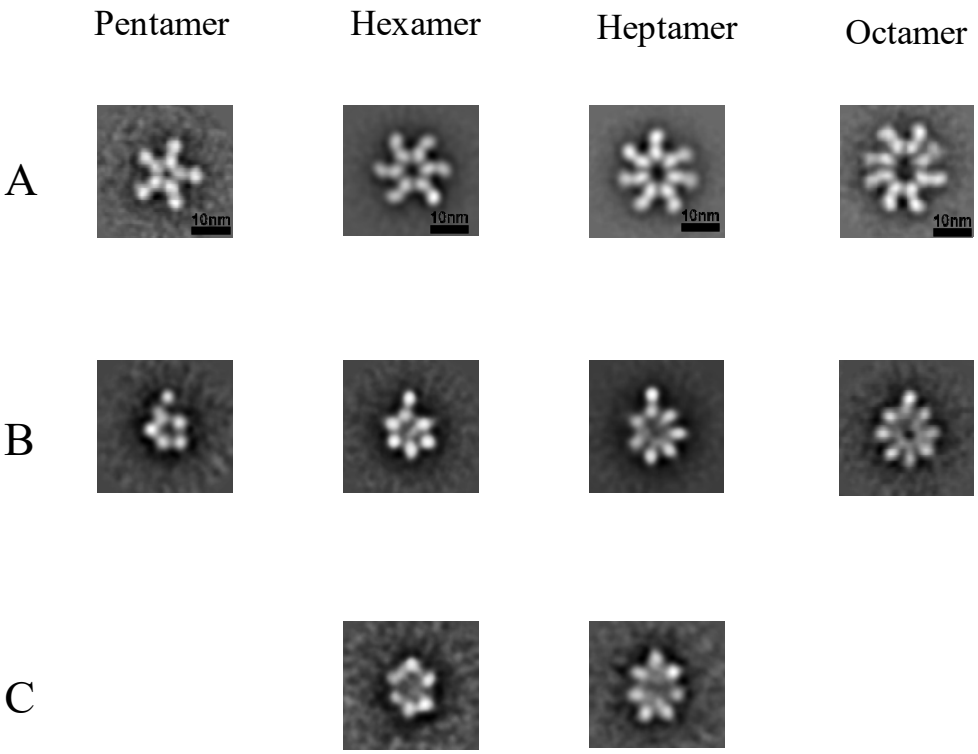

Figure 12. R**epresentative NS-EM 2D images of the ZBD-lacking mtDNA helicase (ΔZBD) at 250 mM NaCl A.** Representation of different types of oligomers: a pentamer, a hexamer, a heptamer and an octamer **B.** One-arm-extended compacted particles **C.** Completely compacted particles Data was produced by collaborators, Ana Lucia Alvarez and Jose Maria Carazo.

DISCUSSION

A ring-shaped replicative helicase often has several different oligomeric states: hexameric and heptameric forms for T7gp4 (16) and the human mtDNA helicase (17), and hexameric to octameric forms for *Mt*MCM (25). It is thought to be caused by their flexible subunit interfaces (18). The functionally active form of these replicative helicases is the hexameric form, while the heptameric form has been detected as an equilibrium partner of the hexameric form (16-18,25). In our study, oligomeric states of the human mitochondrial replicative DNA helicase were detected largely as hexamers or heptamers, ranging from pentamers to octamers by both biochemical and microscopic experiments. However, the biological role of non-hexameric forms of the mtDNA helicase remains uncertain.

The heptamer of T7gp4 is considered an intermediate during the hexamer formation (16) in the ring-opening mechanism that has been proposed based on kinetic data (24). Postulating this ring-opening model, Richardson and coworkers proposed a self-loading model in which a heptamer loses one protomer when it binds to ssDNA. The heptamer of the mtDNA helicase is likely to play the same role in loading itself onto DNA without a helicase loader. Several biochemical findings support this idea. The mtDNA helicase can load itself onto closed circular DNA (26) as for T7gp4 (27), a helicase loader has not been identified in either mitochondria or bacteriophage T7, and the mtDNA helicase binds ssDNA within its NTD (12,28), an important step in the ring-opening mechanism of T7gp4 (24). The open-ring structures and one-arm-extended structures of the mtDNA helicase that have been observed under 2D-NS-EM support the self-directed ring-opening model. We speculate the one-arm-extended structure is the structural conformation used to search for ssDNA.

The equilibrium ratio of heptamers to hexamers is also important for explaining the self-

directed ring-opening model. In T7gp4, the presence of ssDNA and dTTP switches the equilibrium exclusively from heptamers to hexamers (16). In the mtDNA helicase, the ratio may depend on the ionic strength instead of the type of nucleotide (17). In this study, the oligomeric states of the human mtDNA helicase in a high ionic strength condition (330 mM) are mainly a mixture of hexamers and heptamers in both GraFix and 2D-NS-EM, while the hexamer is the dominant oligomeric form at the same high ionic strength condition in previous published research (17). These results imply that equilibrium changes of the oligomeric states of the human mtDNA helicase might not be dependent only on ionic strength. Temperature and concentration could affect its dynamic states. *Mt*MCM, a ring-shaped archaeal replicative DNA helicase, prefers the hexameric form to other oligomeric forms with increased temperature and ionic strength and reduced protein concentration (29). Thus, further investigation to identify a condition that switches the ratio of heptamers to hexamers of the mtDNA helicase might give an insight into the understanding of the ring-opening mechanism.

Another self-loading model for ring-shape helicases was proposed based on discovery of double hexameric forms. Double hexameric forms have been found in replicative helicases such as *Hp*DnaB (in bacteria), SV40 LTag (in virus), *Mt*MCM (in archaea) and Mcm2-7 (in yeast) (30,31). A structural study of the *Hp*DnaB double hexamer demonstrates that its dodecamer form is necessary for self-loading onto DNA (31). The dimeric oligomers we found in this study might provide an alternative manner for the mtDNA helicase to load onto DNA without a helicase loader under physiological conditions.

Our data demonstrates that the ZBD is the main domain that gives structural diversity to the mtDNA helicase. Without the ZBD, the mtDNA helicase exhibits mainly in symmetrical structures, showing limited inter-protomer interactions. A considerable increase in compact

particles in the ΔZBD is also observed, indicating that the ZBD contributes to open arms. Another propensity we observed in the ΔZBD is a decrease in the ratio of heptamers over the total oligomers. It decreases from 50% (wild type) to 30% (ΔZBD). This decrease is also found in T7gp4 by biochemical (32) and microscopic (18) experiments. In the EM data, the percentage of heptamers in the 56 kDa ZBD-lacking isomer of T7gp4 decreases to 5% as compared ~35% in the wild type form (18). Reduction of steric hindrance caused by the ZBD would be a possible explanation. Nevertheless, the various movements of the ZBD of T7gp4 are essential for primase activity; the ZBD cooperates with the RPD of the neighboring protomer in order to synthesize a primer and deliver it to T7gp5, the T7 DNA polymerase (33). Consequently, the highest rate of DNA synthesis is detected at an equimolar mixture of the full-length and 56 kDa protomers in T7gp4 (32). However, the biological meaning of ZBD-related interactions in the mtDNA helicase is most likely different from the roles in T7gp4 because the mtDNA helicase is not a primase. Biochemically, the ZBD of the human mtDNA helicase is not essential for its oligomerization or helicase activities (12); ZBD-lacking variants are able to unwind dsDNA, hydrolyze ATP and support DNA polymerase γ to synthesize DNA, although the efficiency is reduced. Thus, further study about the proposed role of the ZBD of mtDNA helicase in the self-directed ring-opening model could explain the diverse conformations caused by its flexible ZBD.

Sola and coworkers reported a 3D atomic model of human mtDNA helicase based on its structure observed from electron microscopy and small angle X-ray scattering (1), while we were researching the 3D structure of human mtDNA helicase by EM. The structural aspects that we found in high salt conditions, including coexistence of hexamers and heptamers, observations of open-rings, inter-or intra-subunit interactions in the NTD and structural flexibility in the ZBD were also observed by them. In their research, a higher ionic strength (1.5 M NaCl) was used in

the condition, and the ratio of hexmers to heptamers was 3:2, being prone to hexamers. As mentioned above, although the equilibrium ratio is likely to be decided not only by ionic strength, the higher ionic strength probably causes the equilibrium changes. The additives such as L-arginine, L-glutamate, and imidazole or lower pH (pH 6.5) in their buffers may also increase the ratio of hexamers and/ or solubility of the mtDNA helicase. However, octamers, pentamers and one-arm-expended structures that we observed were not reported by them. In addition, the structural dynamicity caused by the ZBD was corroborated clearly by our NS-EM images of the ZBD-lacking variant in addition to observations about the dynamic structure of the full-length mtDNA helicase using our NS-EM and their small angle X-ray scattering. To differentiate our research from theirs, the structure in the physiological condition should be pursued because the published structure is observed under extremely high ionic strength conditions. In particular, roles for multimers of oligomers, which was found in our low salt conditions, are valuable enough to warrant investigation. To overcome a problem of aggregation in low salt conditions, the additives and the lower buffer pH that Sola's group used might be helpful to increase protein solubility. Moreover, because Sola's group obtained cryo-EM images with relatively low resolution (12Å), they had to rely largely on their atomic model to explain the structure of the full-length mtDNA helicase. To the better quality of structures, research of domain-deleted variants and/ or individual domain structures by cryo-EM and X-ray crystallography, respectively will be necessary.

CONCLUSIONS

During last one decade, the mtDNA helicase have been investigated intensively, and recently, an EM-based atomic model was published, showing the structure of human mtDNA helicase (1). Our independent structural study of human mtDNA helicase found the same important features in high salt conditions such as heterogeneous oligomers, dynamic interactions between domains, and flexibility of the ZBD, but we observed exclusively more variable structures including heptamers, octamers and one-arm-extended structures that the other group did not report. Moreover, our research found several important structures such as open-ring structures, one-arm-extended structures and dimers of oligomers. These structures may explain the self-loading mechanism of the mtDNA helicase after biochemical or physiological experiments. Furthermore, the limited structural diversity of the ZBD-deleted demonstrates that the flexible ZBD causes conformational variety. The feature is likely to be necessary to capture ssDNA. Considering the published structure that is made under far distance of physiological ionic strength, we should continue to investigate structures in low salt conditions with an effort to overcome insolubility of the mtDNA helicase at low ionic strength. In addition, to obtain a high quality of molecular-scale structure of the mtDNA helicase, X-ray crystallography and cryo-EM will be employed with individual domains and domain-deleted mtDNA helicases, respectively.

BIBLIOGRAPHY

BIBLIOGRAPHY

1. Fernandez-Millan, P., Lazaro, M., Cansiz-Arda, S., Gerhold, J. M., Rajala, N., Schmitz, C. A., Silva-Espina, C., Gil, D., Bernado, P., Valle, M., Spelbrink, J. N., and Sola, M. (2015) The hexameric structure of the human mitochondrial replicative helicase Twinkle. *Nucleic acids research* **43**, 4284-4295

2. Spelbrink, J. N., Li, F. Y., Tiranti, V., Nikali, K., Yuan, Q. P., Tariq, M., Wanrooij, S., Garrido, N., Comi, G., Morandi, L., Santoro, L., Toscano, A., Fabrizi, G. M., Somer, H., Croxen, R., Beeson, D., Poulton, J., Suomalainen, A., Jacobs, H. T., Zeviani, M., and Larsson, C. (2001) Human mitochondrial DNA deletions associated with mutations in the gene encoding Twinkle, a phage T7 gene 4-like protein localized in mitochondria. *Nature genetics* **28**, 223-231

3. Copeland, W. C. (2008) Inherited mitochondrial diseases of DNA replication. *Annual review of medicine* **59**, 131-146

4. Tyynismaa, H., Sembongi, H., Bokori-Brown, M., Granycome, C., Ashley, N., Poulton, J., Jalanko, A., Spelbrink, J. N., Holt, I. J., and Suomalainen, A. (2004) Twinkle helicase is essential for mtDNA maintenance and regulates mtDNA copy number. *Human molecular genetics* **13**, 3219-3227

5. Tyynismaa, H., Mjosund, K. P., Wanrooij, S., Lappalainen, I., Ylikallio, E., Jalanko, A., Spelbrink, J. N., Paetau, A., and Suomalainen, A. (2005) Mutant mitochondrial helicase Twinkle causes multiple mtDNA deletions and a late-onset mitochondrial disease in mice. *Proceedings of the National Academy of Sciences of the United States of America* **102**, 17687-17692

6. Korhonen, J. A., Gaspari, M., and Falkenberg, M. (2003) TWINKLE Has 5' -> 3' DNA helicase activity and is specifically stimulated by mitochondrial single-stranded DNA-binding protein. *The Journal of biological chemistry* **278**, 48627-48632

7. Sen, D., Nandakumar, D., Tang, G. Q., and Patel, S. S. (2012) Human mitochondrial DNA helicase TWINKLE is both an unwinding and annealing helicase. *The Journal of biological chemistry* **287**, 14545-14556

8. Ziebarth, T. D., Farr, C. L., and Kaguni, L. S. (2007) Modular architecture of the hexameric human mitochondrial DNA helicase. *Journal of molecular biology* **367**, 1382-1391

9. Kaguni, L. S., and Oliveira, M. T. (2016) Structure, function and evolution of the animal mitochondrial replicative DNA helicase. *Critical reviews in biochemistry and molecular biology* **51**, 53-64

10. Kato, M., Ito, T., Wagner, G., and Ellenberger, T. (2004) A molecular handoff between bacteriophage T7 DNA primase and T7 DNA polymerase initiates DNA synthesis. *The Journal of biological chemistry* **279**, 30554-30562

11. Kulczyk, A. W., Akabayov, B., Lee, S. J., Bostina, M., Berkowitz, S. A., and Richardson, C. C. (2012) An interaction between DNA polymerase and helicase is essential for the high processivity of the bacteriophage T7 replisome. *The Journal of biological chemistry* **287**, 39050-39060

12. Farge, G., Holmlund, T., Khvorostova, J., Rofougaran, R., Hofer, A., and Falkenberg, M. (2008) The N-terminal domain of TWINKLE contributes to single-stranded DNA binding and DNA helicase activities. *Nucleic acids research* **36**, 393-403

13. Singleton, M. R., Sawaya, M. R., Ellenberger, T., and Wigley, D. B. (2000) Crystal structure of T7 gene 4 ring helicase indicates a mechanism for sequential hydrolysis of nucleotides. *Cell* **101**, 589-600

14. Lee, S. J., Qimron, U., and Richardson, C. C. (2008) Communication between subunits critical to DNA binding by hexameric helicase of bacteriophage T7. *Proceedings of the National Academy of Sciences of the United States of America* **105**, 8908-8913

15. Patel, S. S., and Hingorani, M. M. (1993) Oligomeric structure of bacteriophage T7 DNA primase/helicase proteins. *The Journal of biological chemistry* **268**, 10668-10675

16. Crampton, D. J., Ohi, M., Qimron, U., Walz, T., and Richardson, C. C. (2006) Oligomeric states of bacteriophage T7 gene 4 primase/helicase. *Journal of molecular biology* **360**, 667-677

17. Ziebarth, T. D., Gonzalez-Soltero, R., Makowska-Grzyska, M. M., Nunez-Ramirez, R., Carazo, J. M., and Kaguni, L. S. (2010) Dynamic effects of cofactors and DNA on the oligomeric state of human mitochondrial DNA helicase. *The Journal of biological chemistry* **285**, 14639-14647

18. Toth, E. A., Li, Y., Sawaya, M. R., Cheng, Y., and Ellenberger, T. (2003) The crystal structure of the bifunctional primase-helicase of bacteriophage T7. *Molecular cell* **12**, 1113-1123

19. Rosado-Ruiz, F. A., So, M., and Kaguni, L. S. (2016) Purification and Comparative Assay of the Human Mitochondrial Replicative DNA Helicase. *Methods in molecular biology* **1351**, 185-198

20. Matsushima, Y., and Kaguni, L. S. (2007) Differential phenotypes of active site and human autosomal dominant progressive external ophthalmoplegia mutations in Drosophila mitochondrial DNA helicase expressed in Schneider cells. *The Journal of biological chemistry* **282**, 9436-9444

21. Peretz, H., and Elson, D. (1976) Synthesis of a cleavable protein-crosslinking reagent for the investigation of ribosome structure. *European journal of biochemistry / FEBS* **63**, 77-82

22. Kastner, B., Fischer, N., Golas, M. M., Sander, B., Dube, P., Boehringer, D., Hartmuth, K., Deckert, J., Hauer, F., Wolf, E., Uchtenhagen, H., Urlaub, H., Herzog, F., Peters, J. M., Poerschke, D., Luhrmann, R., and Stark, H. (2008) GraFix: sample preparation for single-particle electron cryomicroscopy. *Nature methods* **5**, 53-55

23. Stark, H. (2010) GraFix: stabilization of fragile macromolecular complexes for single particle cryo-EM. *Methods in enzymology* **481**, 109-126

24. Ahnert, P., Picha, K. M., and Patel, S. S. (2000) A ring-opening mechanism for DNA binding in the central channel of the T7 helicase-primase protein. *The EMBO journal* **19**, 3418-3427

25. Yu, X., VanLoock, M. S., Poplawski, A., Kelman, Z., Xiang, T., Tye, B. K., and Egelman, E. H. (2002) The Methanobacterium thermoautotrophicum MCM protein can form heptameric rings. *EMBO reports* **3**, 792-797

26. Jemt, E., Farge, G., Backstrom, S., Holmlund, T., Gustafsson, C. M., and Falkenberg, M. (2011) The mitochondrial DNA helicase TWINKLE can assemble on a closed circular template and support initiation of DNA synthesis. *Nucleic acids research* **39**, 9238-9249

27. Matson, S. W., and Richardson, C. C. (1985) Nucleotide-dependent binding of the gene 4 protein of bacteriophage T7 to single-stranded DNA. *The Journal of biological chemistry* **260**, 2281-2287

28. Stiban, J., Farnum, G. A., Hovde, S. L., and Kaguni, L. S. (2014) The N-terminal domain of the Drosophila mitochondrial replicative DNA helicase contains an iron-sulfur cluster and binds DNA. *The Journal of biological chemistry* **289**, 24032-24042

29. Shin, J. H., Heo, G. Y., and Kelman, Z. (2009) The Methanothermobacter thermautotrophicus MCM helicase is active as a hexameric ring. *The Journal of biological chemistry* **284**, 540-546

30. Fletcher, R. J., Bishop, B. E., Leon, R. P., Sclafani, R. A., Ogata, C. M., and Chen, X. S. (2003) The structure and function of MCM from archaeal M. Thermoautotrophicum. *Nature structural biology* **10**, 160-167

31. Stelter, M., Gutsche, I., Kapp, U., Bazin, A., Bajic, G., Goret, G., Jamin, M., Timmins, J., and Terradot, L. (2012) Architecture of a dodecameric bacterial replicative helicase. *Structure* **20**, 554-564

32. Zhang, H., Lee, S. J., Kulczyk, A. W., Zhu, B., and Richardson, C. C. (2012) Heterohexamer of 56- and 63-kDa Gene 4 Helicase-Primase of Bacteriophage T7 in DNA

Replication. *The Journal of biological chemistry* **287**, 34273-34287

33. Kulczyk, A. W., and Richardson, C. C. (2012) Molecular interactions in the priming complex of bacteriophage T7. *Proceedings of the National Academy of Sciences of the United States of America* **109**, 9408-9413

CHAPTER 3
N-terminal domains in mtDNA helicases

ABSTRACT

Recent evidence suggests that iron-sulfur clusters in DNA replicative proteins sense DNA-mediated charge transfer to modulate nuclear DNA replication. In the mitochondrial DNA replisome, only the replicative DNA helicase (mtDNA helicase) from *Drosophila melanogaster* has been shown to contain an iron-sulfur cluster in its N-terminal, primase-like domain. In this chapter, I confirm the presence of the iron-sulfur cluster and show that the N-terminal domain also serves a role in membrane binding. The N-terminal domain binds to asolectin liposomes, which mimic phospholipid membranes, through electrostatic interactions. In particular, membrane binding is more specific with increasing cardiolipin content that is characteristically high in the mitochondrial inner membrane. These results suggest that the N-terminal domain of the mtDNA helicase interacts with the mitochondrial inner membrane to recruit mtDNA and initiate mtDNA replication.

The human pathogenic mutant cluster in the RNA polymerase-like domain has been proposed to serve a role in single-stranded DNA (ssDNA) binding in the N-terminal domain of human mtDNA helicase. In this chapter, I show that the human pathogenic mutant cluster contributes to ssDNA binding using a UV crosslinking assay. This result contribute to our understanding of processes that are likely to be involved in ssDNA binding of mtDNA helicases such as helicase self loading and annealing.

INTRODUCTION

The mitochondrial replicative DNA helicase shows high amino acid sequence homology with bacteriophage T7 gene 4 protein that has an N-terminal primase domain and a C-terminal helicase domain. The N-terminal domain (NTD) of metazoan mtDNA helicases share seven conserved sequence motifs found in bacterial and bacterophage primase regions (1,2) and form a similar overall fold (3). However, primase activity has not been detected in mtDNA helicase because of the absence of a few important residues in its homologous primase active site (2).

The NTD of mtDNA helicase comprises a zinc binding-like domain (ZBD) and an RNA polymerase-like domain (RPD) similar to bacterial and bacteriophage primases (Fig. 2 in chapter 1). The ZBD has a motif I that contains four conserved cysteines for coordination of a zinc ion in bacterial and bacteriophage primases. In T7gp4, the ZBD recognizes a trinucleotide template sequence and delivers it to the primase active site through interactions with its own RPD (cis-) and its neighboring RPD (trans-) in the hexameric form of the protein (4). However, the zinc ion in T7gp4 is not thought to interact with DNA because it faces out from the active site and is surrounded by residues not suitable for DNA binding (5). Rather, the zinc ion is believed to contribute to protein stability (5). Homology models for the ZBD of mtDNA helicase have been published by using T7gp4 or DnaG as a template (3,6), but their reliability is debatable due to low sequence similarities of the ZBDs between the mtDNA helicase and prokaryotic primases (7). Instead, a novel structural fold for the ZBD is expected in the mtDNA helicase. The ZBD of *Dm* mtDNA helicase binds an iron-sulfur cluster instead of the zinc ion in its prokaryotic homolog (8), while the ZBD of human mtDNA helicase cannot bind any metal ion because three of four conserved metal coordinating cysteines are missing (2,9). Alanine substitution of the iron-sulfur cluster ligating cysteines results in a significant reduction in protein stability (8). This

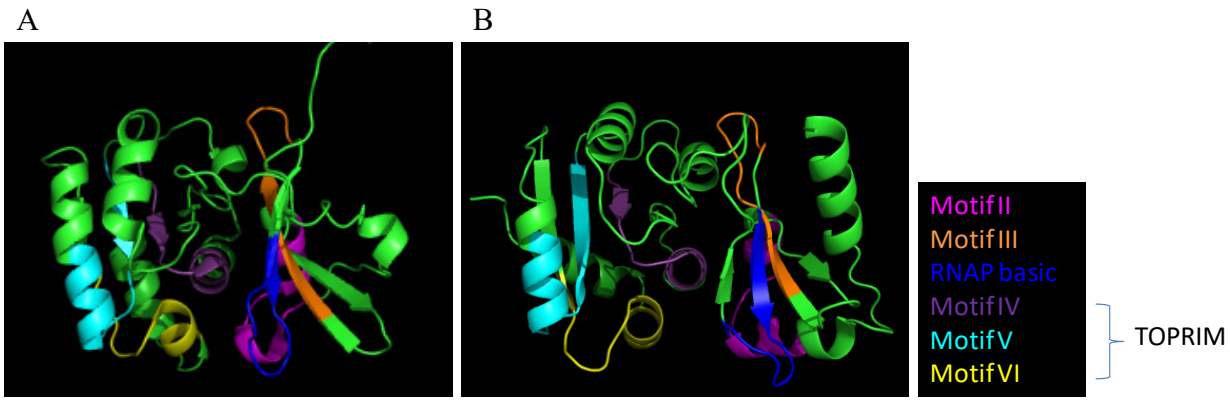

Figure 13. **Conserved motifs in RPDs of bacteriophage T7gp4 (A) and human mtDNA helicase (B) A.** The RPD was taken from the X-ray crystal structure of T7gp4 (1NUI) (10). **B.** A homology model of the RPD of human mtDNA helicase was generated from *E.coli* DnaG (1DDE) (11) as a template. Each motif (2) was coded with different colors as shown in the legend. Motifs IV-VI are called as the TOPRIM subdomain and motifs II, III and the RNAP basic motif corresponds to the N-terminal subdomain. Motif I is the ZBD and not displayed in this figure.

suggests that the iron-sulfur cluster probably plays a role in protein stability similar to the proposed role of the zinc ion in the ZBD of T7gp4 (5). However, the evolutionary reason that insect mtDNA helicase selected an iron-sulfur cluster instead of a zinc ion and the human ortholog has lost the metal ion in its ZBD remains unclear.

The RPD of mtDNA helicase consists of an N-terminal subdomain and a C-terminal TOPRIM subdomain (Fig. 13 B) (7) that show high structural similarity with bacteriophage T7 primase (Fig. 13 A) (5) and *E. coli* DnaG primase (12). Conserved motifs II, III and the RNAP basic motif are located in the N-terminal subdomain where single-stranded DNA (ssDNA) binds in a conserved DNA binding groove in *E. coli* DnaG (11). The TOPRIM subdomain has a primase active site in which functionally important acidic residues in motifs IV to VI form a magnesium ion binding pocket that is necessary for primer synthesis (9,13). Metazoan mtDNA helicases have lost some of these acidic residues, resulting in no primase activity (2). Kaguni and Oliveira propose the absence of the magnesium ion binding pocket in human RPD by showing that the pocket is positively charged in an electrostatic potential surface (EPS) map of their human RPD model (7). In contrast, the pockets in T7gp4 and DnaG primases are negatively charged.

In addition to the lack of primase activity in the NTD of mtDNA helicase, recombinant NTD-only variants do not show oligomerization or catalytic activities including DNA dependent ATPase activity or DNA unwinding activity (14). In contrast, an NTD deletion variant (Δ 1-314) and a ZBD deletion variant (Δ 1- 121) of the full-length mtDNA helicase form hexamers and show diminished ATPase activity and unwinding activity, suggesting the contribution of the NTD to these catalytic activities (14). Interestingly, the NTD deletion variant shows a substantial decrease in ssDNA binding but a mild reduction in double-stranded DNA (dsDNA) binding,

indicating the NTD is involved particularly in ssDNA binding. The ssDNA binding affinity of the NTD-only variant of the *D. melanogaster* homolog was found to be ~120 nM of K_D by fluorescence quenching assay (8).

The NTD is suggested to be a binding module for physical interactions (7). Interactions between the mtDNA helicase and mitochondrial proteins or lipids (or the mitochondrial inner membrane) have been observed in biochemical and physiological studies (15-18), although no component interacting directly with the NTD has been identified. A protein candidate for interaction with the NTD is mitochondrial single-stranded DNA binding protein (mtSSB). Unwinding activity of the mtDNA helicase is stimulated by mtSSB and our group showed that alanine substitution mutants in the loop 1, 2, and loop 4, 5-2 of mtSSB decrease stimulation about 40%, suggesting that the loops interact with the helicase and facilitate dsDNA unwinding (15). Moreover, high through-put scale research has reported several putative interacting partners of the human and *Drosophila* mtDNA helicases (19,20). Among them, *Drosophila* Ind1, an iron-sulfur cluster delivery protein, is interesting because of the presence of an iron-sulfur cluster in the *Drosophila* mtDNA helicase (20). The interaction between *Dm* Ind1 and the *Dm* mtDNA helicase NTD-only variant will be discussed in chapter 4. Besides proteins, lipid binding or membrane association of mtDNA helicases has been proposed (17,18). Endogenous and recombinant mtDNA helicase proteins are often found in the membrane fraction of mitochondria by mitochondrial fractionation and fluorescence microscopy ((17,18), and our unpublished data). Recently, it was reported that replicative proteins, including the mtDNA helicase, cosedimented with cholesterol-rich membranes in human HEK cells (18), implying the possible interaction between mtDNA helicase and cholesterol.

Mutations in human mtDNA helicase cause mitochondrial diseases. Most disease-

associated mutations are in the C-terminal helicase domain and the linker region that are responsible for helicase activity and oligomerization, respectively (21-23). Interestingly, pathogenic mutants in the N-terminal domain are clustered only in the TOPRIM subdomain (7). To date, ten pathogenic mutations have been reported in six amino acid residues in the NTD of human mtDNA helicase (7). Biochemical studies with recombinant full-length helicases that harbor disease mutants reveal that most of the pathogenic mutations in the NTD cause severely decreased ssDNA binding activity but a mild reduction in dsDNA unwinding activity (6,21). An *in vivo* study about three human pathogenic mutants in the NTD of *Dm* mtDNA helicase shows that induction of pathogenic analogs in *Drosophila* S2 cells results in mitochondrial DNA depletion (9), suggesting a physiological role for these amino acids in helicase activity of the mtDNA helicase.

The structure and function of the primase like-NTD of the mtDNA helicase have been investigated for the last decade, but its role remains unclear. In this study, I investigated the NTD of both *Drosophila* and human mtDNA helicases to assess their binding properties and to understand their functions. This chapter focuses on iron-sulfur cluster binding and membrane binding properties of *Dm* mtDNA helicase, as well as ssDNA binding by human mtDNA helicase, demonstrating the presence of the cluster in the NTD from *Drosophila* S2 cells, mitochondrial inner membrane binding of *Dm* NTD through interactions with cardiolipin, and ssDNA binding in human RPD within the disease mutation cluster.

MATERIALS AND METHODS

Cell culture, generation of a stable cell line, and production of a recombinant Drosophila mtDNA helicase NTD in Drosophila cells

To express a C-terminally His-tagged *Drosophila* mtDNA helicase NTD (*Dm* NTD) (Met^{1}-Ala^{333}), stable cell line was generated as described previously (9). *Drosophila melanogaster* Schneider 2 cells (S2 cells) were subcultured to 5 X 10^{6} cells/ ml at 25°C in *Drosophila* Schneider Medium (Invitrogen) with 10% fetal bovine serum (Gibco) one day before transfection. pMt-*Dm* NTD whose gene is under a metallothionein promoter, was transfected using Effecten (Qiagen) by a manufacturer's manual. Transfected cells were selected under 200 μg/ ml hygromycin (Invitrogen) and passed more than five times under the hygromycin-containing medium. The cell line was grown in suspension culture in Insect-XPRESS™ protein-free insect cell medium (Lonza) and protein expression was induced with 0.2 mM $CuSO_4$. After 3-4 days of induction, cells were harvested and mitochondria were isolated by differential centrifugation. A mitochondrial extract was prepared and the *Dm* NTD was purified further by Ni-NTA affinity chromatography as described earlier (8).

Overexpression and purification of Drosophila mtDNA helicase NTD from E. coli

The N-terminally His-tagged *Drosophila* mtDNA helicase NTD (Asn^{24}-Ala^{333}) was produced by overexpression in *E. coli* cells and purified by Ni-NTA affinity chromatography as described previously (8), except that Superdex 200 HR 10/30 (GE Healthcare) gel filtration chromatography was substituted for the glycerol gradient sedimentation.

Cloning and expression of a human mtDNA helicase RPD wild type and its variants

The gene construct coding for the RPD of human mtDNA helicase (Pro^{146}-Ser^{366}) was subcloned into pSUMO vector to express an N-terminally His-SUMO tagged RPD and designated as pSUMO-RPD WT. Expression vectors for RPD variants were constructed by PCR-based site-directed mutagenesis from pSUMO-RPD WT. PCR was performed by using the Expand Long PCR system (Roche Applied Science) with standard laboratory protocols. A specific primer pair was used for each variant as follows: for W315A/ K319A, LSK MS32F 5'-GAT GAC CTT CGG TCC GCG GAA GCC GCC GCG TTG TTT GCA CGA AA-3' and LSK MS 32R 5'-TTT CGT GCA AAC AAC GCG GCG GCT TCC GCG GAC CGA AGG TCA TC-3'; for R303A, LSK MS33F 5'-ACC TGG AAC AGT TCC GGG CGA TTG TAT TCT GGT TGG-3' and LSK MS33R 5'-CCA ACC AGA ATA CAA TCG CCC GGA ACT GTT CCA GGT-3'; for K328A/ R329A,LSK MS34F 5'-TTG CAC GAA AAC TGA ACC CCG CAG CAT GCT TCT TGG TGC GAC CAG-3' and LSK MS34R 5'-CTG GTC GCA CCA AGA AGC ATG CTG CGG GGT TCA GTT TTC GTG CAA-3'; and for K183A/ R329A, LSK MS35F 3'-TAC AAT GTT TGG CCT TAC CGC GGT TAC AGC TGA CAC ACT CAA GCG TTT C-5' and LSK MS35R 3'-GAA ACG CTT GAG TGT GTC AGC TGT AAC CGC GGT AAG GCC AAA CAT TGT A-5'.

The N-terminally His-SUMO-tagged RPD and its variants were produced in *E.coli* BL21 (Rosetta). The bacterial cultures were grown at 37°C until an optical density (OD) of 0.4 at 600 nm was reached. To induce each protein expression, 0.4 mM Isopropyl β-D-1-thiogalactopyranoside (IPTG) was added and cultured at 16°C for 20 hours. Harvested cells were resuspend in lysis buffer A (50 mM Tris-HCl, pH 7.5, 250 mM NaCl, 10% glycerol, 1.5 % *n*-dodecyl β-D-maltoside, and 5 mM β-mercaptoethanol with protease inhibitors (1 mM

phenylmethylsulfonyl fluoride, 10 mM sodium metabisulfite, and 2 μg/ml leupeptin). Cell extracts are prepared in the supernatant fraction after centrifugation of the resulting lysate.

Purification of N-terminally His-SUMO-tagged human mtDNA helicase RPD wild type and its variants

All purification protocols begin with Ni-NTA affinity chromatography of protein from cell extracts. To purify wild type, W315/ K319A, and R303A, the pools of the eluted Ni-NTA peaks were digested by a sumo cleavage enzyme (1mg/ml) with a ratio of 1:1000 at 4°C for overnight during dialysis with 8,000-10,000 Da dialysis tubing (SpectrumLabs) in a dialysis buffer (35 mM Tris-HCl, pH7.5, 500 mM KCl, 10% glycerol, 5mM β-mercaptoethanol). The tag-less RPD proteins were recovered in the unbound fraction and the wash fractions (1CV) by a recovery Ni-NTA affinity chromatography. The recovered RPD wild type and variant R303A were loaded onto the gel filtration column (Superdex 75 HR 10/30 (GE healthcare)) and chromatographed in gel filtration buffer (35mM Tris-HCl pH7.5, 350mM NaCl, 10% glycerol, 5 mM β-mercaptoethanol). The eluted peak fraction were pooled and stored at -80 ºC. On the other hand, the recovered W315A/ K319A variant was loaded on the 12-30% glycerol gradient with Tris-ammonium sulfide buffer (35 mM Tris-HCl, pH7.5, 200 mM $(NH_4)_2SO_4$, 12-30% glycerol, 5 mM β-mercaptoethanol). The pooled peak fractions were pooled and stored at -80 ºC. For the K328A/ R329A variant, a gel filtration followed directly after Ni-NTA affinity chromatography. The pool of gel filtration peak fractions was digested by the sumo cleavage enzyme. Then, the recovery Ni-NTA affinity chromatography was performed. The tag-less target proteins found in the unbound fraction and the wash fractions (1CV), and the pool was concentrated to ~1mg/ml of the total protein. For K183A/ D187A variant, dialysis using centricon (Millipore) was conducted

on ice for 8 hours before the sumo tag was cleaved. After recovery Ni-NTA chromatography, the tag-less target protein from the unbound and the washing fractions was concentrated by centricon (Millipore) and loaded on the 12-30% glycerol gradient with Tris-ammonium sulfide buffer. The pooled peak fractions were stored at -80 ºC.

Protein immunoblot

See Materials and Methods in chapter 1.

Additionally, anti-*Dm* NTD rabbit polyclonal antibody was prepared from a purified N-terminally His-tagged *Drosophila* mtDNA helicase NTD (Asn^{24}-Ala^{333}) (Covance).

N-terminal sequencing

The purified *Dm* mtDNA helicase NTD from the isolated mitochondria of *Drosophila* S2 cells were separated by SDS-PAGE and transferred onto a polyvinylidene difluoride membrane in CAPS buffer at a constant current of 150 mAmp for 16 hours. The membranes were stained with 0.05% R250 Coomassie Blue followed by destaining in 40% methanol. The proteolytic fragments were visualized, cut from the membrane, and submitted for N-terminal sequencing analysis by standard Edman chemistry (UC-Davis).

Potassium ferricyanide staining

After SDS-PAGE, gels were immersed in potassium ferricyanide solution (100 mM potassium ferricyanide, 50 mM Tris-HCl, pH7.5, 100 mM NaCl) in the dark for 1 hour. The gels were transferred to freshly-prepared color-developing solution (10% methanol, 10% trichloroacetic acid) until the protein bands were visible.

Lipid vesicle cosedimentation assay

Asolectin (Sigma) in the presence or absence of additional lipids (cholesterol (Sigma) or cardiolipin (Sigma)) were dissolved in chloroform (Baker) and dried under nitrogen gas. The residual chloroform was eliminated by vacuum desiccation for 8 hours. In the preparation of multilamellar liposomes, the dry lipids were hydrated for 30 minutes in hydration buffer (10 mM NH_4HCO_3, pH7.4, 0.1 mM EDTA). The solution was mixed by vortexing until visible clots disappeared. Then, four cycles of freezing, thawing, sonication, and vortexing were performed. Large unilamellar liposomes were prepared by extrusion through a polycarbonate membrane (100 nm pore size) using a mini-extruder (Avanti Polar Lipids). After incubation of the protein and liposomes for 15 minutes under the stated conditions, the reaction mixtures were centrifuged at 47,000 × *g* in an S120-AT3 rotor (Thermo Scientific) for 1 hour. Equal portions of supernatant and pellet were analyzed by 12% SDS-PAGE followed by immunoblotting. The intensities of the protein signals on the membrane were quantified using the ImageQuant 5.2 software. The fraction of bound protein was determined by dividing the band intensity of the pellet (bound protein) by those of the pellet and the supernatant together (total protein).

Intrinsic tryptophan fluorescent quenching assay

Fluorescence quenching of the *Dm* NTD tryptophan residues was measured after addition of a lipid ligand such as cholesterol (0~140 nM), PE (0~70 nM) and PC (0~7 nM) with serial increase. Tryptophan fluorescence of *Dm* NTD (100 nM) in a buffer (50 mM Tris-HCl, pH7.5, 150 mM NaCl, 5% glycerol, 5mM β-mercaptoethanol) as monitored from 310-400 nm using a Cary Eclipse fluorescence spectrophotometer (Agilent). The excitation wavelength was 288 nm and the measuring temperature was 20ºC. Data was corrected after subtracting the background

scatter of the buffer. The saturation curve was obtained by plotting the maximum fluorescence difference ($\Delta F = Fo - F$) (ΔF, specific) in the presence of different concentrations of a ligand, where F and Fo were the measured fluorescence emission intensity in protein solution with a lipid ligand (F, total) and with solvent (200 proof ethanol (Backer)) of the ligand (Fo), respectively (24).

For the stability assay, the intrinsic tryptophan fluorescence of protein solution in different buffers was measured under same conditions mentioned above except no addition of a lipid ligand or solvent.

Gel mobility shift assay

0.05 μM *Dm* NTD was incubated with 1.44 nM [^{32}P] 5' end labeled 60-mer (LSK911) for 10 minutes at 21ºC in the buffer containing 20 mM Tris-HCl, pH 7.5, 1 mM dithiothreitol, 4 mM $MgCl_2$, 50 mM NaCl. The samples were analyzed by 6% native PAGE (13 cm X 13 cm X 0.15 cm). Gels were dried under vacuum and exposed at -80°C to Kodak X-Omat AR x-ray film using a DuPont NEN Quanta III intensifying screen.

UV crosslinking

The Bromodeoxyuridine (BrdU)-substituted mtDNA 60-mer (5' TGG TAC CGT ACA ATA TTC ATG GTG GC/i5Br-dU/ GGC AGT AAT GTA CGA AAT ACA TAG CGG TTG TTG-3') was end-labeled at the 5' using [γ^{32}P]ATP by T4 Polynucleotide kinase (PNK) (Roche), and unincorporated [γ^{32}P]ATP was removed by P-30 column (Biorad). 1 μM RPD or RPD variants were incubated with the [^{32}P]-labeled BrdU-substituted 60-mer (0-36 nM) for 10 minutes at 20°C in 20 mM Tris-HCl, pH 7.5, 4 mM $MgCl_2$, 1 mM DTT, 0.3 mg/ml BSA with 50 mM NaCl as a

final concentration of salt. The final salt concentration was adjusted with 300 mM NaCl stock solution depending on the salt concentration in protein stocks. The reaction mixtures (total 30 µl) were irradiated for 30 minutes at 0°C with UV light (300 nm) from bulbs (Fotodyne, 4 X 15 watts) at a distance of 8 cm. After irradiation, the samples were analyzed by 12% SDS-PAGE (13 cm X 13 cm X 0.15 cm) and the gel was dried under vacuum and exposed at -80°C to Kodak X-Omat AR x-ray film using a DuPont NEN Quanta III intensifying screen.

RESULTS

Dm mtDNA helicase has a canonical N-terminal mitochondrial targeting sequence and the mature protein starts with the 26th amino acid, alanine.

Dm mtDNA helicase has a low abundance in *Drosophila* cells. Thus, overexpression of *Dm* mtDNA helicase was necessary to investigate its characteristics. Due to the high insolubility of the full-length *Dm* mtDNA helicase recombinant protein, only the N-terminal domain (M1-A333) was cloned to a pMk/Hy vector with a C-terminal His tag. The inserted gene has its endogenous mitochondrial targeting sequence (MTS) at the N-terminus. Thus, the MTS of the overexpressed N-terminal domain protein is cleaved off during transport into the mitochondrial matrix (25). In order to determine the cleavage site, the recombinant NTD was expressed in *Drosophila* S2 cells and purified from isolated mitochondria by affinity chromatography. The size of the purified protein is ~36 kDa on an SDS-PAGE gel (data not shown). N-terminal sequencing of the overexpressed mature NTD by the Edman degradation method demonstrates that the recombinant mature NTD starts with A26, indicating that the mature *Dm* mtDNA helicase contains amino acids A26-N613.

The mature NTD overexpressed from Drosophila S2 cells contains an iron-sulfur cluster.

The presence of an iron-sulfur cluster in *Dm* mtDNA helicase was demonstrated previously (8), but it has been questioned that the insertion of the cluster into the recombinant NTD might be an artifact resulting from an *E. coli* overexpression system (26). To verify the presence of an iron-sulfur cluster in *Dm* mtDNA helicase, the mature NTD expressed from *Drosophila* S2 cells was stained by potassium ferricyanide (27) in which only proteins that contain non-heme iron ions can be stained on an SDS-PAGE gel. NTD protein from S2 cells

(Fig. 14, lane 1) and from *E. coli* BL21 cells (Fig. 14, lane 2) were detected by both Coomassie and potassium ferricyanide staining. A recombinant full-length *Dm* mtDNA helicase from an *E. coli* BL21 cell lysate was also detected at a position corresponding to ~70 kDa by both staining procedures (Fig. 14, lane 3). These data suggest strongly that the iron-sulfur cluster is a *bona fide* component of the *Dm* mtDNA helicase.

Dm NTD binds to asolectin liposomes.

Direct interactions between lipid membranes and a recombinant *Dm* NTD overexpressed in *E. coli* were investigated by using a lipid vesicle cosedimentation assay. Asolectin unilamellar liposomes were prepared as a mimic of cellular membranes. Asolectin is a soybean phospholipid mixture and consists of PE (phosphatidylethanolamine, 34.5 mol%), PC (phosphatidylcholine, 26.7 mol%), PI (phosphatidylinositol, 20.9 mol%), PG (phosphatidylglycerol, 2.3 mol%), PA (phosphatidic acid, 14.2 mol%) and PS (phosphatidylserine, 1.3 mol%) (28). The *Dm* NTD cosedimented with asolectin liposomes and was found in the pellet, indicating that *Dm* NTD binds to liposomes (Fig. 15). However, *Dm* NTD was predominately in the supernatant fraction as an unbound protein, suggesting the binding was not strong. A fraction of the bound protein (the pellet) over total protein (sum of the pellet and the supernatant) was calculated based on signal intensity. The fraction of bound *Dm* NTD (~0.2) was saturated at a concentration of 25 μM liposomes at near-physiological ionic strength (100 mM NaCl) (Fig. 15 A). Binding was abolished completely by an increase in salt concentration, suggesting that liposome binding of *Dm* NTD depends almost entirely on electrostatic interactions (Fig. 15 B).

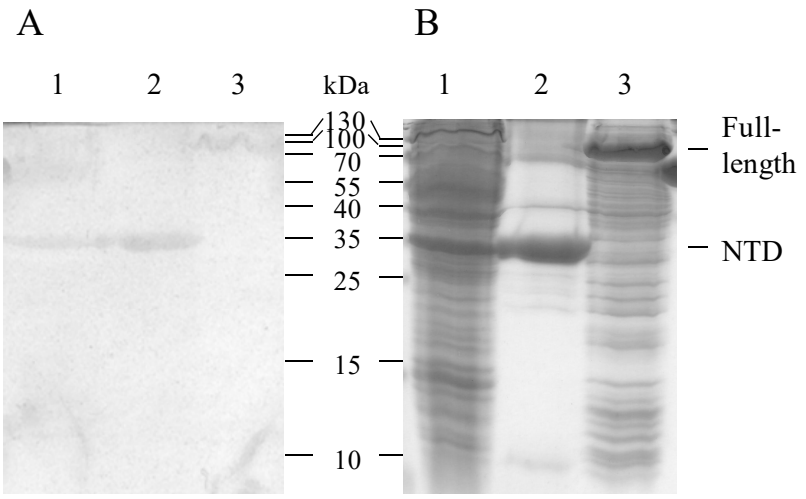

Figure 14. **Detection of non-heme iron in *Dm* NTD** Potassium ferricyanide staining **(A)** and Coomassie brilliant blue staining **(B)** of partially-purified NTD overexpressed in *Drosophila* S2 cells (lane 1), purified NTD overexpressed in *E. coli* BL21 (lane 2) and overexpressed full-length *Dm* mtDNA helicase in an *E. coli* BL21 cell lysate (lane 3). A negative control (BSA) for potassium ferricyanide staining was tested by using the same protocol on three separate gels (data not shown). 1.5 μg, 4.5 μg, and 9 μg of purified *Dm* NTD (0.04 nmol, 0.13 nmol, and 0.25 nmol) and purified BSA (0.02 nmol, 0.07 nmol, and 0.13 nmol) were loaded on 12% SDS-polyacrylamide gels. While the intensities of stained *Dm* NTD bands were proportional to the amounts loaded, no BSA band was detected.

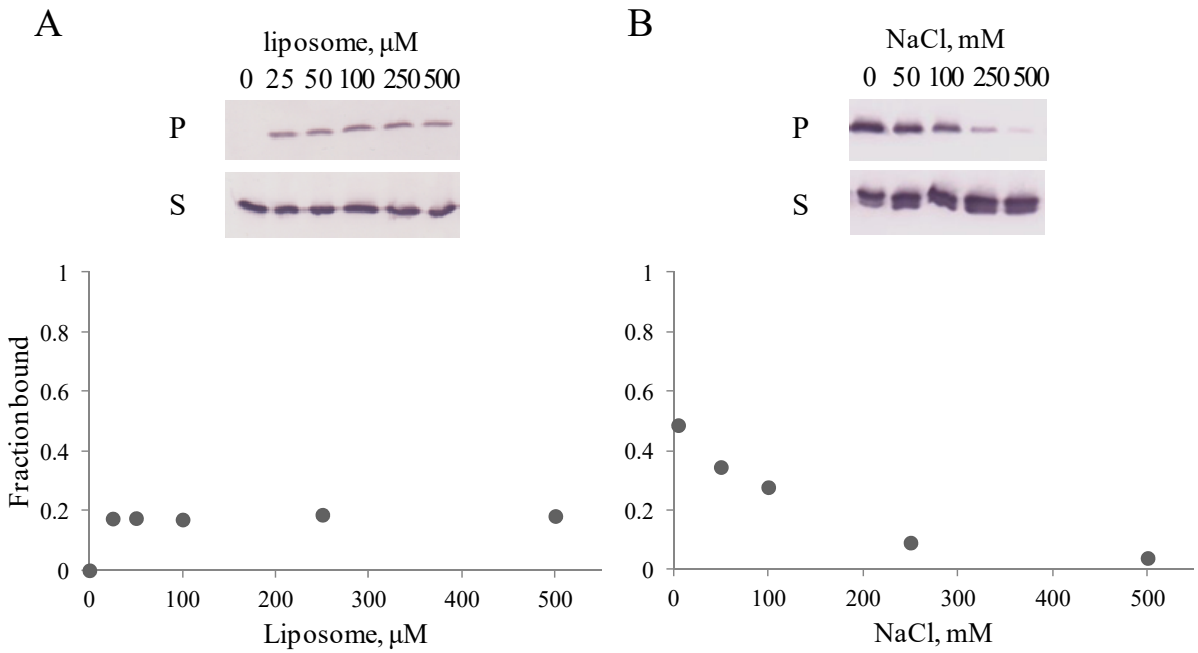

Figure 15. **Binding of *Dm* NTD to asolectin liposomes by lipid vesicle cosedimentation A.** Liposome titration of 0.4 μM *Dm* NTD at 100 mM NaCl showed that *Dm* NTD binds to liposomes. **B.** Salt titration of 0.4 μM *Dm* NTD with 250 μM liposomes reveals that liposome binding is salt-sensitive, suggesting electrostatic interactions. Pellet fraction (P) and supernatant fraction (S) are analyzed by 12% SDS-PAGE (upper). Fraction bound of the NTD was determined by band intensity of pellet (bound protein) over sum of band intensities of pellet and supernatant (total protein) and plotted against concentration of liposomes (A) or NaCl (B) (lower).

Dm NTD binds more efficiently to cardiolipin-containing liposomes, but not to cholesterol-containing liposomes.

A recent report showed that human mitochondrial DNA replicative proteins cosedimented with cholesterol in flotation gradients of purified mitochondria from human HEK293 cells, proposing that the replicative protein complex attaches to a cholesterol-rich membrane (18). In addition, stronger binding affinity to a membrane may be needed for the helicase to fulfill its proposed role in tethering the mtDNA-replisome complex to the mitochondrial inner membrane (17). Thus, membrane lipids that could increase membrane binding affinity of *Dm* NTD were examined. To investigate whether the *Dm* NTD binds to cholesterol in cholesterol-containing liposomes, 30% w/w of cholesterol-containing asolectin liposomes were prepared and diluted with standard asolectin-only liposomes to generate different concentrations of chorelesterol-containing liposomes. The increase of cholesterol concentration had no effect on the bound protein fraction (Fig. 16 A), indicating that *Dm* NTD does not bind to cholesterol in the asolectin liposomes. In contrast, when cardiolipin, an abundant lipid in the mitochondrial membrane, was added to asolectin liposomes, the bound fraction of *Dm* NTD was increased depending on cardiolipin concentration (Fig. 16 B). The fraction of bound protein was proportionally increased from 0.1 to 0.6, as cardiolipin concentration increased from 2% w/w to 20% w/w. The bound fraction was saturated when liposomes contained more than 20% w/w cardiolipin, and the increase at saturation was statistically significant as compared to the bound fraction of cardiolipin-free liposomes (Fig. 16 B). This data demonstrates that *Dm* NTD binds specifically to cardiolipin, and the binding is maximized in liposomes containing 20% w/w cardiolipin that is close to the physiological cardiolipin content in mitochondrial inner membranes (~16% w/w) (29). Next, we compared directly the binding efficiency of *Dm* NTD to asolectin liposomes in the

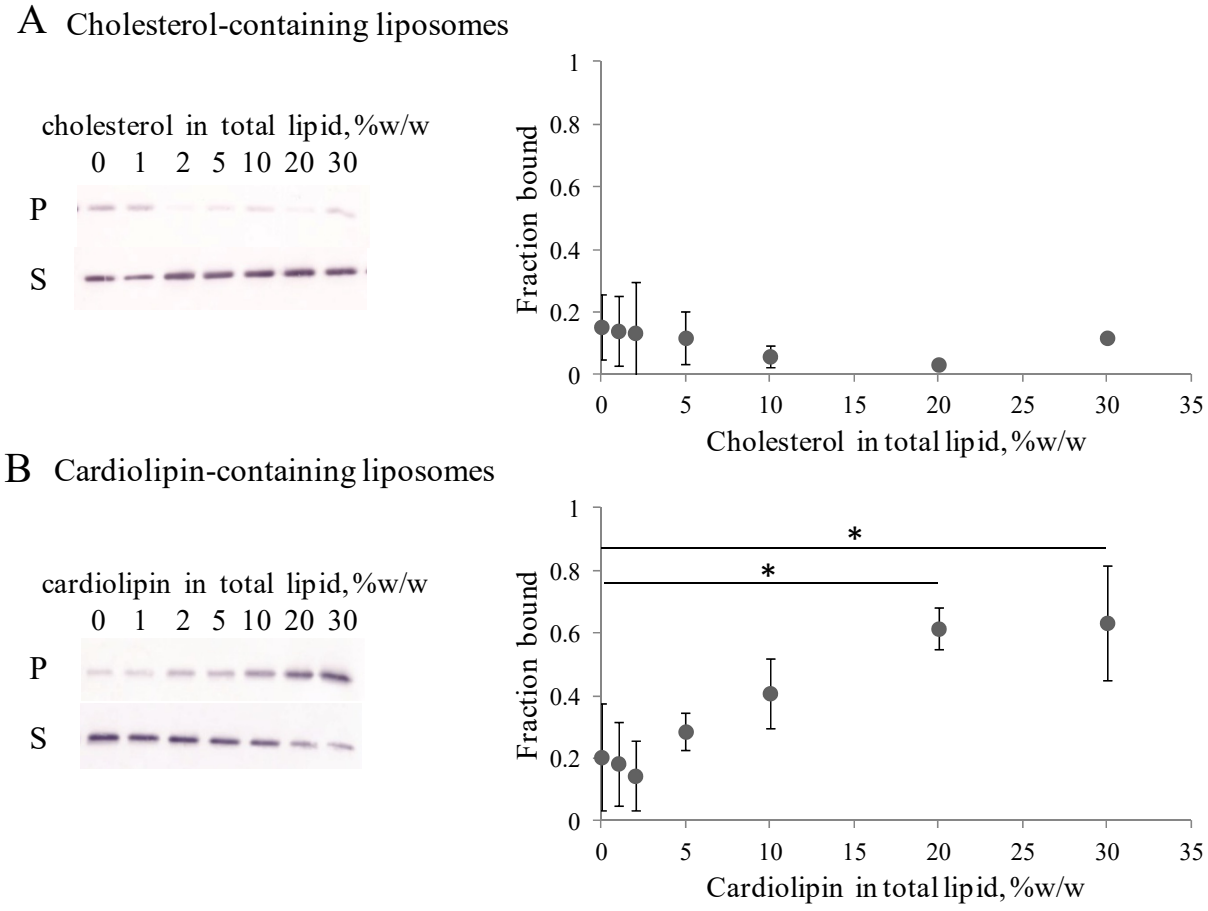

Figure 16. **Binding of *Dm* NTD to asolectin liposomes that contain cholesterol (A) or cardiolipin (B) by lipid vesicle cosedimentation** The final concentration of *Dm* NTD was 0.4 μM in 50 mM Tris-HCl, pH7.5, 100 mM NaCl. The total concentration of liposomes is 100 μM and liposome composition varies as indicated. Pellet fraction (P) and supernatant fraction (S) are analyzed by 12% SDS-PAGE (left) and fraction bound of *Dm* NTD was determined (right) by the same calculation in Figure 15. Each data point represents the mean of triplicate measurements. The error bars indicate ± standard deviation. *P < 0.05 by Student's T-test.

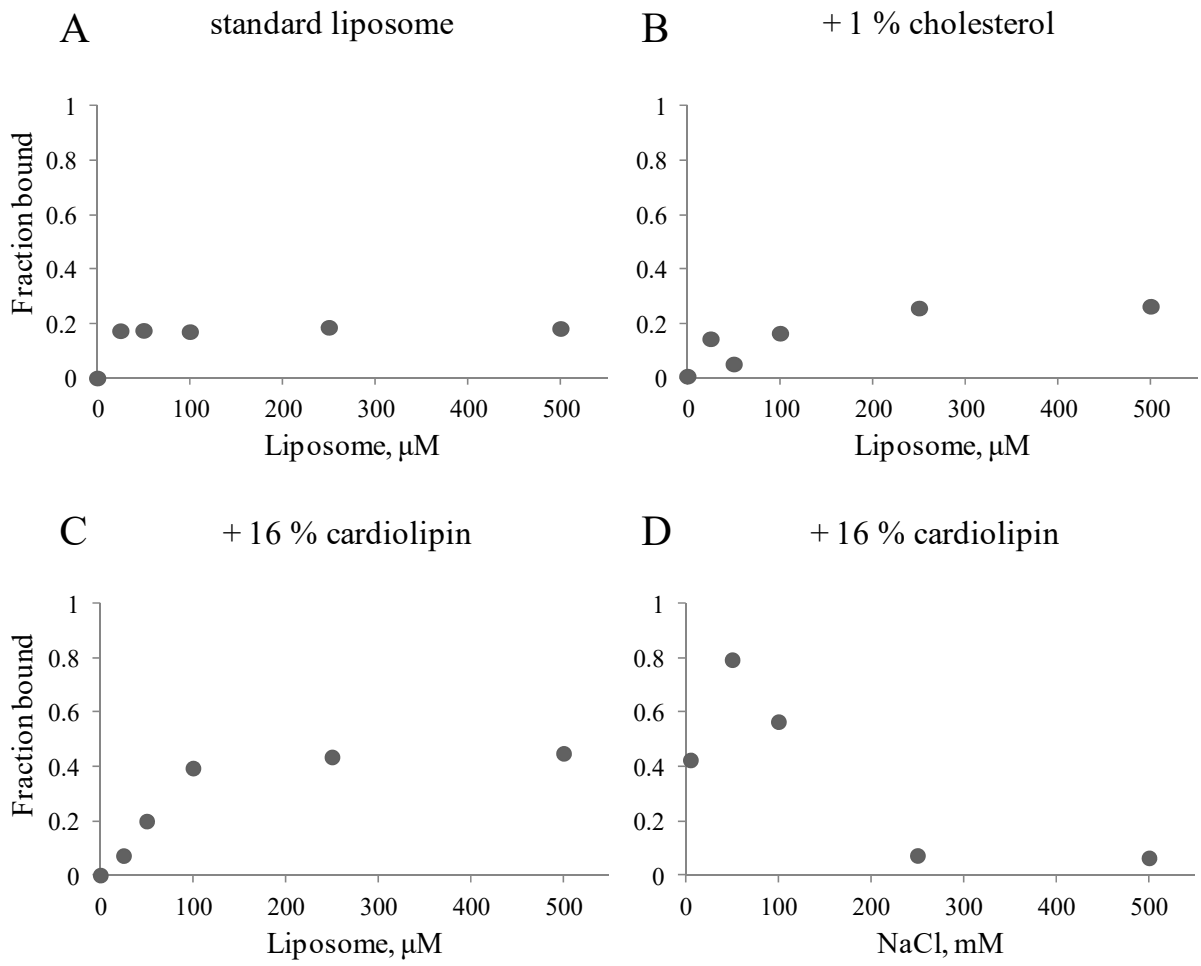

Figure 17. **Binding of *Dm* NTD to different asolectin liposomes by lipid vesicle cosedimentation** Liposome binding of 0.4 µM *Dm* NTD in 50 mM Tris-HCl, pH7.5, 100 mM NaCl with standard asolectin liposomes (A), 1% w/w cholesterol-containing liposomes (B), and 16% w/w cardiolipin-containing liposomes (C) shows that cardiolipin increases liposome binding efficiency of *Dm* NTD. Salt titration of 0.4 µM *Dm* NTD with 250 µM of 16% w/w cardiolipin-containing liposomes (D) shows increasing salt concentration decreases binding. Figure 17 A is a duplicate of Figure 15 A.

presence of 1% w/w cholesterol or 16% w/w cardiolipin, which represent the approximate cholesterol or cardiolipin content found in inner mitochondrial membranes, respectively (29). The fraction of bound NTD increased 2.5 fold at saturation to 16% w/w cardiolipin-containing liposomes as compared to that bound to standard asolectin-only liposomes (Fig. 17 A and C). On the contrary, the fraction of bound NTD to 1% w/w cholesterol-containing liposomes was similar to that bound to the standard liposomes (Fig. 17 A and B). NTD binding to 16% w/w cardiolipin liposomes was decreased with increasing salt concentration, showing the binding is electrostatic (Fig. 17 D). This data demonstrates that *Dm* NTD binds to asolectin liposomes largely by electrostatic interactions between the acidic polar head of cardiolipin and a positively charged surface region of the NTD. They also argue that cholesterol is not involved in membrane attachment of *Dm* NTD.

Intrinsic tryptophan fluorescence quenching shows no specific binding of Dm NTD to cholesterol or the two most abundant lipids in asolectin liposomes.

Binding properties of *Dm* NTD to individual lipids including cholesterol, PE, and PC were investigated by intrinsic tryptophan fluorescence quenching. A stability test was performed prior to the intrinsic tryptophan fluorescence quenching assay to find an optimal buffer for the *Dm* NTD because the emission spectra of the protein near 330 nm decreased over time without adding a lipid in phosphate-buffered saline (PBS) (Fig. A1). This indicates that the environment around tryptophan residues in the protein was changing in the buffer, likely due to protein unfolding or aggregation. Three buffers were tested: (1) Tris-HCl buffer (50 mM Tris-HCl, pH7.5, 150 mM NaCl, Fig. A1 C), (2) Ammonium bicarbonate buffer (10 mM NH_4HCO_3, 10%

glycerol, Fig. A1 D), and (3) PBS (Fig. A1 E). The emission change of the NTD was least in the Tris-HCl buffer, and the emission decrease in the Tris-HCl buffer was mitigated most when 5% glycerol was added (Fig. A1 B).

To evaluate a possible interaction between *Dm* NTD and cholesterol, the intrinsic tryptophan fluorescence quenching assay was conducted by adding various amounts of cholesterol to *Dm* NTD in the selected buffer (50 mM Tris-HCl, pH7.5, 150 mM NaCl, 5% glycerol, 5mM β- mercaptoethanol). The emission of the NTD at the maximum emission wavelength (λ_{max}) decreased as the cholesterol level increased from 0 to 140 μM (Fig.A2 A); however, a similar decrease was observed in the solvent control to which 99.5% ethanol, the solvent for cholesterol, was added instead of cholesterol (Fig. A2 B). Thus, the observed decreases are likely caused by protein instability rather than a hydrophobicity change near tryptophan residues by lipid binding, indicating that *Dm* NTD does not bind to cholesterol *per se*. Consequently, no specific binding to cholesterol was observed in the saturation curve (Fig. A3 A). This result agrees with the lipid vesicle cosedimentation assay data of cholesterol containing-liposomes where the extent of *Dm* NTD binding to liposomes is not altered by various cholesterol levels (Fig. 16 A).

Binding properties of *Dm* NTD to PE and PC, the two most abundant lipids in asolectin liposomes, 35 and 27 mol%, respectively, were also investigated by intrinsic tryptophan fluorescence quenching. Similar to cholesterol, the emission spectra of the solvent controls overlapped with the emission spectra of PE and PC (data not shown). Thus, no significant specific binding to PE or PC was detected in saturation curves (Fig. A3 B and C). This data demonstrates that the *Dm* NTD does not bind specifically to cholesterol, PE or PC. The binding affinity between *Dm* NTD and asolectin liposomes might be caused by the specific combination

of lipids or more likely, other acidic lipids in asolectin liposomes such as PI (21 mol%) or PA (14 mol%).

Four variants that represent potential ssDNA binding areas in the human RPD were designed and produced to identify ssDNA-binding regions.

In addition to binding a metal cofactor and membranes, the NTD of mtDNA helicases binds to ssDNA and dsDNA (8,14). Kaguni and Oliveira showed recently a pathogenic mutant cluster in a human RPD model and proposed the cluster as a possible ssDNA binding region (7). To assess ssDNA binding by the human RPD, four putative ssDNA binding variants were designed based on the human RPD model of Kaguni and Oliveira (7). I subcategorized the cluster into two areas. One contains well-studied adPEO mutants: W315L, K319X, R334Q, and P335L (Fig. 18, blue) and the other contains three arginine residues: R303W/Q, R354P, and R357P (Fig. 18, cyan). In addition, a highly positively charged loop connects two parallel areas at one end. The loop has four positive residues in the context of RKxxxKR between motifs V and VI, although no pathogenic mutations in this loop have been identified (Fig. 18, yellow). One putative ssDNA binding area located in motif II and towards the TOPRIM fold was selected from outside of the pathogenic mutation cluster region. The area represents an entry to the catalytic ssDNA binding groove found in the prokaryotic homologs (11). G181, K184, and D187 are the homologous residues that have interactions with the phosphate backbone or bases of ssDNA. One or two residues per area were chosen for alanine substitution: W315A/ K319A, R303A, K328A/ R329A, and K184A/ D187A, respectively. The mutations were generated by site-directed mutagenesis in a construct of N-terminally SUMO-tagged wild type RPD (P146-S366). The wild type and variant forms were produced in *E. coli* and purified by affinity

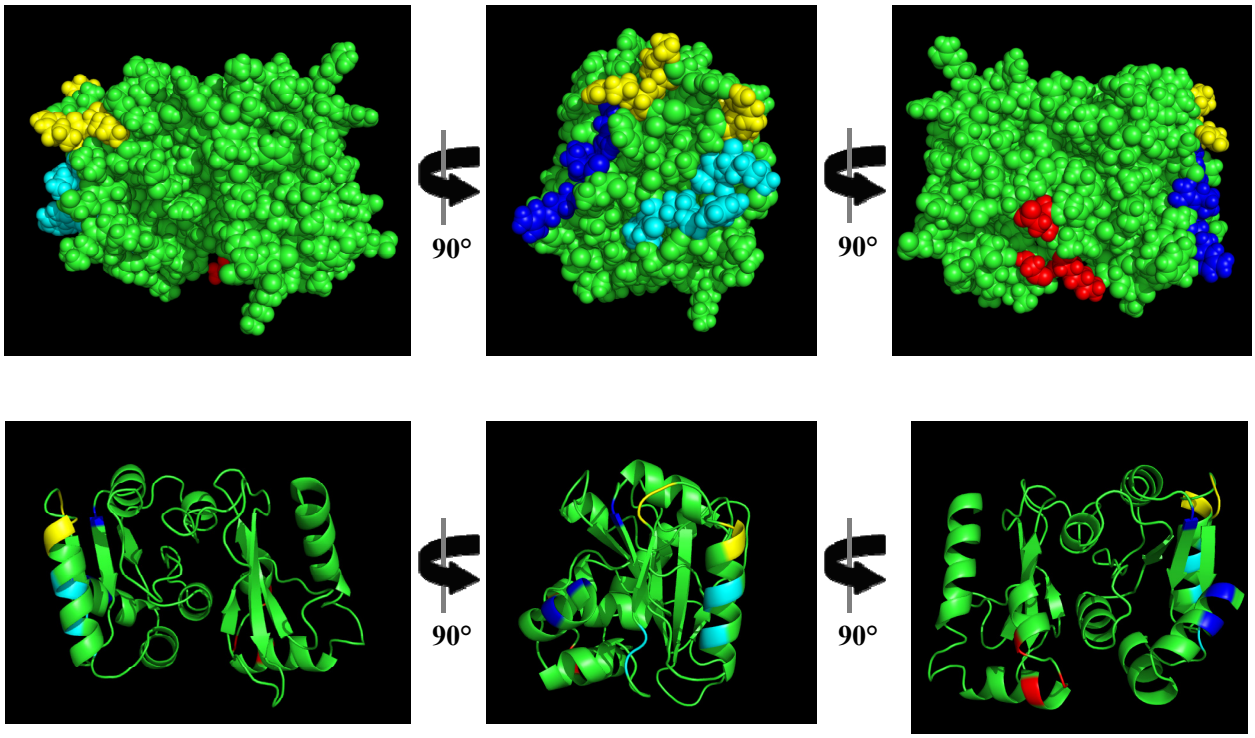

Figure 18. **Putative ssDNA binding areas on a human RPD model** The amino acid residues in the predicted ssDNA binding areas on the human RPD model are colored differently. Residues for disease mutations in two pathogenic mutant areas are colored with cyan and blue. Positively charged residues in the RKxxxKR loop are yellow. Residues at the entrance of the catalytic ssDNA binding groove are colored red. The human RPD model was generated by Kaguni and Oliveira (7).

chromatography and either gel filtration or glycerol gradient sedimentation. The SUMO tag was cleaved after affinity chromatography. The purification method for each protein was optimized to maximize yield (see Materials and Methods). The purified proteins are shown on an SDS-PAGE gel in Figure 19 A.

Variants in the putative ssDNA binding areas show reduced binding affinity to ssDNA.

To investigate ssDNA binding areas in the RPD of human mtDNA helicase, ssDNA binding affinities of the wild type RPD and its variants were measured first by gel mobility shift assay (GMSA). However, signals of ssDNA-bound proteins were not detected probably due to weak and/ or unstable interactions (data not shown). Thus, to capture the interactions, UV crosslinking was applied. A ^{32}P- labeled BrdU-substituted 60-mer oligonucleotide was used to monitor ssDNA binding. A crosslinked 60-mer oligonucleotide-bound wild type RPD was detected and its band intensity was proportional to concentration of the 60-mer oligonucleotide (Fig. 19 B and C). All variants showed reduced ssDNA binding affinity compared to the wild type (Fig. 19 B and C). K184A/ D187A, which lies near the ssDNA binding groove showed ~30% of the wild type activity. K328A/ R329A that is located in a positive loop between two disease mutant areas showed 20% of the wild type ssDNA binding activity. Both W315A/ K319A and R303A in the disease mutant cluster had ~10% of the ssDNA binding activity of the wild type (Fig. 19 B and C). These results indicate that all the hypothesized areas, including the pathogenic mutant cluster area, contribute to ssDNA binding by the human RPD. However, the signifiance of the reduced affinities of the variants remains to be assessed by independent experimental approaches.

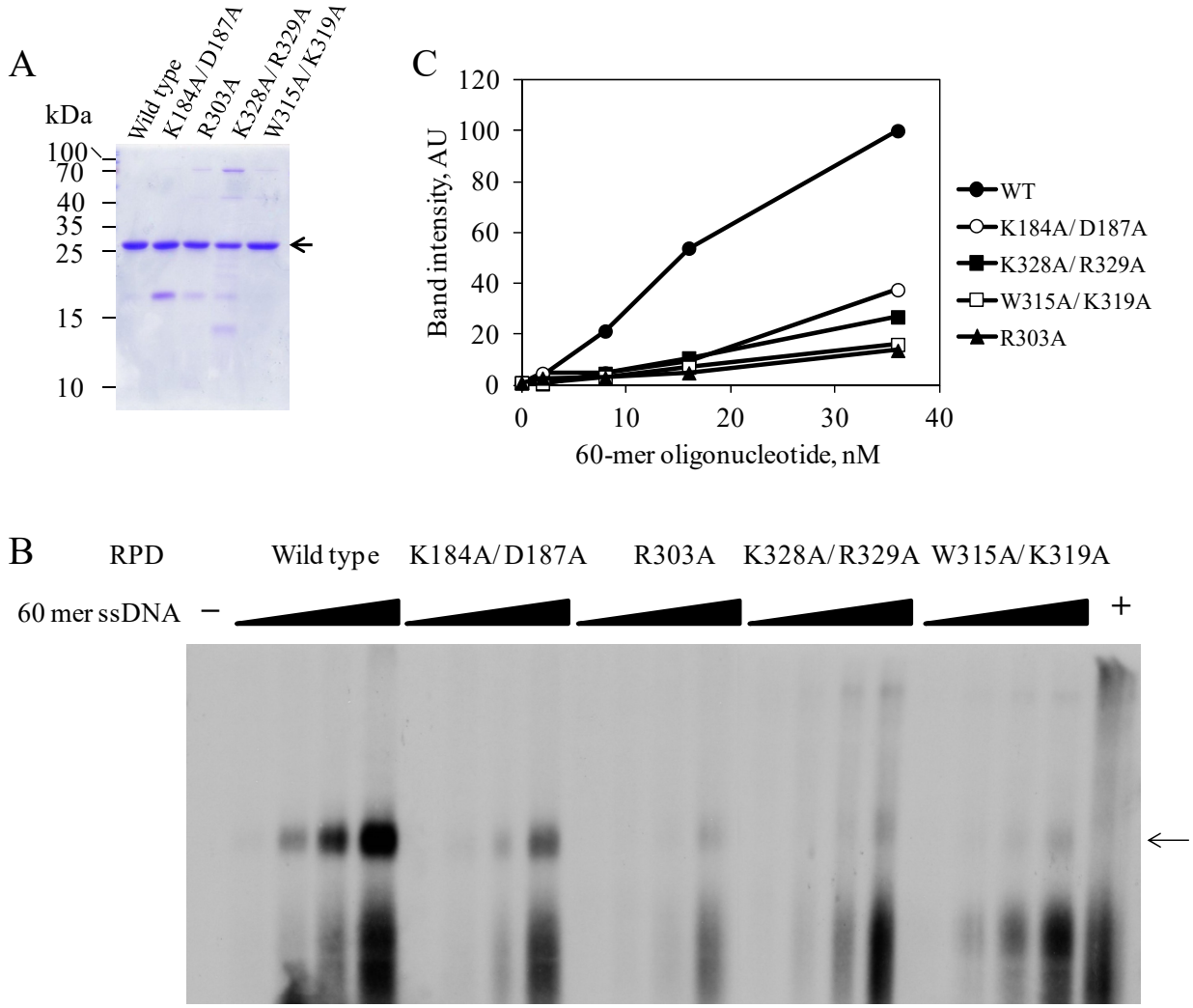

Figure 19. **UV crosslinking between human RPD variants and a BrdU substituted 60-mer oligonucleotide A.** Wild type RPD and its variants were expressed with an N-terminally tagged SUMO. Each variant had a different purification procedure to optimize yield (see Materials and Methods.) 30 pmol of each RPD variant was loaded on a 12% SDS-PAGE gel. Arrow indicates target proteins. **B.** Each RPD variant (30 pmol) was crosslinked with ^{32}P-labeled BrdU substituted 60-mer oligonucleotide (2 - 36 nM) under UV light (300 nm) for 30 min. The crosslinked samples were analyzed by 12% SDS-PAGE, and the gel was dried and exposed to X-ray film. The arrow indicates complexes of ssDNA-crosslinked RPD variants. Two negative controls were used; the lane marked by "–" is no oligo (0 nM) and the lane marked by "+" is oligo-only (10 nM).' **C.** The signal intensities of protein-ssDNA complexes in (B) were analyzed by ImageQuant 5.2 and plotted against the amount of 60-mer oligonucleotide. Protein amounts in the assay were normalized by intensities of target protein bands in the SDS-PAGE gel in (A).

DISCUSSION

Metazoan mitochondrial DNA helicases that do not have primase activity in their primase-like domains (the N-terminal domain) provoke a question about its roles. An interesting study performed by our research group discovered the presence of an iron-sulfur cluster in *Drosophila* mtDNA helicase (8) and prompted further experimentation. In this study, an NTD-only variant-expressing *Drosophila* S2 cell line was established to evaluate structural and functional characteristics of the protein that were demonstrated earlier in the *Dm* NTD (N24-A333) overexpressed in *E. coli* (8). As a homologous recombinant protein, the *Dm* NTD overexpressed in *Drosophila* cells should be structurally and functionally more similar to the endogenous NTD of *Dm* mtDNA helicase than the NTD overexpressed from *E. coli*. It is processed by endogenous mechanisms such as post-translational modifications and mitochondrial transport by its canonical N-terminal mitochondrial targeting sequence, without the metal cofactor misincorporation that occurs occasionally in heterologously-expressed proteins (30,31). Thus, detection of non-heme iron ions in the NTD from overexpressing *Drosophila* S2 cells by potassium ferricyanide staining shows that the iron-sulfur cluster exists as a *bona fide* component in *Dm* mtDNA helicase. In addition, sequence determination of N-terminal residues in the mature NTD from *Drosophila* S2 cells also supports our previous results (8), indicating that our estimation of the first N-terminal residue at position, N24, was close to that of the actual mature protein, A26.

The presence of an iron-sulfur cluster in *Drosophila* mtDNA helicase allows possible roles for the NTD in redox potential sensing and electron transfer. An iron-sulfur cluster has been identified in many nuclear DNA replicative proteins (DNA polymerases α, δ, and ε (32), primase (33), helicase-nuclease Dna2 (34)) and repair proteins (base exclusion repair: Endo III/ MutY

(35,36); nucleotide exclusion repair: XPD (37)). Iron-sulfur clusters of glycosylases have a clear catalytic role, but their roles in other DNA processing proteins have not been clearly elucidated (26). Other nuclear DNA processing, iron-sulfur cluster containing proteins are thought to have the iron-sulfur cluster for structural stability like *Dm* mtDNA helicase. However, when we consider the fact that a zinc ion is more stable and can be substituted instead of an iron-sulfur cluster for structural stability (26), it raises the question why these proteins keep the oxygen labile iron-sulfur cluster over the zinc ion. Recently, an interesting concept called DNA-mediated charge transfer (DNA-CT) was proposed and demonstrated with human DNA primase (38), related to roles of iron-sulfur clusters in redox sensing and electron transfer, particularly in replicative and repair proteins (26,39). DNA binding iron-sulfur cluster proteins can transfer a charge to other DNA binding iron-sulfur cluster proteins through the pi-stacking of DNA base pairs. This is sensitive enough to recognize DNA damage that perturbs base pair stacking. A role for *Dm* mtDNA helicase in DNA-CT is plausible. In *Drosophila* cells, another iron-sulfur cluster nuclease-helicase, Dna2, (34,40) is present, working in long-patch basic excision repair in mitochondrial DNA. *Dm* mtDNA helicase and *Dm* Dna2 might be coordinated by DNA-CT to regulate mtDNA replication and repair.

In this study, the direct interaction between *Dm* NTD and the membrane was demonstrated. Membrane association is expected in both human and *Drosophila* mtDNA helicases. It has been observed that both the endogenous and an overexpressed *Drosophila* mtDNA helicases are found largely in the pellet fraction during preparation of a mitochondrial extract (data not shown). Similarly, Spelbrink and coworkers reported that the mtDNA helicase in human HEK293 cells is also found in the pellet and it is soluble when treated with a detergent (TX100) and a salt (sodium carbonate) (17). In addition, upon digitonin treatment the human

mtDNA helicase behaved similar to COX II, a transmembrane protein (17), implying its membrane association. However, a direct *in vitro* interaction between mtDNA helicases and lipid membranes has not been reported in any organism, and membrane binding motifs in the protein are still unknown, including any potential amphipathic helix, a well-known membrane-associated motif. Thus, the direct interaction between the NTD of *Dm* mtDNA helicase and liposomes in this study demonstrates clearly the membrane binding property of the mtDNA helicase.

Several aspects of mitochondrial membrane binding of *Dm* NTD were identified by lipid vesicle cosedimentation and intrinsic tryptophan fluorescence quenching of *Dm* NTD with liposomes and individual lipids. First, the interaction between the NTD and membranes is mediated largely by cardiolipin, an acidic lipid abundant in the mitochondrial inner membrane. Second, electrostatic interactions are likely formed between the acidic polar head of cardiolipin and a positively charged surface region of the NTD. The abolishment of interactions between *Dm* NTD and cardiolipin-containing liposomes by increased ionic strength supports this notion (Fig. 17. D). Electrostatic interaction is one of major mechanisms for membrane binding of peripheral membrane proteins (41). Though it is nonspecific, it is sufficient to recruit proteins to membranes. Finally, the assays demonstrated that cholesterol is not involved in membrane attachment of *Dm* NTD. The binding efficiency of *Dm* NTD to cholesterol-containing liposomes does not increase even at a level as high as 30% w/w cholesterol, which is similar to the level in lipid rafts (42) (Fig.16 A). The intrinsic tryptophan fluorescence quenching assay also did not show any lipid specific binding between *Dm* NTD and cholesterol (Fig. A2 and A3 A). This suggests that mtDNA helicase-mediated cholesterol-rich membrane binding by the mtDNA replisome might not occur. Cosedimentation of the human mtDNA helicase with cholesterol (18) is instead probably mediated by other cholesterol binding proteins such as ATAD, a

mitochondrial DNA nucleoid component that binds to the mitochondrial inner membrane (43).

ssDNA binding by mtDNA helicase is essential for its ssDNA annealing function (44) and the proposed DNA loading process in the helicase loader-free ring-opening model (45,46). Identification of ssDNA binding regions in the NTD allows study of these processes on a molecular level. The UV crosslinking assay employed here represents the first study to identify ssDNA binding regions within the RPD. Detection of RPD-ssDNA complexes was possible because the weak and transient complexes were trapped successfully by UV crosslinking. To improve detection of weak binding, a specific substrate was also used that contains sequences of the human mitochondrial DNA (the TAS site in D-loop region (Fig. 1 in chapter 1), where human mtDNA helicase is likely to be reloaded and reinitiated (47)). In addition, use of excess BSA helped to maintain the structural stability of the RPD and reduce non-specific binding. Establishment of the UV crosslinking assay for RPD-ssDNA complexes is valuable for X-ray crystallography and facilitates understanding of the binding mechanism between the NTD and ssDNA at the molecular level. However, to confirm the results of the UV crosslinking assay and to measure binding affinity of variant-ssDNA complexes, an alternative method is necessary. Biolayer interferometry, a sensitive and useful method for replicative protein-protein and protein-DNA binding (48), can be pursued in future studies.

The UV crosslinking assay of four human mtDNA RPD variants defined two possible ssDNA binding regions in human RPD: a pathogenic mutant cluster and the entry to the analogous catalytic ssDNA binding shallow groove in prokaryotic primases. The pathogenic mutant cluster presented by variants R303A, W315A/ K319A, and K328A/ R329A in the TOPRIM subdomain faces the C-terminal domain of its neighboring protomer in the EM structure observed by Sola and coworkers (3) and in the unpublished homology model developed

by our research group. Whether the pathogenic mutant cluster region forms a binding interface with residues in the C-terminal domain remains unclear and warrants additional investigation. The ssDNA binding property of this cluster region is supported by the nature of the pathogenic mutations. Eight of twelve pathogenic mutations in the cluster change their amino acids from basic to neutral or acidic, likely abolishing ionic bonds between the positively-charged residues and negatively-charged DNA backbones. Moreover, several biochemical and physiological studies about these pathogenic mutants in the TOPRIM subdomain have been conducted (6,9,21,49). Reduced ssDNA activity has been commonly reported, although the extent of its effects on other helicase activities is variable. The reduction of ssDNA binding in the variant K184A/ D187A identifies ssDNA contacts at the entry of the catalytic ssDNA binding groove in human RPD. However, more variants within this region should be tested to clarify whether this region of the human RPD contains a ssDNA track that is homologous to the catalytic ssDNA binding track in other prokaryotic primases. In addition, exit channel for a DNA template in the prokaryotic homologs is located perpendicular to the catalytic ssDNA binding track in DnaG, but the homologous amino acids in the human RPD model lie on the surface of the RPD model with a different orientation, proposed as another possible ssDNA binding track of the RPD (7,11).

Studies in this chapter demonstrate that the N-terminal domains of human and *Drosophila* mtDNA helicases play roles in binding to cofactors, lipids, and ssDNA. The physiological roles for these physical interactions need to be clarified in future work.

CONCLUSIONS

The N-terminal domains of human and *Drosophila* mtDNA helicases play a role as a binding module. *Drosophila* mtDNA helicase NTD binds to an iron-sulfur cluster and membranes, and human mtDNA helicase NTD has ssDNA binding properties.

Biological and evolutionary roles for the species-specific iron-sulfur cluster in *Dm* mtDNA helicase warrant future investigation. Considering the recent discovery of a DNA-charge transferring role in the human nuclear, 4Fe-4S cluster-containing DNA primase (38), I propose that DNA binding by *Dm* mtDNA helicase may be regulated by redox signaling of the ISC in the NTD through DNA-charge transfer.

The phospholipid membrane binding property of the NTD, which appears to be more specific for liposomes mimicking the lipid content of the mitochondrial inner membrane, supports the idea that the NTD of the helicase docks to the mitochondrial inner membrane and recruits mtDNA to initiate the unwinding process and replication in mitochondria.

The positively-charged region where pathogenic mutants are clustered in the RPD of human mtDNA helicase contributes to ssDNA binding. Further studies of ssDNA binding region will help to understand mechanisms of mtDNA helicase self-loading, translocation, and annealing in which ssDNA contact by the NTD may be required.

APPENDIX

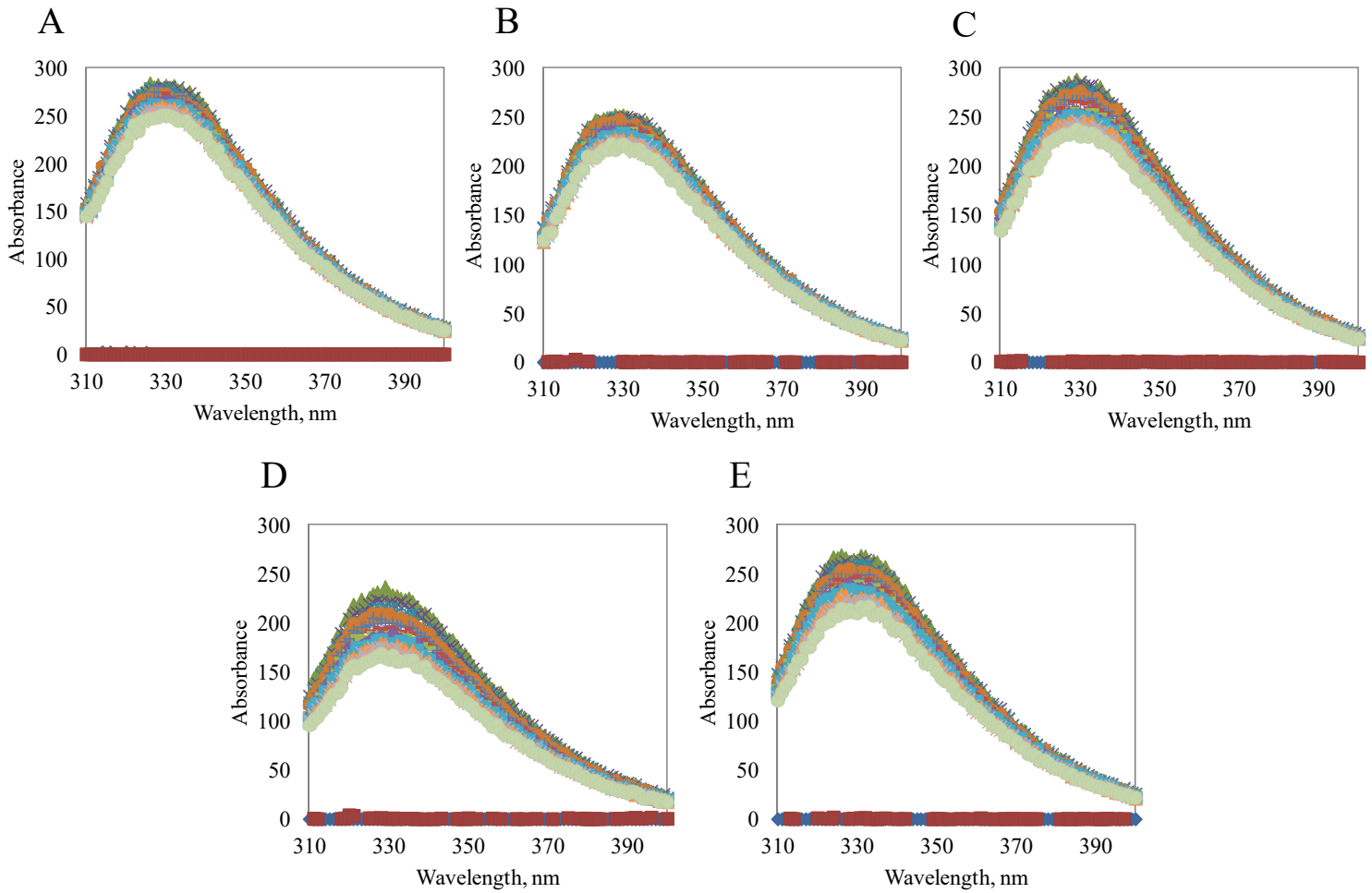

Figure A1. **Emission spectra of *Dm* NTD in various buffers A-C**, Tris-HCl buffer (50 mM Tris-HCl, pH7.5, 150 mM NaCl, 10% glycerol (A), 5% glycerol (B), 0% glycerol(C)) **D,** Ammonium bicarbonate buffer (10 mM NH_4HCO_3, 10% glycerol) **E**, PBS buffer. All buffers have 5 mM β-mercaptoethanol. A spectrum was obtained every 2 minutes for 28 minutes. Dark and faint green spectra are the first and the last measurements, respectively. Red/ blue lines near 0 are the spectra measured without protein.

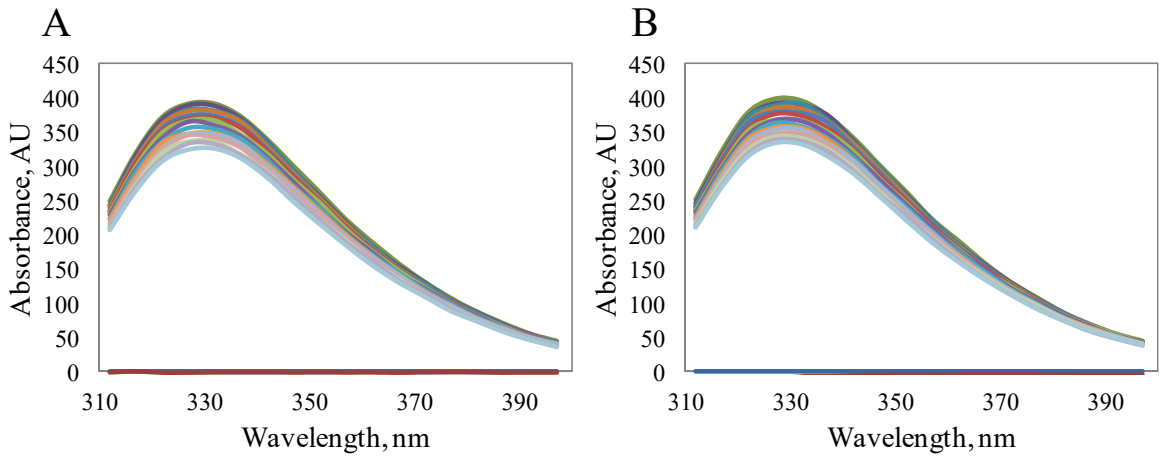

Figure A2. **Emission spectra of *Dm* NTD with cholesterol (A) and with solvent (ethanol) (B) by intrinsic tryptophan fluorescence quenching** The final concentration of *Dm* NTD was 100 nM and the excitation wavelength was 288 nm. Cholesterol (A) was added to the selected buffer (50 mM Tris-HCl, pH7.5, 150 mM NaCl, 5% glycerol, 5 mM β- mercaptoethanol) every 2 minutes for 28 minutes, resulting in 0 - 140 nM of final cholesterol concentration. Alternatively, the same volume of 99.5% ethanol (solvent) (B) was added instead of cholesterol. The dark green spectrum on the top is the first measurement and the faint blue spectrum on the bottom is the last measurement.

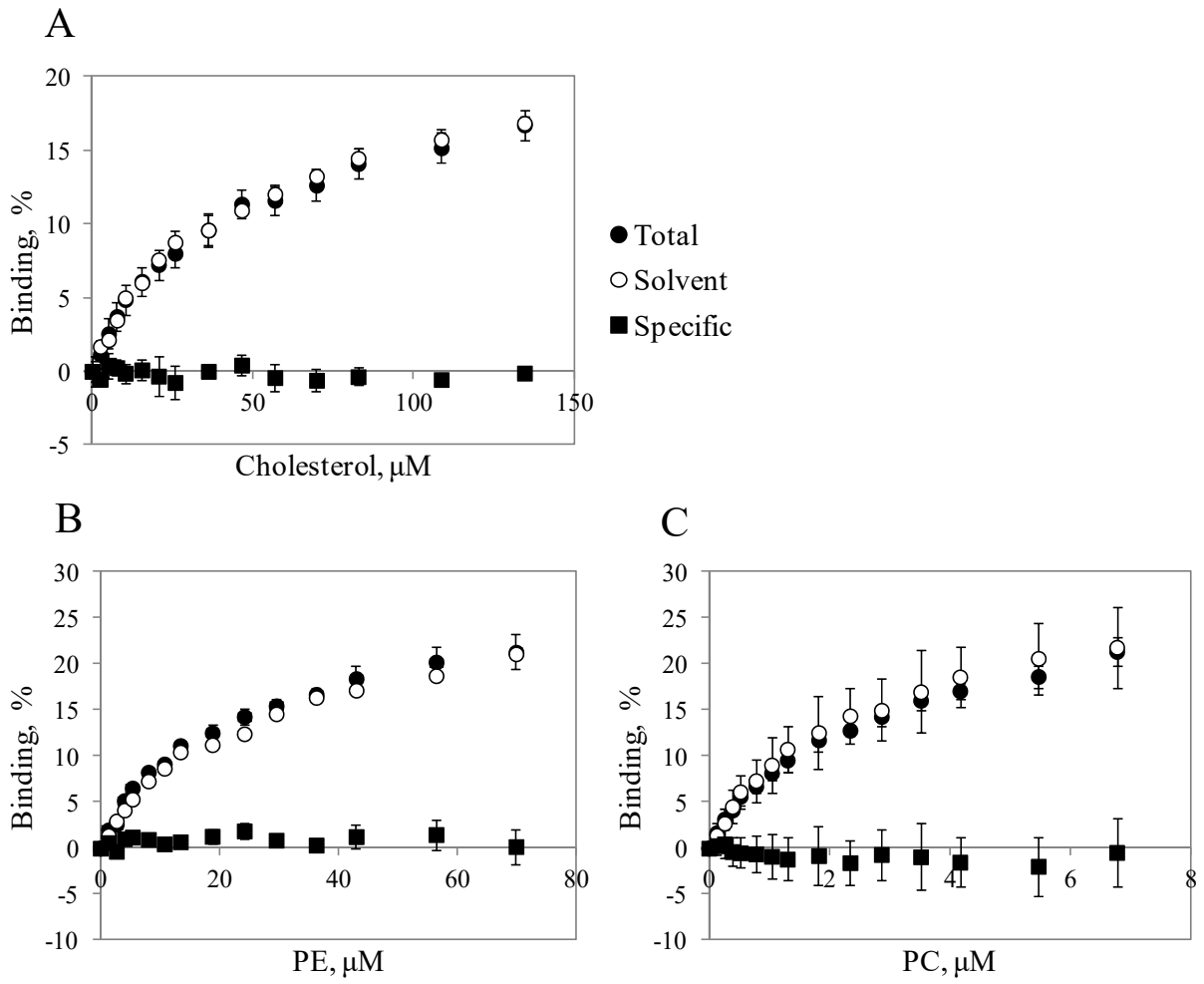

Figure A3. **Saturation curves of *Dm* NTD binding to individual lipids: cholesterol (A), PE (B), or PC (C) by intrinsic tryptophan fluorescence quenching assays** Specific binding (closed squares) was obtained by subtracting solvent binding (open circles) from total binding (closed circles). Each data point represents the mean of triplicate (total) or duplicate (solvent) measurements and the data point of specific binding is the mean of six possible calculations. The error bars indicate ± standard deviation.

BIBLIOGRAPHY

BIBLIOGRAPHY

1. Ilyina, T. V., Gorbalenya, A. E., and Koonin, E. V. (1992) Organization and evolution of bacterial and bacteriophage primase-helicase systems. *Journal of molecular evolution* **34**, 351-357

2. Shutt, T. E., and Gray, M. W. (2006) Twinkle, the mitochondrial replicative DNA helicase, is widespread in the eukaryotic radiation and may also be the mitochondrial DNA primase in most eukaryotes. *Journal of molecular evolution* **62**, 588-599

3. Fernandez-Millan, P., Lazaro, M., Cansiz-Arda, S., Gerhold, J. M., Rajala, N., Schmitz, C. A., Silva-Espina, C., Gil, D., Bernado, P., Valle, M., Spelbrink, J. N., and Sola, M. (2015) The hexameric structure of the human mitochondrial replicative helicase Twinkle. *Nucleic acids research* **43**, 4284-4295

4. Lee, S. J., and Richardson, C. C. (2002) Interaction of adjacent primase domains within the hexameric gene 4 helicase-primase of bacteriophage T7. *Proceedings of the National Academy of Sciences of the United States of America* **99**, 12703-12708

5. Kato, M., Ito, T., Wagner, G., Richardson, C. C., and Ellenberger, T. (2003) Modular architecture of the bacteriophage T7 primase couples RNA primer synthesis to DNA synthesis. *Molecular cell* **11**, 1349-1360

6. Holmlund, T., Farge, G., Pande, V., Korhonen, J., Nilsson, L., and Falkenberg, M. (2009) Structure-function defects of the twinkle amino-terminal region in progressive external ophthalmoplegia. *Biochimica et biophysica acta* **1792**, 132-139

7. Kaguni, L. S., and Oliveira, M. T. (2016) Structure, function and evolution of the animal mitochondrial replicative DNA helicase. *Critical reviews in biochemistry and molecular biology* **51**, 53-64

8. Stiban, J., Farnum, G. A., Hovde, S. L., and Kaguni, L. S. (2014) The N-terminal domain of the Drosophila mitochondrial replicative DNA helicase contains an iron-sulfur cluster and binds DNA. *The Journal of biological chemistry* **289**, 24032-24042

9. Matsushima, Y., and Kaguni, L. S. (2009) Functional importance of the conserved N-terminal domain of the mitochondrial replicative DNA helicase. *Biochimica et biophysica acta* **1787**, 290-295

10. Kato, M., Ito, T., Wagner, G., and Ellenberger, T. (2004) A molecular handoff between bacteriophage T7 DNA primase and T7 DNA polymerase initiates DNA synthesis. *The Journal of biological chemistry* **279**, 30554-30562

11. Corn, J. E., Pelton, J. G., and Berger, J. M. (2008) Identification of a DNA primase

template tracking site redefines the geometry of primer synthesis. *Nature structural & molecular biology* **15**, 163-169

12. Keck, J. L., Roche, D. D., Lynch, A. S., and Berger, J. M. (2000) Structure of the RNA polymerase domain of E. coli primase. *Science* **287**, 2482-2486

13. Lee, S. J., and Richardson, C. C. (2005) Acidic residues in the nucleotide-binding site of the bacteriophage T7 DNA primase. *The Journal of biological chemistry* **280**, 26984-26991

14. Farge, G., Holmlund, T., Khvorostova, J., Rofougaran, R., Hofer, A., and Falkenberg, M. (2008) The N-terminal domain of TWINKLE contributes to single-stranded DNA binding and DNA helicase activities. *Nucleic acids research* **36**, 393-403

15. Oliveira, M. T., and Kaguni, L. S. (2011) Reduced stimulation of recombinant DNA polymerase gamma and mitochondrial DNA (mtDNA) helicase by variants of mitochondrial single-stranded DNA-binding protein (mtSSB) correlates with defects in mtDNA replication in animal cells. *The Journal of biological chemistry* **286**, 40649-40658

16. Guruharsha, K. G., Obar, R. A., Mintseris, J., Aishwarya, K., Krishnan, R. T., Vijayraghavan, K., and Artavanis-Tsakonas, S. (2012) Drosophila protein interaction map (DPiM): a paradigm for metazoan protein complex interactions. *Fly* **6**, 246-253

17. Rajala, N., Gerhold, J. M., Martinsson, P., Klymov, A., and Spelbrink, J. N. (2014) Replication factors transiently associate with mtDNA at the mitochondrial inner membrane to facilitate replication. *Nucleic acids research* **42**, 952-967

18. Gerhold, J. M., Cansiz-Arda, S., Lohmus, M., Engberg, O., Reyes, A., van Rennes, H., Sanz, A., Holt, I. J., Cooper, H. M., and Spelbrink, J. N. (2015) Human Mitochondrial DNA-Protein Complexes Attach to a Cholesterol-Rich Membrane Structure. *Scientific reports* **5**, 15292

19. Hein, M. Y., Hubner, N. C., Poser, I., Cox, J., Nagaraj, N., Toyoda, Y., Gak, I. A., Weisswange, I., Mansfeld, J., Buchholz, F., Hyman, A. A., and Mann, M. (2015) A human interactome in three quantitative dimensions organized by stoichiometries and abundances. *Cell* **163**, 712-723

20. Guruharsha, K. G., Rual, J. F., Zhai, B., Mintseris, J., Vaidya, P., Vaidya, N., Beekman, C., Wong, C., Rhee, D. Y., Cenaj, O., McKillip, E., Shah, S., Stapleton, M., Wan, K. H., Yu, C., Parsa, B., Carlson, J. W., Chen, X., Kapadia, B., VijayRaghavan, K., Gygi, S. P., Celniker, S. E., Obar, R. A., and Artavanis-Tsakonas, S. (2011) A protein complex network of Drosophila melanogaster. *Cell* **147**, 690-703

21. Longley, M. J., Humble, M. M., Sharief, F. S., and Copeland, W. C. (2010) Disease variants of the human mitochondrial DNA helicase encoded by C10orf2 differentially

alter protein stability, nucleotide hydrolysis, and helicase activity. *The Journal of biological chemistry* **285**, 29690-29702

22. Matsushima, Y., and Kaguni, L. S. (2007) Differential phenotypes of active site and human autosomal dominant progressive external ophthalmoplegia mutations in Drosophila mitochondrial DNA helicase expressed in Schneider cells. *The Journal of biological chemistry* **282**, 9436-9444

23. Korhonen, J. A., Pande, V., Holmlund, T., Farge, G., Pham, X. H., Nilsson, L., and Falkenberg, M. (2008) Structure-function defects of the TWINKLE linker region in progressive external ophthalmoplegia. *Journal of molecular biology* **377**, 691-705

24. Najt, C. P., Lwande, J. S., McIntosh, A. L., Senthivinayagam, S., Gupta, S., Kuhn, L. A., and Atshaves, B. P. (2014) Structural and functional assessment of perilipin 2 lipid binding domain(s). *Biochemistry* **53**, 7051-7066

25. Quiros, P. M., Langer, T., and Lopez-Otin, C. (2015) New roles for mitochondrial proteases in health, ageing and disease. *Nature reviews. Molecular cell biology* **16**, 345-359

26. Fuss, J. O., Tsai, C. L., Ishida, J. P., and Tainer, J. A. (2015) Emerging critical roles of Fe-S clusters in DNA replication and repair. *Biochimica et biophysica acta* **1853**, 1253-1271

27. Leong, L. M., Tan, B. H., and Ho, K. K. (1992) A specific stain for the detection of nonheme iron proteins in polyacrylamide gels. *Analytical biochemistry* **207**, 317-320

28. Yamaguchi, M., and Kasamo, K. (2001) Modulation in the activity of purified tonoplast H+-ATPase by tonoplast glycolipids prepared from cultured rice (Oryza sativa L. var. Boro) cells. *Plant & cell physiology* **42**, 516-523

29. Horvath, S. E., and Daum, G. (2013) Lipids of mitochondria. *Progress in lipid research* **52**, 590-614

30. Kocabas, E., Liu, H., and Hernick, M. (2015) Identity of cofactor bound to mycothiol conjugate amidase (Mca) influenced by expression and purification conditions. *Biometals : an international journal on the role of metal ions in biology, biochemistry, and medicine* **28**, 755-763

31. Waldron, K. J., Rutherford, J. C., Ford, D., and Robinson, N. J. (2009) Metalloproteins and metal sensing. *Nature* **460**, 823-830

32. Netz, D. J., Stith, C. M., Stumpfig, M., Kopf, G., Vogel, D., Genau, H. M., Stodola, J. L., Lill, R., Burgers, P. M., and Pierik, A. J. (2012) Eukaryotic DNA polymerases require an iron-sulfur cluster for the formation of active complexes. *Nature chemical biology* **8**, 125-132

33. Weiner, B. E., Huang, H., Dattilo, B. M., Nilges, M. J., Fanning, E., and Chazin, W. J. (2007) An iron-sulfur cluster in the C-terminal domain of the p58 subunit of human DNA primase. *The Journal of biological chemistry* **282**, 33444-33451

34. Pokharel, S., and Campbell, J. L. (2012) Cross talk between the nuclease and helicase activities of Dna2: role of an essential iron-sulfur cluster domain. *Nucleic acids research* **40**, 7821-7830

35. Boal, A. K., Yavin, E., and Barton, J. K. (2007) DNA repair glycosylases with a [4Fe-4S] cluster: a redox cofactor for DNA-mediated charge transport? *Journal of inorganic biochemistry* **101**, 1913-1921

36. Genereux, J. C., Boal, A. K., and Barton, J. K. (2010) DNA-mediated charge transport in redox sensing and signaling. *Journal of the American Chemical Society* **132**, 891-905

37. Fan, L., Fuss, J. O., Cheng, Q. J., Arvai, A. S., Hammel, M., Roberts, V. A., Cooper, P. K., and Tainer, J. A. (2008) XPD helicase structures and activities: insights into the cancer and aging phenotypes from XPD mutations. *Cell* **133**, 789-800

38. O'Brien, E., Holt, M. E., Thompson, M. K., Salay, L. E., Ehlinger, A. C., Chazin, W. J., and Barton, J. K. (2017) The [4Fe4S] cluster of human DNA primase functions as a redox switch using DNA charge transport. *Science* **355**

39. Arnold, A. R., Grodick, M. A., and Barton, J. K. (2016) DNA Charge Transport: from Chemical Principles to the Cell. *Cell chemical biology* **23**, 183-197

40. Duxin, J. P., Dao, B., Martinsson, P., Rajala, N., Guittat, L., Campbell, J. L., Spelbrink, J. N., and Stewart, S. A. (2009) Human Dna2 is a nuclear and mitochondrial DNA maintenance protein. *Molecular and cellular biology* **29**, 4274-4282

41. Whited, A. M., and Johs, A. (2015) The interactions of peripheral membrane proteins with biological membranes. *Chemistry and physics of lipids* **192**, 51-59

42. Pike, L. J. (2003) Lipid rafts: bringing order to chaos. *Journal of lipid research* **44**, 655-667

43. He, J., Cooper, H. M., Reyes, A., Di Re, M., Sembongi, H., Litwin, T. R., Gao, J., Neuman, K. C., Fearnley, I. M., Spinazzola, A., Walker, J. E., and Holt, I. J. (2012) Mitochondrial nucleoid interacting proteins support mitochondrial protein synthesis. *Nucleic acids research* **40**, 6109-6121

44. Sen, D., Nandakumar, D., Tang, G. Q., and Patel, S. S. (2012) Human mitochondrial DNA helicase TWINKLE is both an unwinding and annealing helicase. *The Journal of biological chemistry* **287**, 14545-14556

45. Ahnert, P., Picha, K. M., and Patel, S. S. (2000) A ring-opening mechanism for DNA

binding in the central channel of the T7 helicase-primase protein. *The EMBO journal* **19**, 3418-3427

46. Crampton, D. J., Ohi, M., Qimron, U., Walz, T., and Richardson, C. C. (2006) Oligomeric states of bacteriophage T7 gene 4 primase/helicase. *Journal of molecular biology* **360**, 667-677

47. Jemt, E., Persson, O., Shi, Y., Mehmedovic, M., Uhler, J. P., Davila Lopez, M., Freyer, C., Gustafsson, C. M., Samuelsson, T., and Falkenberg, M. (2015) Regulation of DNA replication at the end of the mitochondrial D-loop involves the helicase TWINKLE and a conserved sequence element. *Nucleic acids research* **43**, 9262-9275

48. Ciesielski, G. L., Hytonen, V. P., and Kaguni, L. S. (2016) Biolayer Interferometry: A Novel Method to Elucidate Protein-Protein and Protein-DNA Interactions in the Mitochondrial DNA Replisome. *Methods in molecular biology* **1351**, 223-231

49. Goffart, S., Cooper, H. M., Tyynismaa, H., Wanrooij, S., Suomalainen, A., and Spelbrink, J. N. (2009) Twinkle mutations associated with autosomal dominant progressive external ophthalmoplegia lead to impaired helicase function and in vivo mtDNA replication stalling. *Human molecular genetics* **18**, 328-340

CHAPTER 4
Biochemical properties of *Drosophila* Ind1

ABSTRACT

The *Drosophila* mitochondrial DNA replicative helicase has an iron-sulfur cluster in its N-terminal domain (1). The cofactor is species-specific. In the *Drosophila* mitochondrial proteome, CG3262 was found as an interacting partner of the *Dm* mtDNA helicase by high-throughput AP-MS (coaffinity purification- mass spectrometry) (2). A homology search identified CG3262 protein (*Dm* Ind1) as the *Drosophila* homolog of human Ind1 that is known as a donor of an iron-sulfur cluster specifically to NADH dehydrogenase (3,4). In considering the possibility that the CG3262 protein serves as the iron-sulfur cluster transfer protein for *Dm* mtDNA helicase, mitochondrial localization, cofactor-independent dimerization and membrane binding property of *Dm* Ind1 were investigated. In particular, the membrane binding properties of *Dm* Ind1 is driven by both electrostatic interactions and hydrophobic interactions and thought to facilitate iron-sulfur cluster transfer of *Dm* Ind1 to membrane-bound recipients including *Dm* mtDNA helicase, a putative partner. Significant physiological effects on mtDNA replication in *Dm* Ind1 knockdown cells, however, were not detected in either mtDNA copy number or mitochondrial mass. This result argues that a reduced level of *Dm* Ind1 is sufficient for cell metabolism as described earlier in several clinical cases (5-7). Comparison of the characterized features of *Dm* Ind1 with other family members that form binding interfaces depending on dimerization, nucleotide binding, ATP hydrolysis and membrane binding, I suggest that protein-protein interactions of *Dm* Ind1 are ATP dependent. Testing this hypothesis will clarify the possibility of complex formation between *Dm* mtDNA helicase and *Dm* Ind1, which was not detected by *in vitro* chemical crosslinking.

INTRODUCTION

Mitochondrial P-loop NTPase Ind1 (an **i**ron-sulfur cluster assembly protein known to be required specifically for **N**ADH **d**ehydrogenase) transfers iron-sulfur clusters to targeted apoproteins at the terminal stage of the iron-sulfur cluster assembly process in mitochondria (3,4,8). Ind1 transfers 4Fe-4S clusters to complex I, which contains six 4Fe-4S clusters out of eight iron-sulfur clusters (3,4,9). In humans, it is also called NUBPL (**nu**cleotide-**b**inding **p**rotein-**l**ike) (4,10).

Ind1 shows strong specificity for complex I proteins in yeast and humans (3,4). The Ind1 deletion mutant in the yeast *Yarrowia lipolytica* shows only ~30% residual activity and ~20% of the relative abundance of complex I compared to wild type, suggesting that the decreased activity is caused by a decrease in the complex I level (3). Likewise, a knockdown mutant of Ind1 in human HeLa cells showed a 3- to 4-fold decrease in complex I activity and reduced complex I assembly (4). However, no such reduction in activity or assembly was detected in other mitochondrial iron-sulfur cluster proteins such as aconitase, complex II or complex III, all of which contain iron-sulfur clusters as cofactors (3,4). Despite its strong specificity for complex I, the 30% residual activity of complex I in the Ind1 deletion mutant suggests the possibility of involvement of other iron-sulfur cluster delivery proteins for insertion of iron-sulfur clusters to complex I in addition to Ind1.

Since Ind1 was identified as a disease-related gene after next-generation exome sequencing from a cohort with complex I deficiency symptoms (11), disease mutants of Ind1 have been investigated with clinical and biochemical approaches (5,6,12). Compound heterozygous mutations are most frequently found in patients with an Ind1 genetic disorder. A missense mutation (c.166G>A (p.G56R)) and a branch-site mutation (c.815-27T>C), in

particular, are found in the same allele in all patients except one who has a balanced familial chromosome translocation that can disrupt Ind1 expression (7). Biochemical studies show that the branch-site mutation causes splicing abnormalities resulting in three Ind1 variants: a frameshifted p.D273QfsX31, a frameshifted and early terminated p.G272VfsX11, and the normally spliced wild type Ind1 (5). A subject with the heterozygous branch-site mutation shows reduced mRNA (74%) and protein (59%) expression of Ind1, but the G56R missense mutant introduced into patient fibroblasts is expressed normally and even rescues complex I activity. Interestingly, a homozygous individual having the branch-site mutation is expected to express ~30% of Ind1 but exhibits subclinical phenotype with only partially impaired complex I function (5). In addition, a healthy sibling of the patient with the balanced familial chromosome translocation was asymptomatic with 30% of the Ind1protein level and the expression of complex I level was not altered significantly (7). These results show that complex I activity is maintained by a minimal level of Ind1 (~30% of wild type).

Ind1 belongs to the Mrp/ MinD family in the P-loop NTPase superfamily (13). Within the Mrp/ MinD family, Ind1 is classified as a Nbp35/ Mrp subfamily member with Nbp35 and Cdf1, which are iron-sulfur cluster scaffold proteins in the cytosolic iron-sulfur cluster assembly (CIA) pathway. An Nbp35 homodimer and a Cdf1 homodimer make a heterotetramer that harbors three 4Fe-4S clusters (14).Members of the Nbp35/ Mrp subfamily including Nbp35, Cdf1, and Ind1 share several conserved motifs: Walker A (P-loop), Walker B, and Mrp signature, as well as CxxC motifs that coordinate an iron-sulfur cluster. The Walker A motif (xKGGxxK[T/S]) is for nucleotide phosphate group binding, and the Walker B motif (DxxG) is involved in binding to magnesium ions (15). The Mrp signature (Wxx[LIVM]D[VFY][LIVM](3)DxPPGT[GS]D) defined in PROSITE (PDOC00935) that follows the P-loop motif is a conserved pattern in Mrp/

MinD family members. The N-terminal part of the Nbp35/ Mrp subfamily, however, has sequence diversity, resulting in different subcelluar localizations (16). Ind1 harbors a canonical N-terminal mitochondrial targeting sequence, while Nbp35 and Cdf1, without the targeting sequence, have cytosolic localization and function in CIA pathway. Compared to proteins in other subfamilies of the Mrp/ MinD family (13), structure-function relationships in protein-protein binding interactions in the Nbp35/ Mrp subfamily remain unclear. The proteins have been studied with a limited emphasis on in iron-sulfur clusters, although it was reported that an Nbp35 homodimer and a Cdf1 homodimer form heterotetramers that harbor three 4Fe-4S clusters (14).

The Mrp/ MinD family encompasses eight subfamilies. The protein members are widespread in all organelles of a cell and have diverse roles: chromosomal partitioning (MinD and Soj) (17,18), drug transport (Mrp) (19), flagellation in polar flagellates (FlhG) (20), electron transfer in nitrogen assimilation (NifH) (21), newly synthesized membrane protein transpor (Get3) (22,23) and iron-sulfur cluster assembly (Nbp35 and Cdf1) (14). These functionally different family members show structural similarity, sharing a featured KGG signature in the Walker A motif (13). All proteins in this Mrp/ MinD family are thought to be dimers because the conserved lysine residue in the signature interacts with the terminal oxygen atom of the β phosphate group of ATP that binds in the other protomer (13,24). Most of the family members, including the above mentioned proteins, form complexes with binding partners to achieve their functions. Conformational changes in their dimeric forms are linked to ATP/ ADP binding and ATP hydrolysis, regulating protein-protein interactions or membrane association (17,21,25). Association to a specific membrane is observed in some proteins in this family. They use an amphipathic helix to bind to a membrane or to transport an amphipathic helix to a membrane. For instance, MinD and FlhG use the C-terminal amphipathic helix to anchor to the plasma

membrane and make a binding interface for interacting partners (MinE (26) and FlhM/Y(20), respectively). Get3 uses a membrane-bound interacting partner to tether itself to the ER membrane where it transfers a newly synthesized amphipathic helix (27,28). However, these common features have not been evaluated in proteins of the NBP35/ Mrp subfamily including Ind1.

In addition to a role in complex I assembly, Ind1 may serve other roles in *Drosophila* mitochondria. In *D. melanogaster* mitochondria, a physical interaction between a homolog of Ind1 (CG3262) and the mtDNA helicase was found by high-throughput co-affinity purification coupled with mass spectrometry (2), suggesting an expanded role for *Drosophila* Ind1 in mitochondrial DNA replication. This notion is supported by our recent discovery that the *Drosophila* mtDNA replicative helicase contains an iron-sulfur cluster (1).

Thus, I studied the structure and function of *Drosophila* Ind1 in order to understand its protein-protein interactions. Although the putative interaction between *Dm* mtDNA helicase and *Dm* Ind1was not detected *in vivo* or *in vitro* experiments under given conditions, mitochondrial localization, cofactor-independent dimerization, and membrane association of *Dm* Ind1 were demonstrated, and these characteristics allow new scientifically-plausible hypotheses about interactions between *Dm* Ind1 and its binding partner proteins (chapter 5). These are the first biochemical results to characterize Ind1 from this point of view. This research will contribute to understanding the binding mechanism(s) of Ind1 to the interacting partners for its proper function.

MATERIALS AND METHODS

cDNA preparation of CG3292

The CG3292 cDNA (Berkeley *Drosophila* Genome Project *Drosophila* Gene Collection clone, RE72832) was purchased from the *Drosophila* Genomics Resource Center. Because the RE72832 clone lacks 16 base pairs in its ORF, the missing nucleotides (5'-GCA GTT AAT TTT GCC T-3') were inserted by two cycles of site-directed mutagenesis using the following primers: LSK MS11-1F 5' GGA AAA AGC ACC GTG TTT TGC CTG CAG CTT GGC AAA AC-3', LSK MS11-1R 5'-GTT TTG CCA AGC TGC AGG CAA AAC ACG GTG CTT TTT CC-3, LSK MS11-2F 5'-GGA AAA AGC ACC GTG GCA GTT AAT TTT GCC TGC AGC-3', LSK MS11-2R 5'-GCT GCA GGC AAA ATT AAC TGC CAC GGT GCT TTT TCC-3'. The full-length ORF was confirmed by DNA sequencing and designated as pFlc-Ind1.

Construction of inducible expression vectors for Dm Ind1 in Drosophila S2 cells

The pMt-EGFP and pMt-HA vectors were constructed by insertion of PCR-amplified EGFP (enhanced GFP, 209 amino acids) or HA fragments (hemagglutinin, 9 amino acids), respectively, into the *Drosophila* expression vector, pMt (29). The following primers were used for the pMt-EGFP construct (LSK MS1F 5'-GGA GGA TCC ATG GTG AGC AAG GGC GAG GA-3' and LSK MS1R 5'- TCC ACT AGT TTA CTT GTA CAG CTC GTC CAT GC-3') and for the pMt-HA construct (LSK MS3F 5' GGA GGA TCC TAC CCA TAC GAT GTT C-3' and LSK MS3R 5'- AAC ACT AGT CTA CTA CAA GCT AGC-3').

For both C-terminally EGFP-tagged *Dm* Ind1 (M^1-H^{293}) and C-terminally HA-tagged *Dm* Ind1 (M^1-H^{293}), the ORF of the full-length CG3292 was amplified by PCR from pFlc-Ind1 with following primers: LSK MS13F, 5'-GGA CTC GAG ATG GAG CGT CTA TTG ATC-3' and

LSK MS13R, 5'- CCC GGA TCC ATG TGC ACT GTT ATT TTG-3.' To express recombinant *Dm* Ind1 proteins in *Drosophila* S2 cells, the PCR products were ligated to pMt-EGFP to obtain pMt-EGFP-Ind1, and pMt-HA to obtain pMt-HA-Ind1.

Generation and induction of transient cell lines and induction for Drosophila Ind1 in Drosophila S2 cells

S2 cells were transiently transfected with pMt-EGFP-Ind1 and pMt-HA-Ind1 by subculture and transfection as in the generation of stable cell lines of the *Dm* NTD (see Materials and Methods in chapter 2), except that the selection procedure was omitted. The recombinant *Dm* Ind1 proteins were induced for 3 days with 0.2 mM $CuSO_4$ at 48 hours after transfection.

Cloning, overexpression, and purification of Drosophila Ind1 in E. coli cells

For *E. coli* cell expression of the N-terminally His-tagged Ind1 (Met^{25}-His^{293}), the ORF was amplified by PCR from pFlc-Ind1 with the following primers: LSK MS25F 5'-TTA GGA TCC ATG GCG CGG GGA TTG C-3' and LSK MS17R 5'- CCA GTC GAC CTA CTA CAA GCT AGC GTA ATC-3'. The PCR product was then ligated into the pET28a vector (Novagen), generating pET28a-Ind1. Iron-sulfur cluster-deficient variant (C214A/ C217A) was constructed by side directed mutagenesis of pET28a-Ind1 using following primers LSK MS19F 5'-GAG AAC ATG AAG TAC ACC ATT GCT CAG AAC GCT AAT CAA CGA TTG GAG TTT TTT AAA G-3' and LSK MS 19R 5'- CTT TAA AAA ACT CCA ATC GTT GAT-3'.

The N-terminally His-tagged Ind1 ($Met2^{5}$-H^{293}) and its iron-sulfur cluster-deficient variant (C214A/C217A) were produced by overexpression in *E.coli* BL21 (Rosetta) cells (Novagen) in auto-induction media as described (30). Briefly, transformed cells were cultured at

37 °C with aeration until an OD_{600} of 1 was reached. Then, the cultures were shifted to 25°C until an OD_{600} of ~15-20 was reached (~48-60 hours). Cell harvest and protein purification were performed as described (1). Briefly, after harvest, cells were suspended in cold Tris-sucrose buffer (50 mM TrisHCl, pH 7.5, 10% sucrose, 250 mM NaCl, 1.5% *n*-dodecyl β-D-maltoside, 2 μg/ml of leupeptin, 1 mM phenylmethylsulfonyl fluoride, 5 mM β-mercaptoethanol, and 10 mM sodium metabisulfite) and lysed by a freeze-thaw cycle. The resulting lysate was centrifuged at 17,000 × *g* for 50 minutes at 4 °C and the recombinant Ind1 proteins were purified by Ni-NTA affinity chromatography.

Fluorescence microscopy

Transiently-transfected, C-terminally EGFP-tagged Ind1-expressing S2 cells and wild type S2 cells were grown to 70% confluence on a cover glass inside a 6-well tissue culture plate (Corning). Mitochondria within the cells were stained with MitoTracker Red (10 μM final concentration, Molecular Probes) for 1 hour in the dark before observation in an Olympus FluoView FV1000 confocal laser scanning microscope (CLSM). The instrument was equipped with 488 nm argon and 543 nm helium-neon lasers for GFP and MitoTracker Red excitation, respectively. Fluorescence emission detected with a 505-525 nm band-pass filter for GFP, and a 560 nm long-pass filter for MitoTracker Red. Images were obtained using a 60X PlanApo oil objective.

Gel filtration

Dm Ind1 (0.5 mg/ml, total 1 mg) was loaded onto a Superdex 75 HR 10/30 gel filtration column (GE healthcare) and chromatographed in gel filtration buffer (35 mM Tris-HCl pH 7.5,

350 mM NaCl, 10% glycerol, 5 mM β-mercaptoethanol) in the presence or absence of EDTA. Target protein eluted in the peak fractions was analyzed by 12% SDS-PAGE. Band intensities were measured using the ImageQuant 5.2 software after Coomassie blue staining.

ATPase assay

To measure ATP hydrolysis activity of *Dm* Ind1, 0~1 μM of *Dm* Ind1was incubated with 2 mM ATP and 1 μM [γ-^{32}P]ATP (PerkinElmer) in an ATPase assay buffer (50 mM Tris-HCl, pH7.5, 0.1 mM EGTA, 10 mM $MgCl_2$, and 1mg/ml BSA) (total reaction volume was 20 ul) at 37 °C for 30 minutes. After the incubation, 0.5 μl of each reaction mixture was spotted onto 1 cm from the bottom of polyethylenimine (PEI) cellulose paper (20 cm X 10cm) (Millipore). After drying the spots, the sheet was immersed in a developing buffer (1 M formic acid, 0.5 M LiCl) for about 30 minutes. After drying the sheet, the area containing ATP was cut out and detected under UV. The radioactive content was measured by liquid scintillation counting.

Lipid vesicle cosedimentation assay

See Materials and Methods in chapter 2.

Intrinsic tryptophan fluorescent quenching assay

See Materials and Methods in chapter 2.

Crosslinking analysis between Dm mtDNA helicase NTD and Dm Ind1

2.4 μM of each Ni-NTA purified protein (N-terminally His-tagged human mtDNA helicase NTD and N-terminally His-tagged *Dm* Ind1) was incubated in presence or absence of

chemical crosslinking agents (0.04% glutaraldehyde (Sigma) or 10mM DTBP (PIERES)) in a reaction buffer (50 mM Tris-HCl, pH 7.5, 80 mM KCl, 5mM β mercaptoethanol) for 20 minutes at 20 °C. The reaction mixtures (total volume is 25 µl) were separated in 7-15% SDS-polyacrylamide gels. Proteins were visualized by Coomassie staining or immunoblotting.

RNAi treatment

RNAi knockdown of Ind1 in S2 cells was performed as described (31). Briefly, to prepare PCR template for dsRNA synthesis, primers (LSK MS 23F and LSK MS 23R) were designed by SnapDragon (http://www.flyrnai.org/snapdragon, Harvard Medical School), a web-based software. A T7 RNA polymerase binding site (5'-GAA TTA ATA CGA CTC ACT ATA GGG AGA-3') at 5' end of the PCR product was added through primers. The purified PCR product is transcribed *in vitro* to generate dsRNA (T7 MEGAscript Kit, Ambion). dsRNA was purified with ethanol purification and treated directly to subcultured S2 cells (~1 X 10^6 cells/ml) in Insect-XPRESS™ protein-free insect cell medium (Lonza). Cells were harvested at 3 days, 5 days, and 7days after the dsRNA treatment.

Mitochondrial DNA Copy number

mtDNA copy number was determined by ratio of relative amount of mtDNA to nuclear DNA. Total DNA was prepared by phenol/ chloroform DNA extraction. SYBR Green JumpStartTM Taq Ready Mix (Sigma) was used for reaction mixtures according to manufacturer's instruction. Real time PCR was performed on a 7500 Real Time PCR System instrument (Applied Biosystems) to quantify amounts of the mitochondrial 16S gene and the nuclear RpL32 gene using following primers (16S-F: 5'-AAA AAG ATT GCG ACC TCG AT-3'

and 16S R 5’-AAC CAA CCT GGC TTA CAC C-3’; RpL32F: 5’-AGG CCC AAG ATC GTG AAG AA-3’ and RpL32R 5’-TGT GCA CCA GGA ACT TCT TGA A-3’)

Protein immunoblot

See Materials and Methods in chapter 1.

Additionally, anti-*Dm* Ind1rabbit polyclonal antibody was prepared from a purified N-terminally His tagged *Dm* Ind1 (Met^{25}-His^{329}) (Covance).

Flow cytometry

The LSR II flow cytometer analyzer (BD Bioscience) was used for the flow-cytometry analysis. To measure mitochondrial mass and select dead/ live cells, fluorescent dyes (MitoTracker Green FM (10 μM final concentration, Molecular Probes) and propidium iodide (10 μM final concentration, Molecular Probes), respectively) were treated on prepared wild type S2 cells and Ind1-knockdown cells. Cells were incubated for 30 minutes at 25 °C in the dark for MitoTracker Green staining and then counted, but for propidium iodide staining, cells were measured immediately by the instrument (LSR II) using 488 nm excitation. The emission wavelength was 530±30 nm (FL1) for green fluorescence and 630±30 nm (FL2) for propidium iodide. Data acquisition and analysis was done using FACSDiva software (DB bioscience).

Protein Modeling

To obtain a homology model of *Dm* Ind1, the *Dm* Ind1 sequence was submitted to Phyre2 using the default parameters (32). The dimer structure was derived by Dali (33) and PDBEditor to superimpose the Ind1 monomer model on the dimer crystal structure of nucleotide-binding

protein AF2269 from *A. fulgidus* as a template (PDB #:3KB1). The electrostatic surface potential (ESP) map of *Dm* Ind1 was generated using the APBS Tools in PyMol with the default parameters.

To generate helical wheel projections, predicted secondary structures were obtained first using PsiPred (34) from the primary amino acid sequences of the proteins. The corresponding sequence of the last predicted helix at the C-terminus of each protein was submitted to NetWheels (http://lbqp.unb.br/NetWheels/) to obtain a helical wheel projection.

RESULTS

CG3262 in D. melanogaster is a homolog of Ind1 in humans and yeast, and its encoded protein localizes to mitochondria.

CG3262 in *D. melanogaster* is a gene encoding a putative interacting partner of *Dm* mtDNA helicase (2). According to a NCBI BLAST search, the CG3262 protein belongs to the Mrp-like proteins in a P-loop NTPase superfamily and shows a homology to human NUBPL, or human Ind1, with 44% amino acid sequence identity.

In considering the possibility that the CG3262 protein (*Dm* Ind1) serves as the transfer protein for *Dm* mtDNA helicase, mitochondrial localization was examined. Primary sequence analyses with MitoProt II and iPSORT predicted its mitochondrial localization via a canonical N-terminal mitochondrial targeting sequence with a high probability (0.7036 and positive, respectively). To demonstrate the mitochondrial localization *in vivo*, a C-terminal EGFP tag was inserted into the ORF containing CG3262, and the recombinant protein expressed *Drosophila* S2 cells was observed by confocal microscopy (Fig. 20 A). The green fluorescent signal in successfully transfected cells overlapped completely the red fluorescent signal from mitochondria stained with MitoTracker Red. Moreover, subcellular fractionation of a C-terminally HA-tagged *Dm* Ind1 showed localization to the mitochondrial fraction (M) but not the cytosolic fraction (C) when proteins derived from equal cell equivalents were analyzed by 12% SDS-PAGE and immunoblotting (Fig. 20 B). In composite, the *in silico*, *in vivo* and *in vitro* experiments demonstrate that *Dm* Ind1 (CG3262) is a mitochondrial protein.

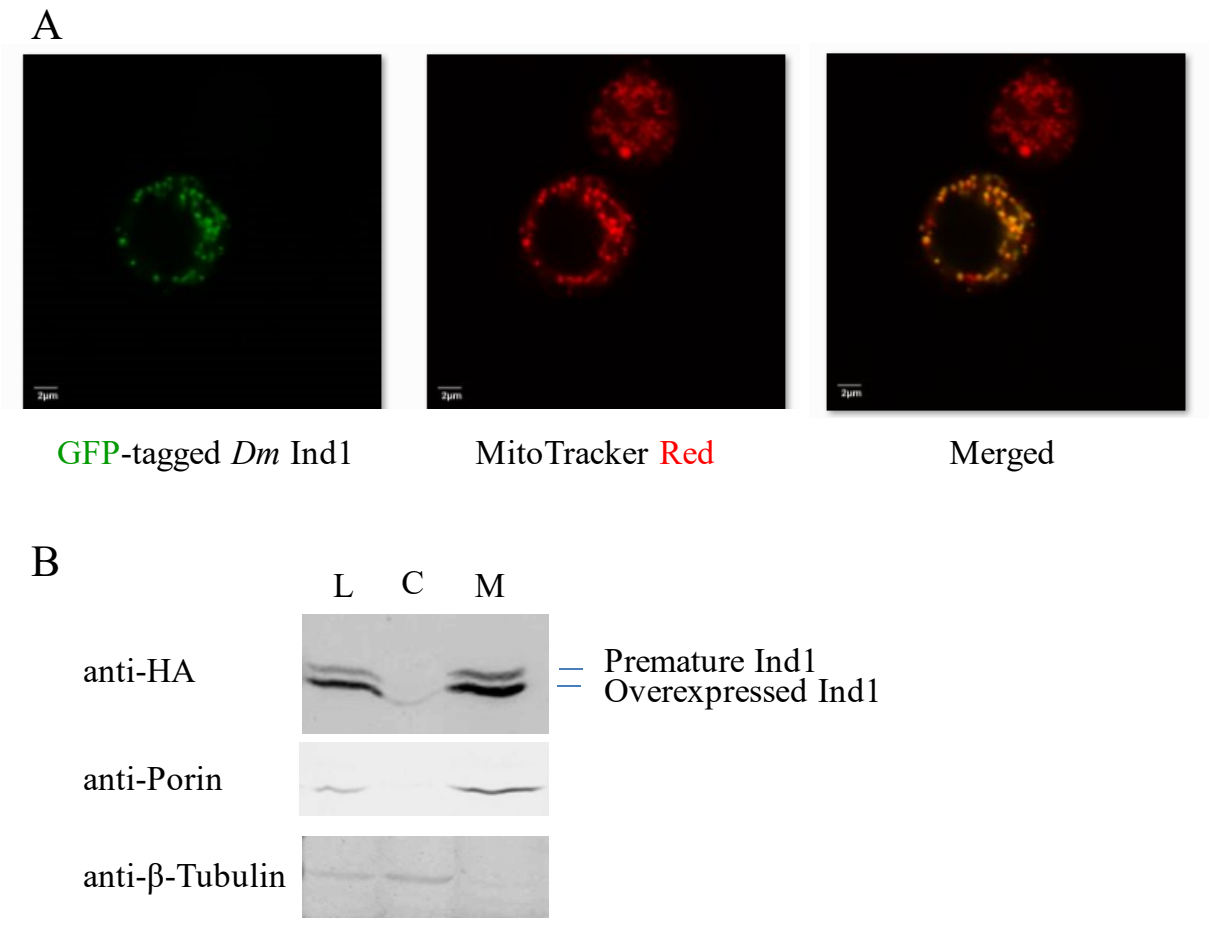

Figure 20. **Localization analyses of recombinant *Dm* Ind1 proteins: representative confocal microscopic images of a GFP-tagged *Dm* Ind1 (A) and immunoblot of a HA-tagged *Dm* Ind1 (B) A.** A C-terminally GFP-tagged full-length *Dm* Ind1 was constructed under the control of metallothionein promoter. The construct was transfected transiently into *Drosophila* S2 cells for two days. After induction by 0.2 mM $CuSO_4$ for 4 days, mitochondria in the cells were stained with MitoTracker Red and observed by confocal microscopy. **B.** A construct for a C-terminally HA tagged full-length *Dm* Ind1 was transfected stably into S2 cells. After induction by 0.2 mM $CuSO_4$ for 4 days, a total cell lysate (L) was fractionated to cytosol (C) and mitochondria (M) by differential centrifugation. Porin and β-tubulin were used as loading controls for mitochondria and cytosol, respectively.

Dm Ind1 is a homodimer that does not require an iron-sulfur cluster or a nucleotide for dimerization.

The Ind1 monomer contains only a single CXXC motif, a common cysteine-containing motif for coordinating metal ions. Homodimerization of Ind1 was expected (Fig. 21) because four cysteines are required typically to coordinate an iron-sulfur cluster (35). This speculation, however, has not yet been demonstrated. Thus, to investigate the oligomeric state of *Dm* Ind1, a N-terminally His-tagged recombinant form was subjected to gel filtration in the absence of an iron-sulfur cluster and nucleotides (Fig. 22). A metal chelator (EDTA) was used to reduce the possibility that the recombinant *Dm* Ind1 contains an iron-sulfur cluster or a zinc ion. *Dm* Ind1 in the presence (closed circles in Fig. 22) or absence of EDTA (open circles in Fig. 22) produced a single chromatographic peak with a Stokes radius of 37 Å and an estimated molecular mass of 66 kDa, which corresponds to the theoretical molecular mass of a dimer (62 kDa) for the recombinant *Dm* Ind1.This data suggests that the presence/ insertion of an iron-sulfur cluster in *Dm* Ind is not obligatory for its dimerization.

As an alternative approach, an Ind1 variant (C214A/ C217A) lacking the iron-sulfur cluster-coordinating capability was produced by alanine substitution of the two cysteines in the CXXC motif. The C214A/ C217A variant (closed squares in Fig. 22) demonstrated a single peak in the same fractions as the dimerized wild type *Dm* Ind1. This result confirms that an iron-sulfur cluster or a metal ion is not required for dimerization. Considering the fact that the C214A/ C217A variant had significantly lower solubility than the wild type form, the coordinating cysteines are likely important for protein stability. These results also suggest that a nucleotide is not required for dimerization of *Dm* Ind1, because all gel filtration runs were performed with nucleotide-free buffers.

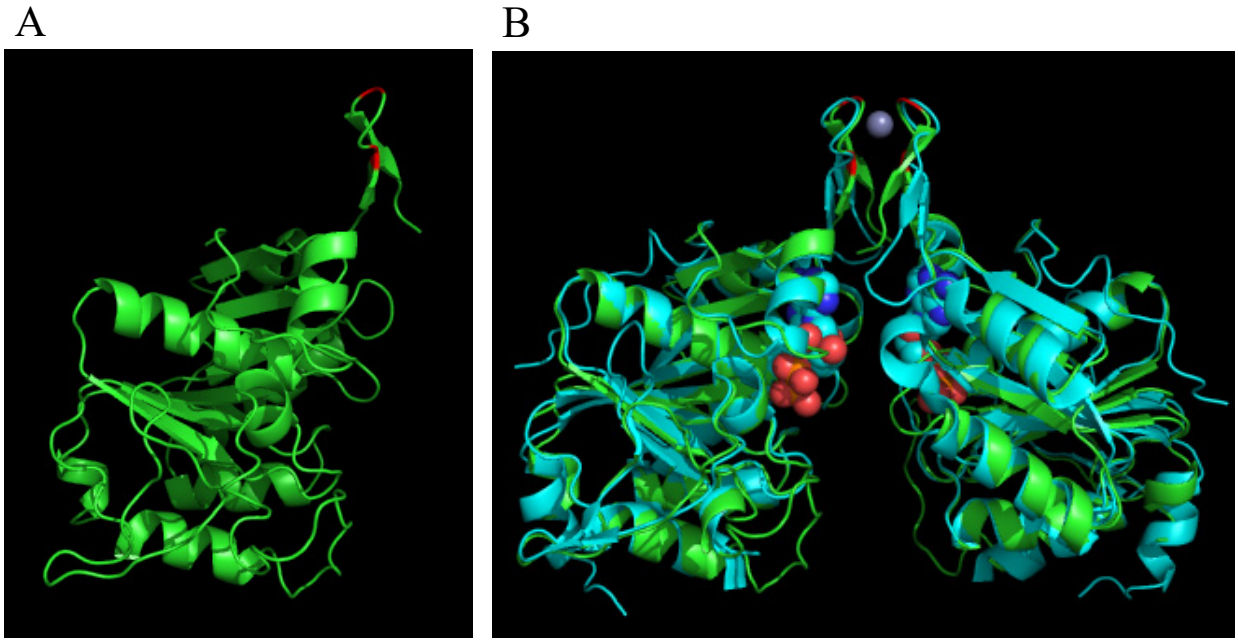

Figure 21. **Homology models of a *Dm* Ind1 monomer (A) and a dimer superimposed with its template (B) A.** Homology model of a monomer of *Dm* Ind1 (green) was generated by Phyre2 using nucleotide-binding protein AF2382 from *Archaeoglobus fulgidus* (PDB #: 2Ph1) as a template. Metal coordinating cysteines are colored red. **B.** A dimer model of *Dm* Ind1 (green) was generated by PyMOL and superimposed on the dimer template (blue), the complex of nucleotide-binding protein AF2269 from *Archaeoglobus fulgidus* with ADP (PDB #: 3KB1). ADP molecules are shown in the space-filling model at the interface of the two protomers. The purple sphere represents the zinc atom in 3KB1 that is likely an iron-sulfur cluster in the *Dm* Ind1 structure.

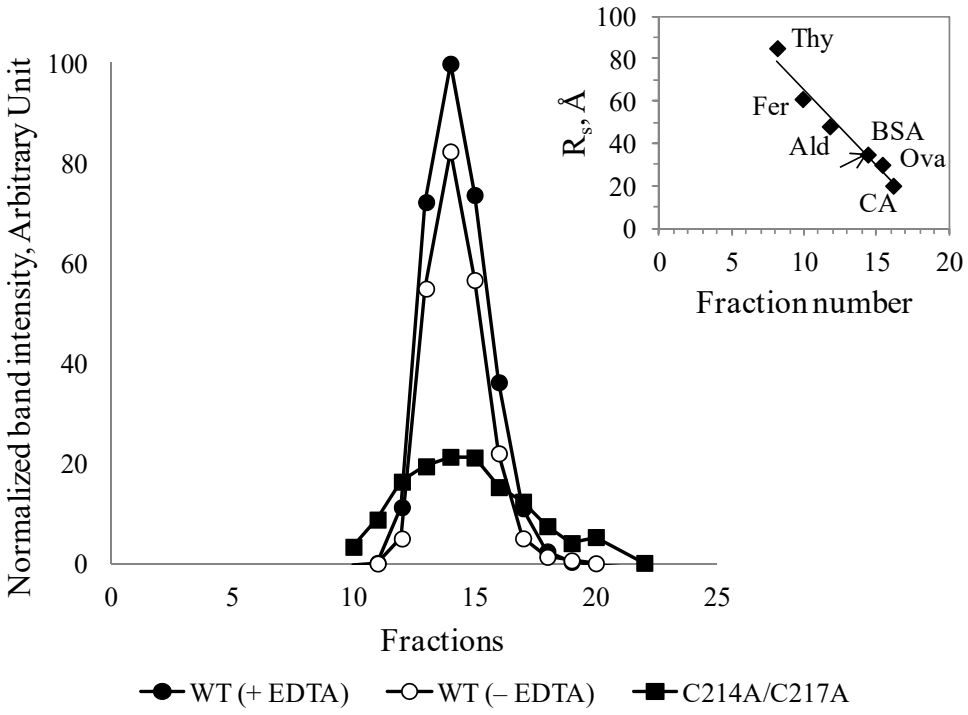

Figure 22. **Gel filtration of an N-terminally His-tagged recombinant *Dm* Ind1** *Dm* Ind1 forms a homodimer regardless of the presence of an apparent iron-sulfur cluster or nucleotides. Gel filtration of an N-terminally His-tagged recombinant *Dm* Ind1 shows that *Dm* Ind1 in the presence (closed circles) or absence of EDTA (open circles), and an iron-sulfur cluster-deficient variant (C214A/ C217A) (closed squares) produced a single peak with the same Stokes radius of 37 Å and an estimated molecular mass of 66 kDa, corresponding to the theoretical molecular mass (62 kDa) of a dimer of the recombinant *Dm* Ind1. Protein standards used to calibrate the column were: carbonic anhydrase (CA, 20 Å, 29 kDa), ovalbumin (Ova, 30 Å, 45 kDa), bovine serum albumin (BSA, 35 Å, 66 kDa), aldolase (Ald, 48 Å, 158 kDa), ferritin (Fer, 61 Å, 440 kDa), and thyroglobulin (Thy, 85 Å, 669 kDa). The position of the eluted recombinant Ind1 peak is indicated by an arrow on the standard protein curve in the inset.

Dm Ind1 has ATPase activity.

The ATPase activity of the recombinant *Dm* Ind1 was assayed by mixing 0~1 μM Ind1 with 2 mM ATP and 0.05 μM [γ-^{32}P] ATP. The remaining labeled ATP was measured after separation by thin layer chromatography (TLC). ATPase activity of *Dm* Ind1 displayed by percentage of hydrolyzed ATP (Fig. 23 A), and yielded ~10% of hydrolyzed ATP at the saturated state in the samples with higher protein concentration. However, because increasing protein concentration also increased salt concentration in the reactions, when hydrolyzed ATP is represented as molar quantity per minute and mg of protein (Fig. 23 B), activity is decreased with increasing salt concentration, indicating the saturation observed with highly-concentrated protein samples (Fig. 23 A) is the result of salt inhibition. This data shows that *Dm* Ind1 has ATPase activity but its basal level could not calculated using this data. A time course experiment with different inhibitors and/ or activators will be required to make such a determination.

Dm Ind1binds to liposomes as predicted for a peripheral membrane protein.

Because Ind1 is an iron-sulfur cluster-transferring protein specific for respiratory complex I, it is expected to associate with the mitochondrial inner membrane where complex I resides. In addition, the overexpressed HA-tagged *Dm* Ind1 in isolated mitochondria from *Drosophila* S2 cells (Fig. 20 B) is found largely in the pellet fraction of the mitochondrial lysate (data not shown). Thus, the membrane binding properties of *Dm* Ind1 were tested. Purified N-terminally His-tagged *Dm* Ind1 was mixed with unilamellar soybean asolectin liposomes, and protein-liposome complexes were demonstrated by lipid vesicle cosedimentation. In the absence of liposomes, *Dm* Ind1 was predominantly in the supernatant fraction (S) after ultracentrifugation, while in the

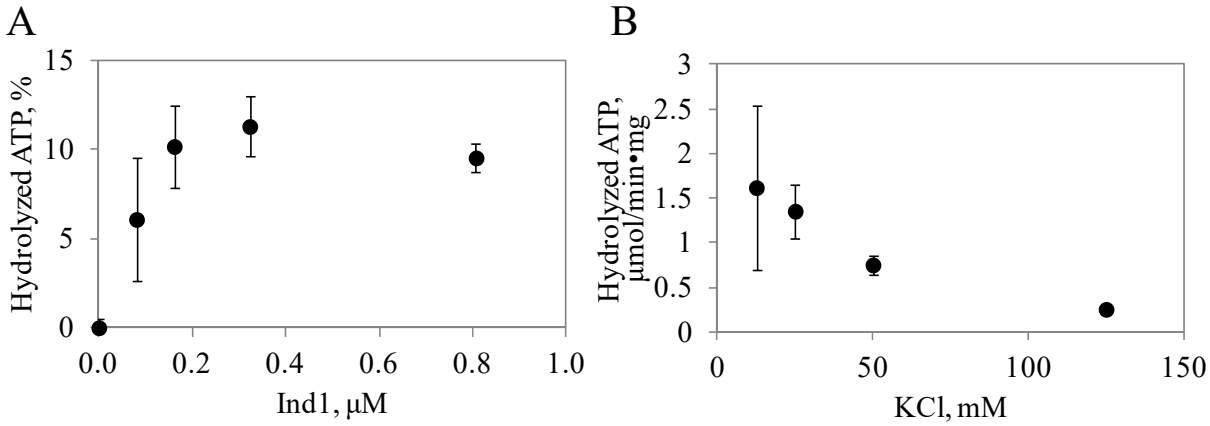

Figure 23. **ATP hydrolysis by *Dm* Ind1** 0~1 μM of Ind1 was incubated with 2 mM ATP and 0.05 μM [γ-^{32}P] ATP at 37ºC for 30 minutes (see Material and Methods). The remaining ATP was measured after separation using thin layer chromatography. **A**. Hydrolyzed ATP is presented by percentage of hydrolyzed ATP (1-remaining ATP/ input ATP). The input ATP is a remaining ATP without protein. **B.** Hydrolyzed ATP is presented by molar quantity per minute and per mg of protein against KCl concentration. Molar quantity was obtained from percentage of hydrolyzed ATP at each data point and divided by the reaction time (30 minutes) and protein amount that was given in each reaction mixture. Each data point represents the mean of triplicates. The error bars indicate means ± standard deviation.

presence of liposomes, the protein was found in the pellet (P) (Fig. 24 A), indicating that *Dm* Ind1 binds to liposomes. The fraction of bound Ind1 (0.8) was saturated at a concentration of 100 μM of liposomes. Liposome binding increased when the NaCl concentration was increased up to 50 mM, but it was inhibited at higher concentrations (Fig. 24 C). The loss of cosedimentation of *Dm* Ind1 and liposomes by increased salt concentration indicates that its interaction with asolectin liposomes is electrostatic. However, the residual fraction (~0.2) of bound Ind1 remaining at elevated salt concentration implicates involvement of another binding force. Hydrophobic interaction seems a likely possibility because a C-terminal amphipathic helix is predicted in human, *Drosophila* and *Y. lipolytica* Ind1 by the helical wheel projection program NetWheels (Fig. A4). These results suggest that Ind1 may be a peripheral membrane protein, and its membrane binding likely facilitates access to its membrane-bound iron-sulfur cluster recipient, complex I or a putative recipient, *Dm* mtDNA helicase.

Neither cholesterol nor cardiolipin change substantially the liposome binding properties of Dm Ind1.

The putative binding partner, *Dm* NTD showed a specific binding to cardiolipin-containing liposomes but not to cholesterol-containing liposomes (see chapter 3). Thus, to test whether *Dm* Ind1 binds to cholesterol or to cardiolipin, which are enriched in lipid raft or the mitochondrial inner membrane, respectively, asolectin liposomes with different concentrations of cholesterol or cardiolipin were prepared. The bound fraction of *Dm* Ind1 was not altered by increasing cholesterol levels in liposomes (Fig. 25 A), indicating that there is no specific binding of Ind1 to cholesterol in the asolectin liposomes. Moreover, an increase of cardiolipin

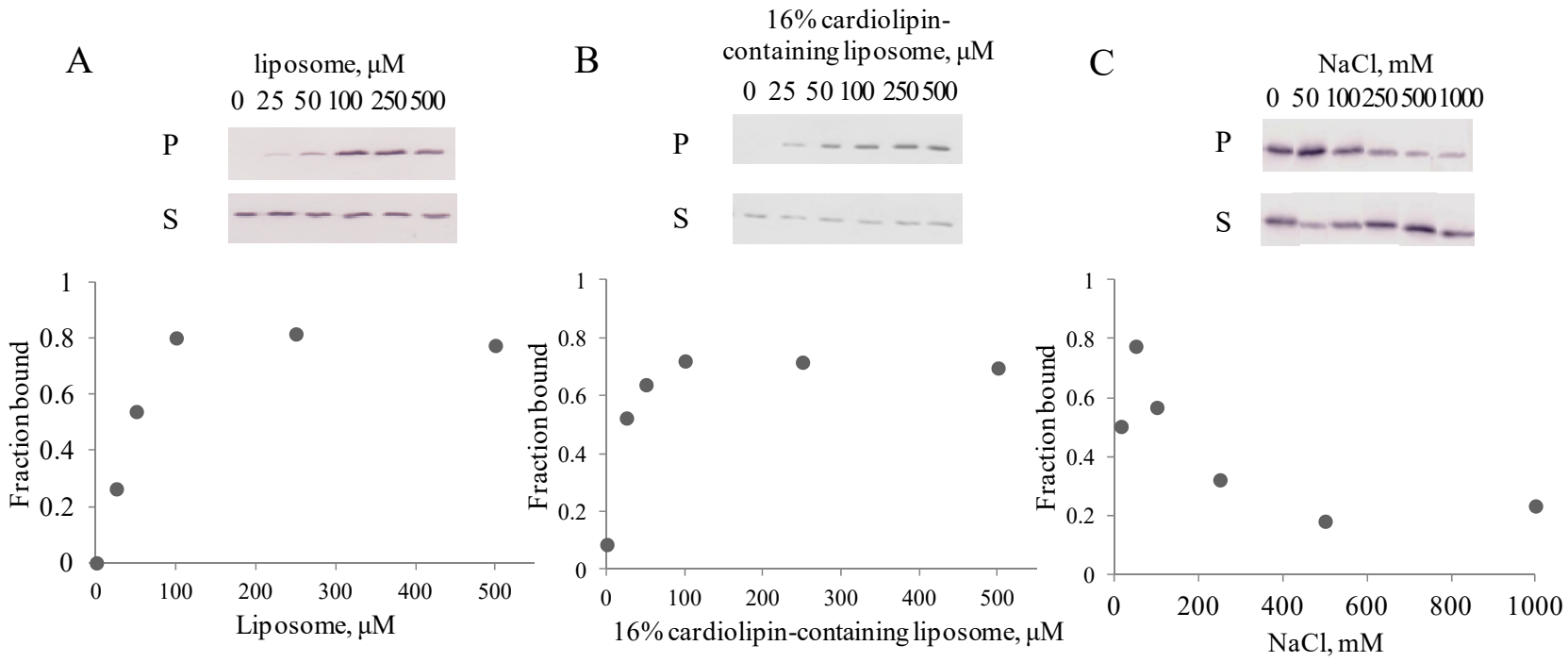

Figure 24. **Binding of *Dm* Ind1 to different asolectin liposomes by lipid vesicle cosedimentation** Liposome titration of 0.4 µM *Dm* Ind1 in 50 mM Tris-HCl, pH7.5, 100 mM NaCl with standard asolectin liposomes (A), and 16% w/w cardiolipin-containing liposomes (B). Salt titration of 0.4 µM *Dm* Ind1 with 250 µM standard liposomes reveals that the binding is salt-sensitive, suggesting electrostatic interactions (C). Pellet fraction (P) and supernatant fraction (S) are analyzed by 12% SDS-PAGE (upper). Fraction bound of *Dm* Ind1 was determined by band intensity of pellet (bound protein) over sum of band intensities of pellet and supernatant (total protein) and plotted against concentration of liposomes (A and B) or NaCl (C) (lower).

concentration did not show a positive correlation in the lipid vesicle cosedimentation that was observed with *Dm* NTD (see chapter 3). The bound fraction of *Dm* Ind1decreased mildly from ~ 0.8 to ~ 0.6 as the cardiolipin level increased from 1% w/w to 10% w/w (Fig. 25 B). However, the mild reduction was not statistically significant, implying *Dm* Ind1 does not have specificity to cardiolipin. The fraction of bound *Dm* Ind1 to 16% w/w cardiolipin-containing liposomes (Fig. 24 B) was also not significantly different from binding to standard liposomes (Fig. 24 A), indicating that liposome binding of *Dm* Ind1is not promoted by cardiolipin.

Intrinsic tryptophan quenching assays show that Dm Ind1 does not bind directly to cholesterol or PE.

To investigate binding properties of *Dm* Ind1 to an individual lipid, I employed an intrinsic tryptophan quenching assay and tested cholesterol and PE, an abundant lipid in lipid rafts and the most abundant lipid in asolectin, respectively. Stability of *Dm* Ind1 was tested prior to the intrinsic tryptophan quenching assay to find an optimal buffer condition. N-dodecyl β-D-maltoside (0.05% w/v) and/ or glycerol (5% v/v or 10% v/v) were added to the buffer (50 mM TrisHCl, pH7.5, 150 mM NaCl) and the emission change of *Dm* Ind1was monitored over time (Fig. A5). Although N-dodecyl β-D-maltoside stabilized *Dm* Ind1in an *in vitro* stability test (data not shown), *Dm* Ind1in N-dodecyl β-D-maltoside-containing buffers (Fig. A5 D and E) showed substantial emission changes, indicating that N-dodecyl β-D-maltoside binds to *Dm* Ind1 and causes a conformational change near tryptophan residues. However, glycerol does not affect emission spectra significantly (Fig. A5 A-C). Thus, the buffer (50 mM TrisHCl, pH 7.5, 150 mM NaCl, 5% glycerol) (Fig. A5 B), which is identical to the one used in the intrinsic tryptophan quenching assay for *Dm* NTD in chapter 2, was chosen. In an intrinsic tryptophan quenching

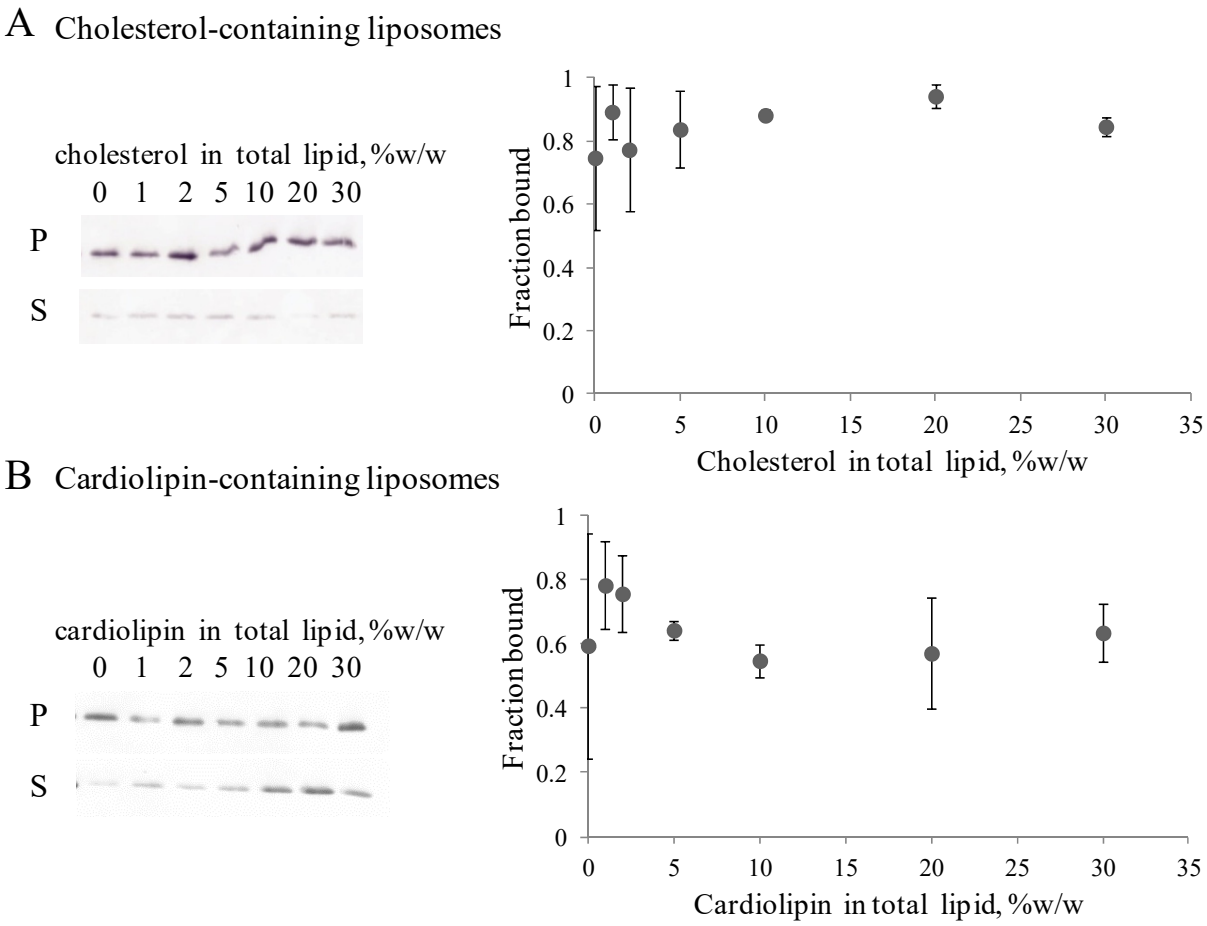

Figure 25. **Binding of *Dm* Ind1 to asolectin liposomes that contain cholesterol (A) or cardiolipin (B) by lipid vesicle cosedimentation** The final concentration of *Dm* Ind1 was 0.4 μM in 50 mM Tris-HCl, pH7.5, 100 mM NaCl. The total concentration of liposomes is 100 μM and liposome composition varies as indicated. Pellet fraction (P) and supernatant fraction (S) are analyzed by 12% SDS-PAGE (left). Fraction bound of *Dm* Ind1 was determined (right) by the same calculation in Figure 21. Each data point represents the mean of triplicate measurements. The error bars indicate means ± standard deviation.

assay of *Dm* Ind1 with cholesterol, intrinsic tryptophan quenching assay of *Dm* Ind1 with cholesterol, the emission of *Dm* Ind1 at the maximum emission wavelength (~330 nm) decreased as the cholesterol level was increased from 0 to 140 nM (Fig. A6 A, closed circles), but similar decreases were also observed in the solvent control (Fig. A6 A, open circles). Consequently, no specific binding to cholesterol was observed in the saturation curve (Fig. A6 A, closed squares). This result agrees with the data from cholesterol-containing liposome cosedimentation, which showed that the increase of cholesterol concentration has no effect on the liposome binding properties of *Dm* Ind1. Similar to cholesterol, the total binding curve of *Dm* Ind1 to PE overlapped the solvent binding curve, indicating no specific binding between PE and *Dm* Ind1 (Fig. A6 B). These data demonstrate that Ind1 does not bind to either cholesterol or PE.

Dm Ind1 does not interact physically with the mtDNA helicase N-terminal domain in vitro.

To confirm the putative physical protein interaction between *Dm* Ind1 and the *Dm* mtDNA helicase that was found by high-throughput AP-MS (2), chemical crosslinking reagents such as glutaraldehyde and DTBP were used to fix the predicted weak and dynamic interactions between *Dm* Ind1 and the *Dm* NTD (Fig. 26). Both proteins were detected on a SDS-PAGE gel as monomers without a crosslinking reagent or with DTBP, while with glutaraldehyde, the monomer bands of the NTD or Ind1 were either blurred or faint, respectively; however, oligomeric bands were somewhat visible in the Commassie stained gel (Fig. 26 A). To clarify the presence or absence of crosslinked oligomeric forms and hetero-complexes, immunoblots were performed with an anti-Ind1 antibody (Fig. 26 B) and an anti-NTD antibody (Fig. 26 C). Glutaraldehyde treatment resulted in a considerable decrease in the monomer signal of Ind1 (Fig. 26 B), generating dimer signals of Ind1 on the membrane, whereas the NTD was detected largely

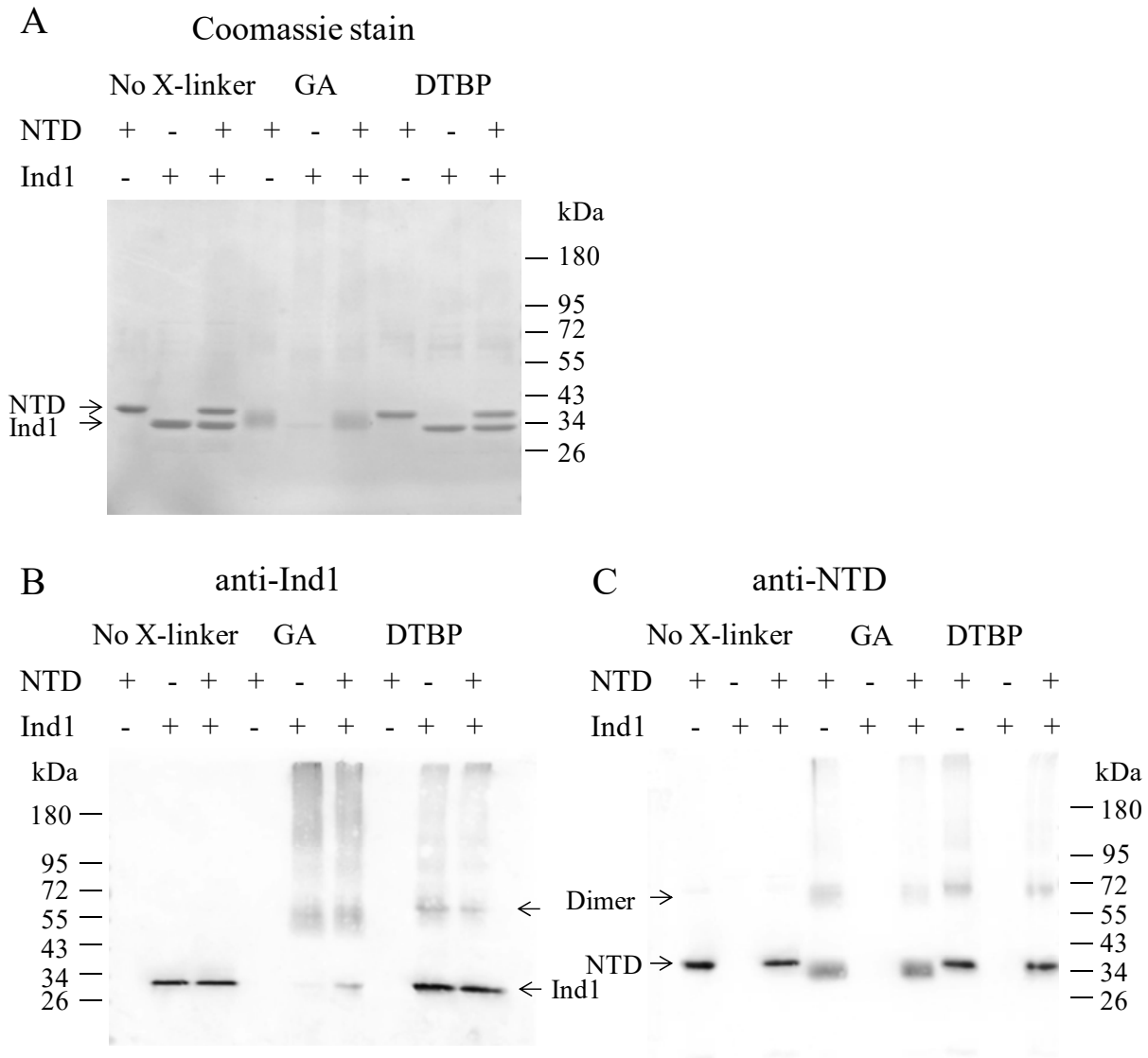

Figure 26. ***In vitro*** **chemical crosslinking between** ***Dm*** **Ind1 and** ***Dm*** **NTD** 2.4 μM of each protein was incubated with or without chemical crosslinking reagents (0.04% Glutaraldehyde (GA) or 10 mM DTBP) in a buffer (50mM TrisHCl, pH7.5, 80 mM KCl) for 20 minutes at 20 ºC. The reactions were quenched with SDS-sample buffer and analyzed by 7-15 % SDS-PAGE. The gels were visualized by Coomassie stain (A) and immunoblots probed by anti-Ind1 antibody (B) and anti-*Dm* NTD antibody (C).

as a monomer (Fig. 26 C). Putative Ind1-NTD complex bands were not found, suggesting that the recombinant *Dm* Ind1does not interact with the N-terminal domain of *Dm* mtDNA helicase *in vitro.* The dimer signal of *Dm* Ind1 in this experiment corroborates the result from gel filtration, confirming the homodimeric state of *Dm* Ind1.

To test a membrane-mediated interaction, which is known in the case of a family member MinD and its interacting partner MinE (26), a liposome cosedimentation assay was performed in the presence of both *Dm* NTD and *Dm* Ind1. However, no significant change was detected in the fractions of the liposome-bound NTD or the liposome-bound Ind1, indicating that a membrane does not trigger their physical interaction (data not shown).

Reduced Dm Ind1protein levels do not affect mtDNA copy number or a mitochondrial mass.

To investigate physiological changes induced by a reduced level of Ind1, RNAi dependent knockdown of Ind1 was used with a dsRNA against *Dm* Ind1 (see Material and Methods). The *Dm* Ind1 protein level was reduced with statistical significance ($P < 0.05$) in knockdown cells over the duration of the time course (Fig. 27 A). Less than 10% of Ind1 was found at day 3, and the Ind1 protein level in knockdown cells remained lower than the wild type during the entire observation period. However, this apparent reduction of the *Dm* Ind1 protein level changed neither the relative TFAM protein level, an indicator of mitochondrial DNA copy number, nor mitochondrial DNA copy number itself. No statistically meaningful difference ($P > 0.1$) was observed between wild type and knockdown cells (Fig. 27 B and C).

Mitochondrial mass change upon knockdown of *Dm* Ind1 was assessed because abnormal mitochondrial morphology was detected in a human Ind1 knockdown cell-line (4). To measure mitochondrial mass by flow cytometry, *Dm* Ind1 knockdown cells were prepared by treatment of

Dm Ind1-targeted dsRNA for 3 days and MitoTracker Green was used to stain mitochondria. A slight (1.1 fold) increase was observed in mitochondrial mass of knockdown cells over wild type in the flow cytometry profiles (Fig. 27 D and E); however, it was not statistically significant, although it was at the margin of statistical significance ($p = 0.06$ in both live (Q4) and total (Q2+Q4) cells). The flow cytomerty data indicates that mitochondrial mass is not changed by the reduced Ind1 protein level. Taken together, there is no biologically significant difference in mitochondrial DNA level or mitochondrial mass between wild type S2 cells and Ind1 knockdown cells.

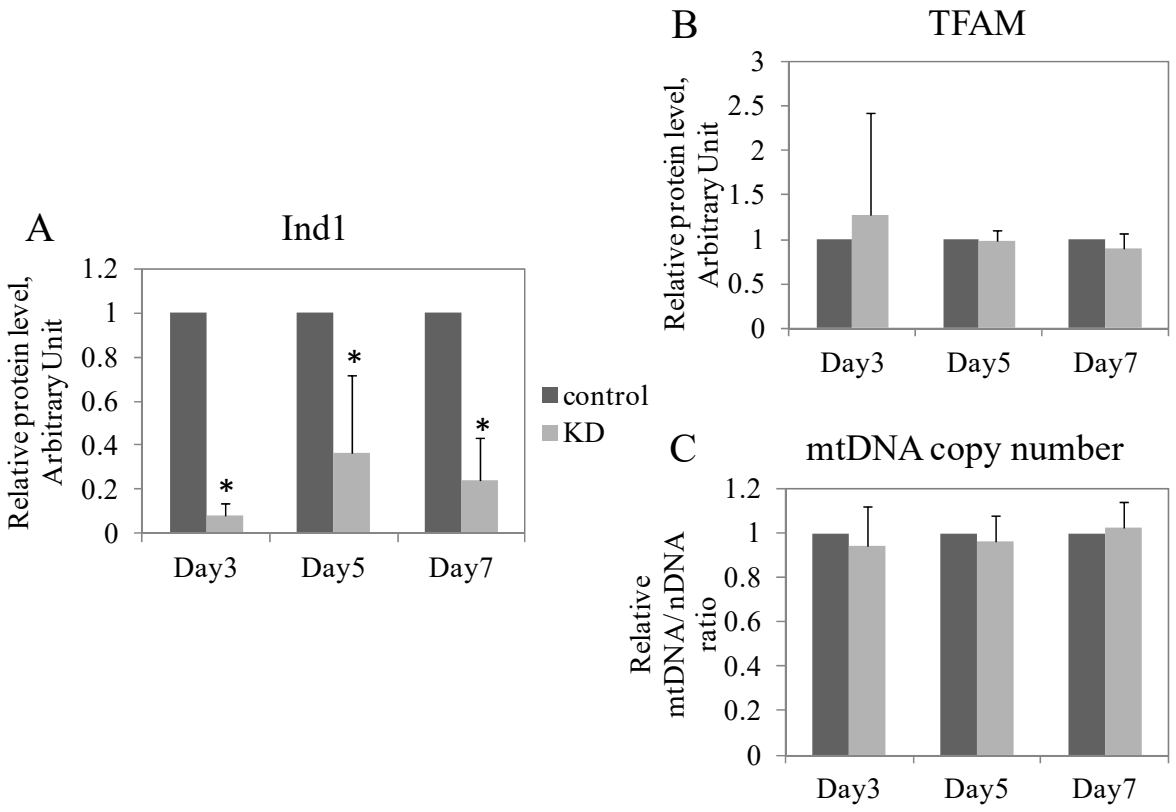

Figure 27. **Characterization of relative protein levels of mitochondrial proteins, mtDNA copy number, and mitochondrial mass in *Dm* Ind1 knockdown (KD) cells** Relative protein levels of Ind1 (A) and TFAM (B) in total cell extracts were measured 3, 5, and 7 days after treatment of the *Dm* Ind1-targeted dsRNA. Protein signals in the immunoblots were quantitated using ImageQuant 5.2, and normalized to the level of β-tubulin. The relative protein level of Ind1 (A) was significantly decreased in KD cells, but TFAM protein level, an indicator of mtDNA replication (B), and mtDNA copy number (C) did not show significant changes in KD cells. Error bars indicate means ± standard deviation of four independent experiments.*P<0.05 by Student's T-test.

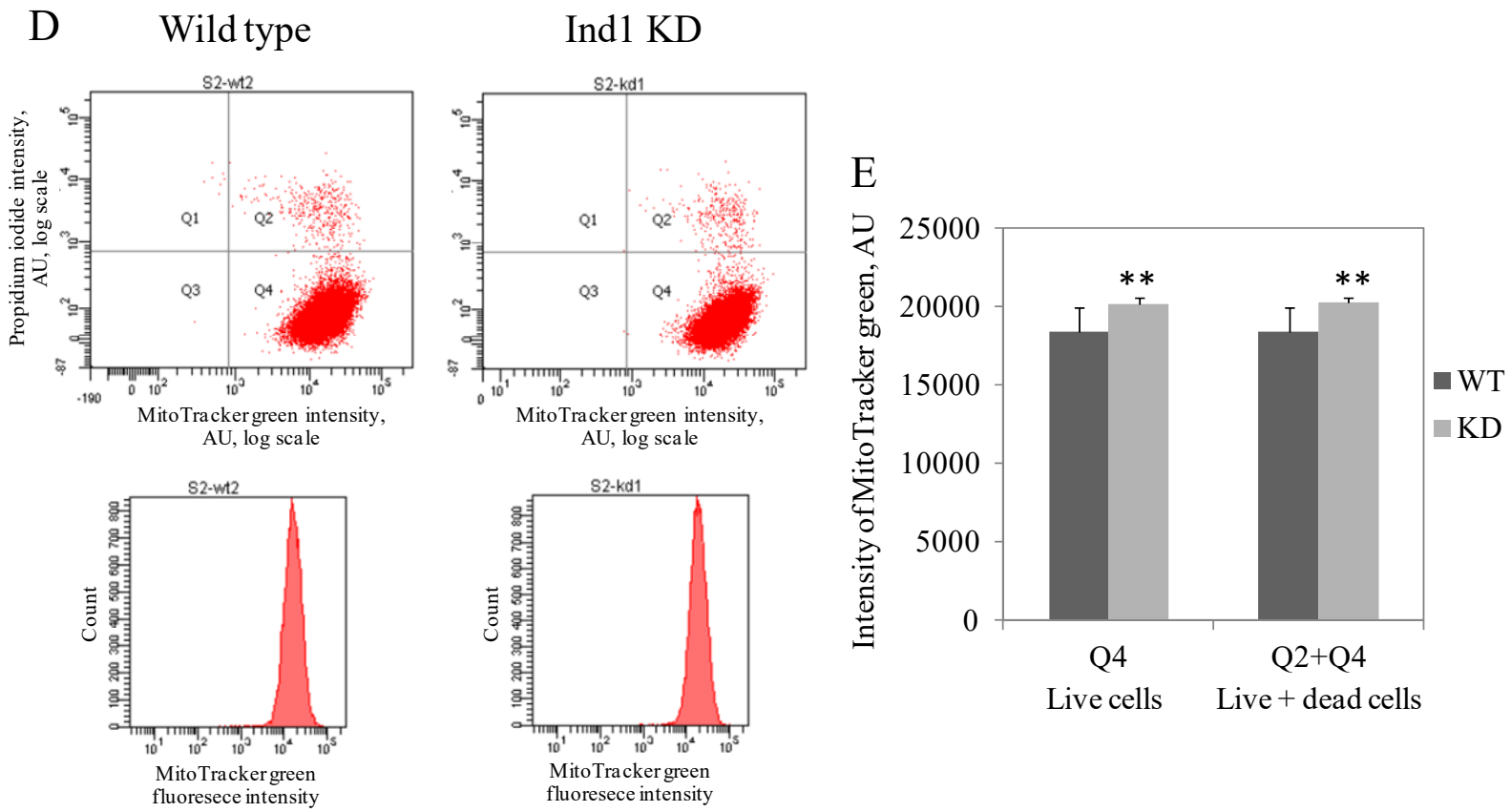

Figure 27. (cont'd) **Characterization of relative protein levels of mitochondrial proteins, mtDNA copy number, and mitochondrial mass in *Dm* Ind1 knockdown (KD) cells** Mitochondrial mass (representative profiles (D), bar graphs of MitoTracker green intensity (E)) in wild type and KD cells was determined at day 3 after transfection by flow cytometry. Error bars indicate means ± standard deviation of five replicates. **P<0.1 by Student's T-test.

DISCUSSION

The putative interaction between *Dm* Ind1and *Dm* mtDNA helicase found in *Drosophila* proteomic research (36) seems plausible because the *Dm* apomtDNA helicase needs an iron-sulfur cluster donor for incorporation of the cluster, and *Dm* Ind1is known to deliver an iron-sulfur clusters in mitochondria (3,4). In addition, the mtDNA helicase is likely to be localized at the mitochondrial inner membrane (see chapter 3)(37) where complex I, a known iron-sulfur cluster recipient of Ind1, resides.

Surprisingly, *in vitro* chemical crosslinking approach showed no direct interaction between the purified proteins. The lack of a chemically crosslinked complex between *Dm* Ind1 and the NTD of *Dm* mtDNA helicase may imply that the protein-protein interaction might be iron-sulfur cluster-dependent and/ or related in redox potential; the conformations of these proteins may be more prone to form a heterocomplex when *Dm* mtDNA helicase is an apoenzyme as a recipient and *Dm* Ind1 is a holoenzyme as a donor, which was contrary in the crosslinking assay. The interaction might also be ATP/ ADP-dependent. Several proteins in the Mrp/ MinD family undergo substantial conformational changes when they bind to ATP to form binding interfaces (17,21,24,28). A possible role for the CTD of the mtDNA helicase in incorporation of an iron-sulfur cluster might be an alternative explanation for no detection of interactions between *Dm* NTD and *Dm* Ind1. Improvement in protein preparation such as increasing stability of a full-length *Dm* apomtDNA helicase and stable reconstitution of *Dm* Ind1may be required for identification of the putative interaction.

To circumvent technical limitations from the *in vitro* study, an *in vivo Dm* Ind1 knockdown study was pursued. Despite the apparent decrease of the *Dm* Ind1 protein level, no statistically significant changes in mitochondrial DNA copy number and mitochondrial mass

were observed in the *Dm* Ind1knockdown cells. This result agrees with the *in vitro* crosslinking study, implying that *Dm* Ind1might not be an iron-sulfur cluster donor for *Dm* apomtDNA helicase. However, the residual Ind1 level under the knockdown might be sufficient for its cellular functions because the target protein is not eliminated completely by RNAi. Case studies about family members of patients with Ind1 mutations support this hypothesis. Wild type Ind1 protein levels of the family members who have a defective Ind1 gene but no pathogenic symptoms were 30~50% of healthy controls (5-7), suggesting that the limited amount of wild type Ind1is sufficient to maintain cellular activity, or that a second unidentified protein has an overlapping function. To investigate the effect of Ind1 in mitochondrial DNA replication, CRISPR-Cas9 would be a good technique to eliminate the Ind1 protein completely.

Complex formation among Mrp/ MinD family members are relatively well-studied (17,18,20,21). Binding interfaces for their interacting partners are created by orchestration of protein dimerization, nucleotide binding, ATPase activity, and membrane binding properties, although the mechanistic details vary among the family members (17,18,20,21,25). In this study, the characteristics of a recombinant *Dm* Ind1were investigated to understand aspects of formation of a binding interface in *Dm* Ind1.

First, the binding interface might be created when ATP binds to *Dm* Ind1, forcing a favorable conformational change. *Dm* Ind1 forms a stable homodimer in the absence of both a nucleotide and an iron-sulfur cluster. NifH and Get3 in the Mrp/ MinD family, which have an iron-sulfur cluster or zinc ion in their dimeric states, respectively, dimerize in a similar fashion (21,24,28). Their dimers have an inactive open form with ADP or no nucleotide and an active closed form with ATP upon protein-protein interaction. The nucleotide-free dimerized Ind structure may be an inactive open form that is similar to the homology model of *Dm* Ind1 dimer

(Fig. 18 B), which was generated by using the ADP bound protein dimer as a template, whereas a *Dm* Ind1dimer is expected to have a closed form when it binds to ATP, like other metal binding family members.

The conformational change induced by ATP/ ADP binding in this family regulates the binding interface for interacting partners (17,22). For instance, the 4Fe-4S cluster position in the NifH dimer at the docking region to the MoFe-protein within a nitrogenase complex moves significantly depending on bound nucleotides: AMPPCP (ATP analog), ADP, and free nucleotide (24,38). Also, the yeast Get3 dimer, which transfers a newly synthesized helix to the ER (Endoplasmic Reticulum) membrane, changes its structure from the cargo unloaded open form without nucleotide to the cargo loaded closed form with an ATP analog, ADP•$AlF4^-$ (22,28). On the contrary, proteins that do not have a metal cofactor in this family such as MinD or Soj need ATP for homodimerization, and ADP bound forms remain as monomers (17,18). ATP-dependent dimerization of MinD also recruits interacting partners, MinC or MinE (17).

The integrity of the iron-sulfur cluster binding region of *Dm* Ind1 is important for stable homodimerization. The gel filtration result with the coordinating cysteine-deficient mutant of *Dm* Ind1 in this study indicates that metal binding is not essential for dimerization of *Dm* Ind1, but the coordinating cysteines of Ind1is important for protein stability. According to crystal structures of yeast Get3 dimer, nucleotide-free Get3 has ~900$Å^2$ of buried area in the interface including zinc ion bound region, and the interface expands to ~2,400 $Å^2$ in the ADP•$AlF4^-$ bound closed form of Get3 (28). Interestingly, the crystal structure of *A. fumigatus* apoGet3 shows disulfide bonds between coordinating cysteines of protomers instead of a zinc ion (39). Thus, *Dm* apoInd1 is likely to form disulfide bonds in the dimeric state, and the intersubunit contact between coordinating cysteines is important for stable dimerization as for metal binding proteins

in the Mrp/ MinD family.

Although demonstration of ATPase activity of *Dm* Ind1was in conclusive in this study, it is possible that a required binding partner may stimulate the ATPase activity of Ind1. Proteins in this family use ATPase activity to dissociate from their interacting partner in a complex and/ or to detach from the membrane (17,21,26). In the absence of an interacting partner or membrane, ATP hydrolysis by *Dm* Ind1 might maintain a basal level in order to minimize unnecessary use of ATP. In Get3, a non-catalytic conformation of the ATP bound closed form was detected in the absence of its binding partner, Get1/ 2 receptor (28), indicating necessity of the binding partner for its ATP hydrolysis. Soj also shows the very low basal ATPase activity in an *in vitro* ATPase assay, but the activity increases approximately three-fold with Spo0J, an interacting partner of Soj (18).

Both electrostatic interaction and hydrophobic interactions in *Dm* Ind1 provide the driving force for membrane binding. *Dm* Ind1 binds the asolectin membranes strongly; the bound protein fraction at equilibration was four times higher than the fraction of bound *Dm* NTD (see chapter 3). The abolishment of the liposome binding by increased salt concentration suggests electrostatic interaction is mainly involved. This result is supported by a broad, positively charged region found in an ESP map of the *Dm* Ind1 dimer homology model (Fig. A7). If the positively charged region is true membrane binding region, the iron-sulfur cluster binding region of Ind1faces toward the mitochondrial matrix because the charged region is on the opposite side of the iron-sulfur cluster binding region. Surprisingly, unlike the *Dm* NTD, liposome interaction was not increased by addition of cardiolipin, which has an acidic polar head, implying a different type of interaction. In the Mrp/ MinD family, proteins such as MinD and FlhG use an amphipathic helix at the end of the C-terminus in order to attach to the membrane. In the *Gt*FlhG

monomeric crystal, the amphipathic helix (helix 10 in *Gt*FlhG) binds to the hydrophobic groove between helix 4 and helix 5, and binding inhibits the dimerization (20). Although the amphipathic helix has not been crystallized in any dimeric form, helix 4 and helix 5 in the dimeric form show significant structural rearrangements, as compared to those in the monomeric form. A C-terminal amphipathic helix that is predicted in Ind1 of humans, *Drosophila*, and *Y. lipolytica* (Fig. A4) supports the implication of an amphipathic helix of Ind1 in membrane association. The amphipathic property of the *Dm* Ind1C-terminal helix is conserved across the C-terminal helixes in MinD and FlhG, but the helix of *Dm* Ind1 has negatively charged residues on the polar surface side unlike MinD or FlhG, which have positively charged residues (Fig. A4) in the helical wheel projection. Hydrophobic interaction of the amphipathic helix that has an acidic hydrophilic side might explain why there was no significant effect of the increased cardiolipin level on membrane association of *Dm* Ind1. A hydrophobic interaction through the amphipathic helix and an electrostatic interaction through the highly positively area are likely to contribute together to membrane association of *Dm* Ind1. It also might be the reason for the relatively strong binding property of *Dm* Ind1 under the nucleotide-free condition in which MinD and FlhG show low basal level binding to membrane. MinD and FlhG form a new binding region after membrane association. In the same way, Ind1 might use membrane association in its function and/ or protein-protein interactions, although the interaction between the NTD of *Dm* mtDNA helicase and *Dm* Ind1was not observed in the presence of liposomes in the cosedimentation assay (data not shown).

The C-terminal region of Ind1 is of interest because in addition to the C-terminal amphipathic helix, it has a CxxC motif to coordinate a 4Fe-4S cluster in *Drosophila*. Furthermore, the most common disease mutant, c.815-27T>C, produces C-terminal deleted

variants, resulting in the loss of two helixes from the C-terminus, while it retains all important conserved motifs such as Walker A and B, a Mrp family signature and a CxxC motif (5,12). This might indicate importance of the amphipathic helix and its putative the implication for membrane association. Thus, further investigation of how recipient protein binding is affected by membrane binding, ATP binding, and ATPase hydrolysis are warranted to understand the Ind1 disease mutant, c.815-27T>C, which is carried in 1.2% of the European population (6).

CONCLUSIONS

Dm Ind1 is a plausible binding partner of *Dm* mtDNA helicase. In addition to the high throughput protein-protein interaction research data, *Dm* Ind1 and *Dm* mtDNA helicase are likely to contact each other for delivery of an iron-sulfur cluster. Several features of *Dm* Ind1 that are shared with *Dm* mtDNA helicase were indentified in this study. *Dm* Ind1, as for *Dm* mtDNA helicase, localizes in mitochondria and binds to mitochondrial membranes as a peripheral membrane protein. In particular, the membrane binding property of *Dm* Ind1 suggests that the Ind1 has an advantage in location to transfer an iron-sulfur cluster to membrane-bound recipients: complex I and possibly *Dm* mtDNA helicase. Furthermore, homodimerization of *Dm* Ind1 occurs regardless of the presence of nucleotide or cofactors, but coordinating cysteines are important for stable dimerization. The characteristics in dimerization are found in other metal cofactor-bound proteins of the Mrp/ MinD family. Because the proteins require ATP-bound active forms to bind to interacting partners and ADP-bound or nucleotide-free inactive forms in the dissociating state, I propose that ATP is necessary to form the interaction between Ind1 and its interacting partners. In this way, ATP may promote formation of a complex of *Dm* mtDNA helicase and *Dm* Ind1 that was not detected by *in vitro* chemical crosslinking. Moreover, because a reduced level of Ind1 by RNAi is likely to be sufficient for its functions, a knockout experiment by CRISPR/ Cas9 will be employed to show an unambiguous effect on mtDNA replication.

APPENDIX

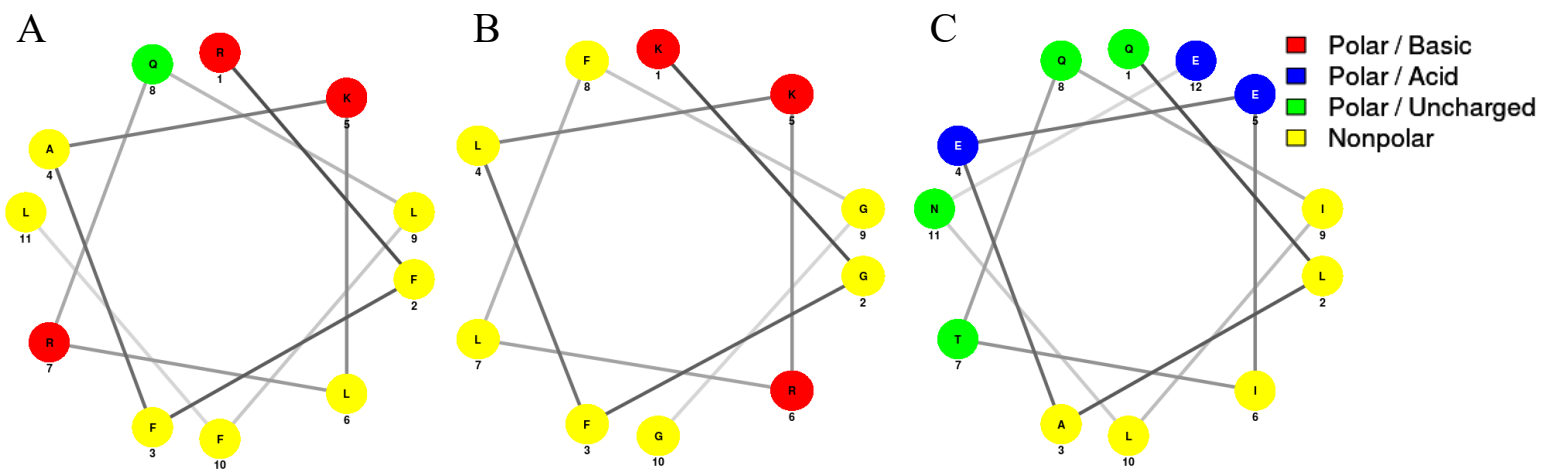

Figure A4. **Helical wheel projection of the C-terminal helix in FlhG (A) MinD (B) *Dm* Ind1(C)** Helical wheel projection of the C-terminal helix of each protein was constructed by the NetWheels program. The helixes show hydrophobic residues (yellow) at one side of the helix and uncharged polar residues (green), hydrophilic/ charged residues (with basic residues in blue and with acidic residues in red) on the other side, indicating that the amphipathic characteristic is conserved in all three proteins. Hydrophilic side of the helix of *Dm* Ind1(C) is negatively charged, while FlhG (A) and MinD (B) are positively charged on the hydrophilic side.

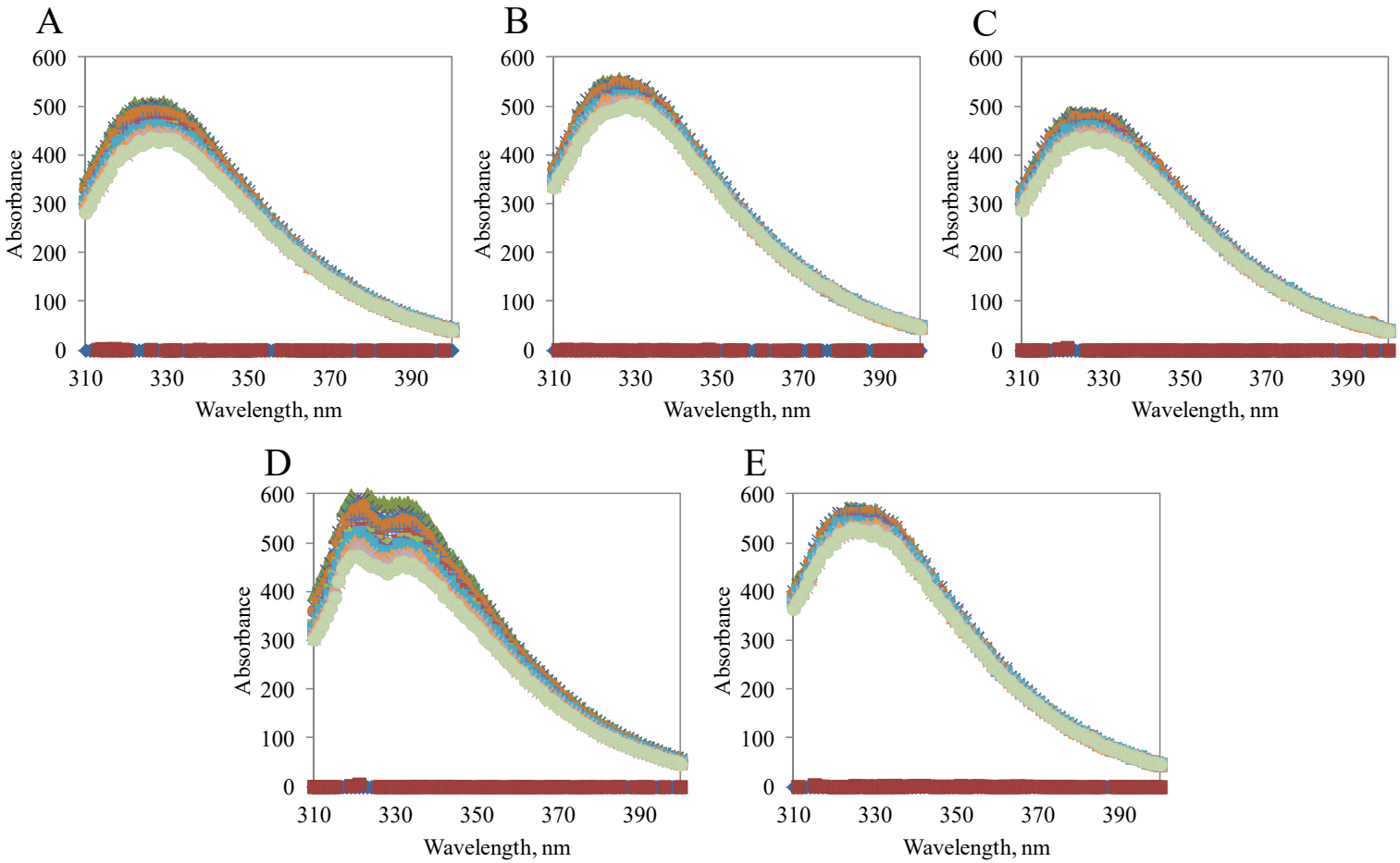

Figure A5. **Emission spectra of *Dm* Ind1 in various buffers A-C,** Tris-HCl buffers (50 mM Tris-HCl, pH7.5, 150mM NaCl, 0% glycerol (A), 5% glycerol (B), 10% glycerol(C)) are used. 0.05% N-dodecyl β-D-maltoside (D) and 0.05% N-dodecyl β-D-maltoside and 5% glycerol (E) were added in buffer A. All buffers have 5 mM β-mercaptoethanol. The spectrum was obtained every 2 minutes for 28 minutes. Dark and faint green spectra are the first and the last measurements, respectively. Red/ blue lines near 0 are the spectra measured without protein.

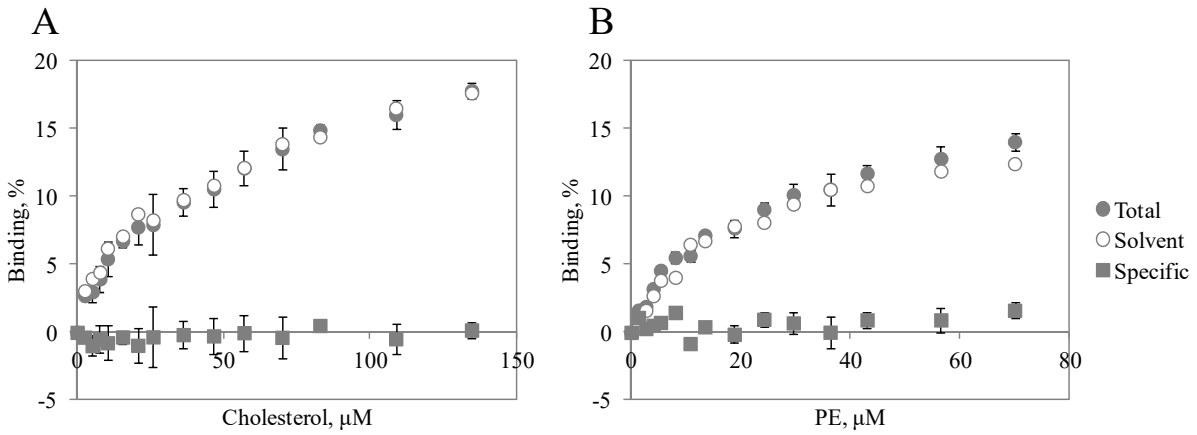

Figure A6. **Saturation curves of *Dm* Ind1 binding to individual lipids: cholesterol (A) and PE (B) by intrinsic tryptophan fluorescence quenching assays** Specific binding (closed squares) was obtained by subtracting solvent binding (open circles) from total binding (closed circles). Each data point represents the mean of triplicate (total) or duplicate (solvent) measurements and the data point of specific binding is the mean of six possible calculations. The error bars indicate ± standard deviation.

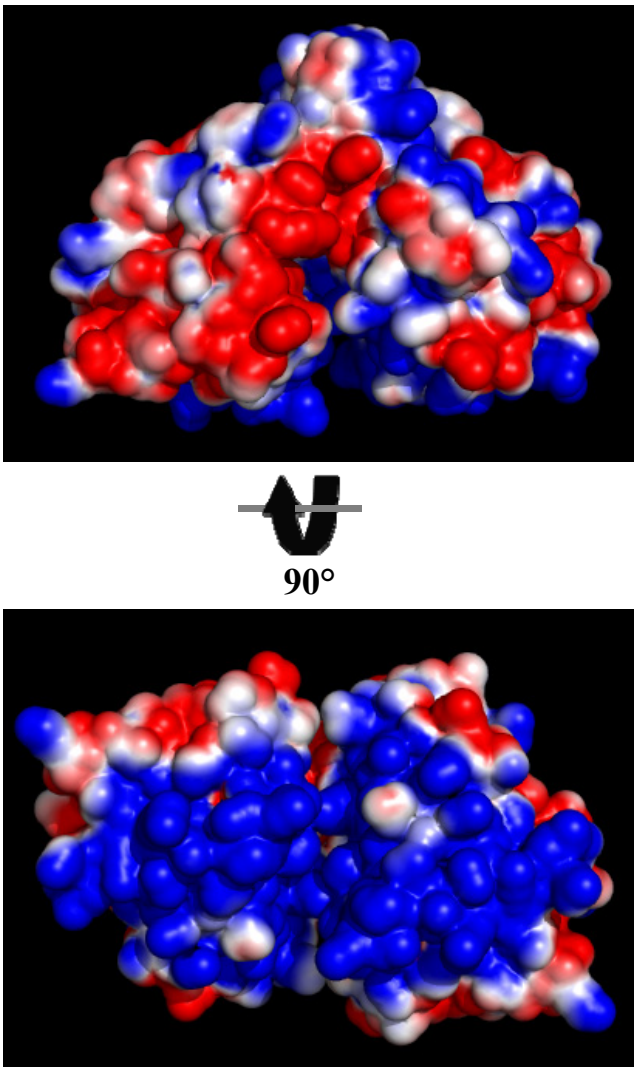

Figure A7. **Surface electrostatic potential map for the *Dm* Ind1 dimer** Front view and bottom view for the snapshot of *Dm* Ind1 dimer shown in Figure 21 B are displayed in surface electrostatic potential map made by PyMOL APBS Tools. Positive, negative and hydrophobic electrostatic potential are colored by blue, red, and white, respectively.

BIBLIOGRAPHY

BIBLIOGRAPHY

1. Stiban, J., Farnum, G. A., Hovde, S. L., and Kaguni, L. S. (2014) The N-terminal domain of the Drosophila mitochondrial replicative DNA helicase contains an iron-sulfur cluster and binds DNA. *The Journal of biological chemistry* **289**, 24032-24042

2. Guruharsha, K. G., Rual, J. F., Zhai, B., Mintseris, J., Vaidya, P., Vaidya, N., Beekman, C., Wong, C., Rhee, D. Y., Cenaj, O., McKillip, E., Shah, S., Stapleton, M., Wan, K. H., Yu, C., Parsa, B., Carlson, J. W., Chen, X., Kapadia, B., VijayRaghavan, K., Gygi, S. P., Celniker, S. E., Obar, R. A., and Artavanis-Tsakonas, S. (2011) A protein complex network of Drosophila melanogaster. *Cell* **147**, 690-703

3. Bych, K., Kerscher, S., Netz, D. J., Pierik, A. J., Zwicker, K., Huynen, M. A., Lill, R., Brandt, U., and Balk, J. (2008) The iron-sulphur protein Ind1 is required for effective complex I assembly. *The EMBO journal* **27**, 1736-1746

4. Sheftel, A. D., Stehling, O., Pierik, A. J., Netz, D. J., Kerscher, S., Elsasser, H. P., Wittig, I., Balk, J., Brandt, U., and Lill, R. (2009) Human ind1, an iron-sulfur cluster assembly factor for respiratory complex I. *Molecular and cellular biology* **29**, 6059-6073

5. Tucker, E. J., Mimaki, M., Compton, A. G., McKenzie, M., Ryan, M. T., and Thorburn, D. R. (2012) Next-generation sequencing in molecular diagnosis: NUBPL mutations highlight the challenges of variant detection and interpretation. *Human mutation* **33**, 411-418

6. Wydro, M. M., and Balk, J. (2013) Insights into the pathogenic character of a common NUBPL branch-site mutation associated with mitochondrial disease and complex I deficiency using a yeast model. *Disease models & mechanisms* **6**, 1279-1284

7. David, D., Almeida, L. S., Maggi, M., Araujo, C., Imreh, S., Valentini, G., Fekete, G., and Haltrich, I. (2015) Clinical Severity of PGK1 Deficiency Due To a Novel p.E120K Substitution Is Exacerbated by Co-inheritance of a Subclinical Translocation t(3;14)(q26.33;q12), Disrupting NUBPL Gene. *JIMD reports* **23**, 55-65

8. Lill, R., Hoffmann, B., Molik, S., Pierik, A. J., Rietzschel, N., Stehling, O., Uzarska, M. A., Webert, H., Wilbrecht, C., and Muhlenhoff, U. (2012) The role of mitochondria in cellular iron-sulfur protein biogenesis and iron metabolism. *Biochimica et biophysica acta* **1823**, 1491-1508

9. Stiban, J., So, M., and Kaguni, L. S. (2016) Iron-sulfur clusters in mitochondrial metabolism: Multifaceted roles of a simple cofactor. *Biochemistry (Moscow)* **81**, 1066-1080

10. Mimaki, M., Wang, X., McKenzie, M., Thorburn, D. R., and Ryan, M. T. (2012) Understanding mitochondrial complex I assembly in health and disease. *Biochimica et*

biophysica acta **1817**, 851-862

11. Calvo, S. E., and Mootha, V. K. (2010) The mitochondrial proteome and human disease. *Annual review of genomics and human genetics* **11**, 25-44

12. Kevelam, S. H., Rodenburg, R. J., Wolf, N. I., Ferreira, P., Lunsing, R. J., Nijtmans, L. G., Mitchell, A., Arroyo, H. A., Rating, D., Vanderver, A., van Berkel, C. G., Abbink, T. E., Heutink, P., and van der Knaap, M. S. (2013) NUBPL mutations in patients with complex I deficiency and a distinct MRI pattern. *Neurology* **80**, 1577-1583

13. Leipe, D. D., Wolf, Y. I., Koonin, E. V., and Aravind, L. (2002) Classification and evolution of P-loop GTPases and related ATPases. *Journal of molecular biology* **317**, 41-72

14. Netz, D. J., Pierik, A. J., Stumpfig, M., Muhlenhoff, U., and Lill, R. (2007) The Cfd1-Nbp35 complex acts as a scaffold for iron-sulfur protein assembly in the yeast cytosol. *Nature chemical biology* **3**, 278-286

15. Via, A., Ferre, F., Brannetti, B., Valencia, A., and Helmer-Citterich, M. (2000) Three-dimensional view of the surface motif associated with the P-loop structure: cis and trans cases of convergent evolution. *Journal of molecular biology* **303**, 455-465

16. Schwenkert, S., Netz, D. J., Frazzon, J., Pierik, A. J., Bill, E., Gross, J., Lill, R., and Meurer, J. (2010) Chloroplast HCF101 is a scaffold protein for [4Fe-4S] cluster assembly. *The Biochemical journal* **425**, 207-214

17. Lutkenhaus, J., and Sundaramoorthy, M. (2003) MinD and role of the deviant Walker A motif, dimerization and membrane binding in oscillation. *Molecular microbiology* **48**, 295-303

18. Leonard, T. A., Butler, P. J., and Lowe, J. (2005) Bacterial chromosome segregation: structure and DNA binding of the Soj dimer--a conserved biological switch. *The EMBO journal* **24**, 270-282

19. Ishikawa, T., Kuo, M. T., Furuta, K., and Suzuki, M. (2000) The human multidrug resistance-associated protein (MRP) gene family: from biological function to drug molecular design. *Clinical chemistry and laboratory medicine : CCLM / FESCC* **38**, 893-897

20. Schuhmacher, J. S., Rossmann, F., Dempwolff, F., Knauer, C., Altegoer, F., Steinchen, W., Dorrich, A. K., Klingl, A., Stephan, M., Linne, U., Thormann, K. M., and Bange, G. (2015) MinD-like ATPase FlhG effects location and number of bacterial flagella during C-ring assembly. *Proceedings of the National Academy of Sciences of the United States of America* **112**, 3092-3097

21. Tezcan, F. A., Kaiser, J. T., Howard, J. B., and Rees, D. C. (2015) Structural evidence for asymmetrical nucleotide interactions in nitrogenase. *Journal of the American Chemical*

Society **137**, 146-149

22. Mateja, A., Paduch, M., Chang, H. Y., Szydlowska, A., Kossiakoff, A. A., Hegde, R. S., and Keenan, R. J. (2015) Protein targeting. Structure of the Get3 targeting factor in complex with its membrane protein cargo. *Science* **347**, 1152-1155

23. Bozkurt, G., Stjepanovic, G., Vilardi, F., Amlacher, S., Wild, K., Bange, G., Favaloro, V., Rippe, K., Hurt, E., Dobberstein, B., and Sinning, I. (2009) Structural insights into tail-anchored protein binding and membrane insertion by Get3. *Proceedings of the National Academy of Sciences of the United States of America* **106**, 21131-21136

24. Tezcan, F. A., Kaiser, J. T., Mustafi, D., Walton, M. Y., Howard, J. B., and Rees, D. C. (2005) Nitrogenase complexes: multiple docking sites for a nucleotide switch protein. *Science* **309**, 1377-1380

25. Netz, D. J., Pierik, A. J., Stumpfig, M., Bill, E., Sharma, A. K., Pallesen, L. J., Walden, W. E., and Lill, R. (2012) A bridging [4Fe-4S] cluster and nucleotide binding are essential for function of the Cfd1-Nbp35 complex as a scaffold in iron-sulfur protein maturation. *The Journal of biological chemistry* **287**, 12365-12378

26. Vecchiarelli, A. G., Li, M., Mizuuchi, M., Hwang, L. C., Seol, Y., Neuman, K. C., and Mizuuchi, K. (2016) Membrane-bound MinDE complex acts as a toggle switch that drives Min oscillation coupled to cytoplasmic depletion of MinD. *Proceedings of the National Academy of Sciences of the United States of America* **113**, E1479-1488

27. Mariappan, M., Mateja, A., Dobosz, M., Bove, E., Hegde, R. S., and Keenan, R. J. (2011) The mechanism of membrane-associated steps in tail-anchored protein insertion. *Nature* **477**, 61-66

28. Mateja, A., Szlachcic, A., Downing, M. E., Dobosz, M., Mariappan, M., Hegde, R. S., and Keenan, R. J. (2009) The structural basis of tail-anchored membrane protein recognition by Get3. *Nature* **461**, 361-366

29. Matsushima, Y., and Kaguni, L. S. (2009) Functional importance of the conserved N-terminal domain of the mitochondrial replicative DNA helicase. *Biochimica et biophysica acta* **1787**, 290-295

30. Gajewski, J. P., Arnold, J. J., Salminen, T. S., Kaguni, L. S., and Cameron, C. E. (2016) Expression and Purification of Mitochondrial RNA Polymerase and Transcription Factor A from Drosophila melanogaster. *Methods in molecular biology* **1351**, 199-210

31. Worby, C. A., Simonson-Leff, N., and Dixon, J. E. (2001) RNA interference of gene expression (RNAi) in cultured Drosophila cells. *Science's STKE : signal transduction knowledge environment* **2001**, pl1

32. Kelley, L. A., Mezulis, S., Yates, C. M., Wass, M. N., and Sternberg, M. J. E. (2015) The Phyre2 web portal for protein modeling, prediction and analysis. *Nat. Protocols* **10**, 845-

858

33. Holm, L., and Rosenström, P. (2010) Dali server: conservation mapping in 3D. *Nucleic acids research* **38**, W545-W549

34. Buchan, D. W., Minneci, F., Nugent, T. C., Bryson, K., and Jones, D. T. (2013) Scalable web services for the PSIPRED Protein Analysis Workbench. *Nucleic acids research* **41**, W349-357

35. Maio, N., and Rouault, T. A. (2016) Mammalian Fe-S proteins: definition of a consensus motif recognized by the co-chaperone HSC20. *Metallomics : integrated biometal science* **8**, 1032-1046

36. Guruharsha, K. G., Obar, R. A., Mintseris, J., Aishwarya, K., Krishnan, R. T., Vijayraghavan, K., and Artavanis-Tsakonas, S. (2012) Drosophila protein interaction map (DPiM): a paradigm for metazoan protein complex interactions. *Fly* **6**, 246-253

37. Rajala, N., Gerhold, J. M., Martinsson, P., Klymov, A., and Spelbrink, J. N. (2014) Replication factors transiently associate with mtDNA at the mitochondrial inner membrane to facilitate replication. *Nucleic acids research* **42**, 952-967

38. Schindelin, H., Kisker, C., Schlessman, J. L., Howard, J. B., and Rees, D. C. (1997) Structure of ADP x AIF4(-)-stabilized nitrogenase complex and its implications for signal transduction. *Nature* **387**, 370-376

39. Suloway, C. J., Chartron, J. W., Zaslaver, M., and Clemons, W. M., Jr. (2009) Model for eukaryotic tail-anchored protein binding based on the structure of Get3. *Proceedings of the National Academy of Sciences of the United States of America* **106**, 14849-14854

CHAPTER 5
Perspectives

INTRODUCTION

In this dissertation, the comprehensive investigation of the structural and functional roles for both human and *Drosophila* mtDNA helicase has been discussed. A different distribution of oligomeric states and reduced dynamic conformations of the ZBD-deficient human mtDNA helicase demonstrated that the ZBD causes the dynamic changes (Chapter 2). In addition, confirmation of the presence of an iron-sulfur cluster in *Drosophila* mtDNA helicase from *Drosophila* S2 cells, discovery of the binding property of *Drosophila* NTD to the mitochondrial inner membrane through cardiolipin, and evaluation of the ssDNA binding properties in the human RPD showed that the NTDs in mtDNA helicases serve as a binding module (Chapter 3). *Drosophila* Ind1, as a putative iron-sulfur donor to *Dm* mtDNA helicase, has been characterized; its mitochondrial localization, dimerization, and the membrane binding property driven by electrostatic and hydrophobic interactions were demonstrated (Chapter 4).

Three aims are proposed in this chapter to expand the studies in this dissertation. The biological function of the iron-sulfur cluster in *Dm* mtDNA helicase can be questioned by measuring protein activities in the absence and presence of the cluster, and by monitoring the biologically-active form of the cluster (see 1.1 and 1.2., respectively). The expected protein-protein interactions between *Dm* Ind1 and *Dm* NTD/ or *Dm* mtDNA helicase may occur under optimized conditions with an appropriate cofactor (ATP) and chaperone proteins. To evaluate this hypothesis, a further experimental plan is proposed in this chapter (see 2.1.). To investigate roles for Ind1 in oxidative phosphorylation and mtDNA replication, measurement of complex I activity and analysis of replicative intermediates by two-dimensional agarose-gel electrophoresis (2D-AGE), respectively, are suggested (see 2.2). Lastly, an experimental plan to select new interacting partners of *Dm* mtDNA helicase from mitochondrial extracts was proposed based on

established methods that were introduced in chapters 3 and 4. New protein partners that may explain new roles for *Dm* mtDNA helicase and its iron-sulfur cluster in mtDNA maintenance are expected to be identified.

Besides three aims, I also propose additional experimental plans for some studies that are incomplete, and in particular, to allow publication. For example, the investigation of the human mtDNA helicase structure at physiological ionic strength needs additional EM data to clarify the hypothesis about double oligomers that I proposed in chapter 2 as a helicase self-loading mechanism. This would be publishable with *in vitro* data regarding self-loading onto circular dsDNA (or D-loop containing dsDNA) by human mtDNA helicase under various salt conditions. As another example, in addition to the ssDNA binding by UV-crosslinking in chapter 3, fluorescent quenching (1) or biolayer interferometry (2) will be required to provide detailed information such as binding affinity to document the ssDNA binding properties of the human mtDNA helicase RPD. These experiments will confirm the hypothesis regarding the disease mutation cluster in the human RPD (3).Investigation of an *in vivo* relationship between *Dm* Ind1 and mtDNA replication was also incomplete, likely as a result of the fact that Ind1 may remain functional even at a reduced protein level as low as ~30-50% (4-6). To complete the investigation about loss-of function of Ind1, gene knock-out by CRISPR-Cas9 in *Drosophila* S2 cells can be conducted. Comparison of effects of Ind1 gene knock-out with theses of gene knock-down (Chapter 4) may yield an interesting finding for publication. This research may also be combined with research proposed in this chapter (see 2.2.).

AIMS

Aim1-Biological roles of the iron-sulfur cluster in Drosophila mtDNA helicase

1.1. Comparison of enzymatic activities between full-length *Dm* mtDNA helicase and its iron-sulfur cluster-deficient variants

Background and Rationale - Roles for the iron-sulfur cluster of *Dm* mtDNA helicase in structural stability and ssDNA binding were demonstrated in our previous study (1); however, the effect of the iron-sulfur cluster on catalytic activities of *Dm* mtDNA helicase was not tested due to insolubility of the full-length protein. Recent successful purification of full-length *Dm* mtDNA helicase from an *E. coli* overexpression system in our group now enables us to investigate a possible role of the iron-sulfur cluster in the catalytic activities of *Dm* mtDNA helicase *in vitro.* Iron-sulfur clusters in some SF1 or SF2 helicases such as XPD (7), FancJ (8), DinG (9) and Dna2 (10) are known to be essential for their helicase activities. In particular, the X-ray crystal structure of XPD reveals that the iron-sulfur cluster plays a role in separating the DNA strands at the ssDNA-dsDNA junction (11). *Dm* mtDNA helicase is the only known iron-sulfur cluster helicase among the SF4 helicases and its human homolog does not have the cofactor. Thus, investigation of activities of holo- or apo-*Dm* mtDNA helicase is important and necessary to understand the roles of its iron-sulfur cluster in the mtDNA helicase. It may also provide a clue to an evolutionary reason for the cofactor change from T7gp4 (a zinc ion) to *Drosophila* mtDNA helicase (an iron-sulfur cluster) and to human mtDNA helicase (none).

Production of altered iron-sulfur cluster-containing variants - To prepare an apo-*Dm* mtDNA helicase, I propose to generate iron-sulfur cluster coordinating cysteine-deficient variants by serine (or alanine) substitution mutagenesis. Reduction and oxidation with dithionite and ferricyanide, respectively (9), provide an alternative to prepare *Dm* mtDNA helicases whose

redox states in the iron-sulfur cluster are modified. Additionally, 100-times excess glutathione might produce structurally stable apo-enzyme (See Aim 1.3.).

Enzyme activity assays - Helicase unwinding assay, ssDNA or dsDNA binding assays, and ATPase assay will be pursued in order to compare enzymatic activities of *Dm* holo-mtDNA helicase to iron-sulfur cluster-deficient variants, and/ or to reduced or oxidative iron-sulfur cluster-containing *Dm* mtDNA helicase. Our group has well-established protocols for the activity assays. R576A (an arginine finger variant) (12) and W282L (the *Drosophila* homolog of human W315L, a human adPEO mutation, see Chapter 3) (13) can be used as negative controls for ATP hydrolysis and unwinding activity, and ssDNA binding activity, respectively. Wild-type human mtDNA helicase can be used as a positive control for all enzymatic activity assays.

Circular dichroism (CD) and velocity sedimentation - Structural stability and oligomeric states of the wild-type *Dm* mtDNA helicase and iron-sulfur cluster-deficient variants will be determined by CD and velocity sedimentation, respectively.

1.2. Identification of a biologically active iron-sulfur cluster type in *Dm* mtDNA helicase

Background and Rationale - Catalytic activities of the full-length *Dm* holo-mtDNA helicase *per se* are important to evaluate the endogenous type of the iron-sulfur cluster in the biologically active *Dm* mtDNA helicase. I propose an exploration of iron-sulfur cluster types in the purified full-length mtDNA helicase. It is likely to be a 2Fe2S cluster, as the purified NTD has a 2Fe2S cluster (1). However, if the 2Fe2S cluster-containing full-length helicase does not show catalytic activities *in vitro* under aerobic conditions, it is plausible that it has a 4Fe4S cluster *in vivo,* or under anaerobic conditions. Similarly, conversion from a 4Fe4S cluster to a 2Fe2S cluster by O_2 causes a loss of biological activity in a few iron-sulfur cluster proteins

including a transcription factor FNR (14). This conversion is an important part of oxygen sensing mechanism in proteins such as FNR (15,16), biotin synthase (BioB) (17) and a ribosomal RNA methyl transferase (RumA) (18). In addition, UV-vis spectra of Cdf1 and Mbp35 before reconstitution, which have 4Fe4S clusters after reconstruction and contain Walker A motifs (19), show the identical pattern as the spectra of *Dm* NTD under aerobic conditions (1), suggesting a possibility that *Dm* mtDNA helicase, which also contains a Walker A motif, might contain a 4Fe4S cluster inside cells or under anaerobic conditions. Thus, if the catalytic activities of *Dm* mtDNA helicase are not detected in aim 1.1., I propose an investigation of the conversion of iron-sulfur cluster type.

UV/visible spectroscopy and inductively coupled plasma optical emission spectrometry (ICP-OES) - To measure types of iron-sulfur clusters before and after a chemical reconstitution (19), UV/visible spectroscopy can be used. As an independent alternative, Fe and S content can be measured by ICP-OES and/ or colorimetric chemical experiments following the procedure described by Cheng (20). Recording changes in UV/vis spectra of the reconstituted *Dm* mtDNA helicase during oxygen exposure will show whether or not the conversion from a 4Fe4S cluster to a 2Fe2S cluster occurs in *Dm* mtDNA helicase (14).

Surface plasmon resonance (SPR) and/ or Mössbauer spectroscopy - To obtain an unambiguous type of clusters in *Dm* mtDNA helicase, SPR and/ or Mössbauer spectroscopy is recommended.

ATPase activity assay with malachite green - The activity of reconstituted *Dm* mtDNA helicase can be measured inside an anaerobic chamber by using an isotope-free ATPase assay such as the malachite green ATPase assay (21).

1.3. Effects of a glutathione-coordinated 2Fe2S cluster on *Dm* mtDNA helicase

Background and Rationale - Glutathione regulates redox-sensitive proteins (22). In particular, it is involved in incorporation of iron-sulfur clusters in iron-sulfur cluster biosynthetic and trafficking proteins such as ISCU(23), GLRX5 (24), Nfu (25) and Atm1 (26-28). Two molecules of glutathione coordinates a 2Fe2S cluster together with two ligating cysteines of some iron-sulfur protein such as GLRX5 (24). In addition, four glutathione molecules coordinates a 2Fe2S cluster and form a water stable [2Fe2S] $(GS)_4$ complex(29-31). The [2Fe2S]$(GS)_4$ complex transfers the 2Fe2S cluster to apo-protein such as ISU (32), Isa1(23) and Nfu (25). The [2Fe2S]$(GS)_4$ complex is considered as either a storage of the cluster or a vehicle for cluster trafficking (23,25). More importantly, glutathione serves a role in stabilizing proteins for a few iron-sulfur cluster proteins including GLRX5 (24) and Atm1 (27). Thus, study of cluster exchange between *Dm* mtDNA helicase and glutathione might explain whether or not the helicase is regulated by glutathione in stabilization or insertion of its iron-sulfur cluster depending on oxidative stress level. In addition, if glutathione increases the stability of *Dm* mtDNA helicase, investigation is warranted in further *in vitro* experiments such as crystal generation.

[2Fe2S]$(GS)_4$ synthesis and cluster exchange chemistry of *Dm* mtDNA helicase – [2Fe2S]$(GS)_4$ will be synthesized by *in vitro* chemical reactions as described by Cowan and coworkers (31). To evaluate whether *Dm* mtDNA helicase can use the glutathione conjugated 2Fe2S cluster, extraction of the cluster from *Dm* mtDNA helicase by free glutathione and reconstitution of apo-*Dm* mtDNA helicase by [2Fe-2S] $(GS)_4$ will be investigated. Directionality of reversible cluster exchange reactions between the complex and an apo-protein depends on relative concentrations of the species (23). Rate constants for cluster reconstitution to apo-

proteins are considerably higher than for cluster extraction; therefore, for reconstruction of *Dm* apo-mtDNA helicase, a ratio of 1:1 (apo-protein and the complex), and a100-fold excess of glutathione over apo-protein for cluster extraction will be employed. In addition, effects of [2Fe-2S] $(GS)_4$ or free glutathione on the stability of *Dm* mtDNA helicase will be assessed as in our previous study (1).

Circular dichroism (CD) - To analyze the iron-sulfur cluster containing structures: apo-, holo- and complex bound intermediate *Dm* mtDNA helicase, and to monitor uptake/ transfer of iron-sulfur clusters (23,25), CD spectroscopy will be employed. The spectra will be recorded over time in an air-tight anaerobic cuvette.

1.4. Expected Impact

The presence of iron-sulfur clusters in DNA-processing proteins is not rare; however, *Dm* mtDNA helicase is the only known iron-sulfur cluster protein among mitochondrial DNA replicative proteins and SF4 helicases. Its existence also shows species specificity. Thus, investigation of the biochemical and physiological roles of the iron-sulfur cluster in the mtDNA helicase will show whether it affects enzymatic activities, and whether the helicase can sense redox through changes in iron-sulfur cluster types. These results extend our knowledge of functions of mtDNA helicases and mechanistic details in mitochondrial DNA processes, and give us new insight into the evolutionary reason why the cofactor resides in the ZBD, which is responsible for dynamic structural conformations in the helicase (see Chapter 2). Structural study of the human ZBD would be a good counterpart that can be published with this aim.

Aim2-Effects of Dm Ind1 on oxidative phosphorylation and mtDNA replication in Drosophila mitochondria

2.1. *In vitro* assessment of a putative physical interaction between *Dm* Ind1 and *Dm* helicase

Background and Rationale - The putative interaction between *Dm* mtDNA helicase and *Dm* Ind1 found in *Drosophila* proteomics research (33) was not detected in this study (Chapter 4). However, assessment and comparison of the characteristics of *Dm* Ind1 in the binding interfaces of the Mrp/ MinD family members suggests protein complex formation between *Dm* Ind1 and its putative binding partners (Chapter 4). I hypothesize that (1) protein complex formation is likely to be ATP-dependent and/ or stabilized by chaperone proteins, and (2) ATP hydrolysis by *Dm* Ind1 might be promoted by a stabilized protein complex. It is frequently observed that conformational changes by ATP binding stimulate protein-protein interactions in MinD/ Mrp family (34-37) and bacterial DnaB (38). In addition, chaperone proteins such as HSC20 (39) or HSP70 (or DnaK) (40) form stable complexes with iron-sulfur cluster assembly proteins in mitochondria. Such an increased stability of a protein complex of *Dm* Ind1 might promote ATPase activity as it does in SoJ (41).These studies will help to determine whether *Dm* Ind1binds to *Dm* mtDNA helicase to transfer an iron-sulfur cluster, and also to understand how *Dm* Ind1 binds to its interacting partners, elucidating the mechanistic details of the mitochondrial iron-sulfur cluster assembly pathway.

Chemical crosslinking assay and GraFix in the presence of ATP - The proposed ATP-dependent complex formation between *Dm* Ind1 and *Dm* mtDNA helicase and/ or chaperones will be evaluated by the chemical crosslinking assay in chapter 4 under different nucleotide-containing buffer conditions: ATP analog (ATPγS) or ADP. GraFix (Chapter 2) or a pull-down are alternative assays to detect the possible complexes. An expected pitfall is that if the presence

of the iron-sulfur cluster of *Dm* Ind1is required for creation of ATP-driven binding interface, iron-sulfur cluster reconstitution under an anaerobic condition would be necessary in order to prepare holo-Ind1.

ATPase assay - The ATPase assay established in chapter 3 will be used to test whether formation of a complex with an interacting partner (the full-length or the NTD of the mtDNA helicase as putative partner proteins of *Dm* Ind1) and/ or chaperone proteins promotes ATPase activity of *Dm* Ind1. In addition, effects of chaperones in ATPase activity of the putative Ind1-mtDNA helicase complex will be investigated. One caveat is that an ATP hydrolysis-deficient mtDNA helicase variant should be prepared as a control to rule out ATPase activity by mtDNA helicase itself. The alanine-substituted variant of the arginine finger (R576A in *Dm* mtDNA helicase), which lacks ATPase activity but still maintains its hexameric state (12) can serve a negative control.

2.2. Effects of modified protein levels of *Dm* Ind1 on oxidative phosphorylation and mtDNA replication

Background and Rationale - A major pitfall of *in vitro* studies (Aim 2.1.) is the absence of a positive control, a known binding partner of *Dm* Ind1. Complex I (subunits NDUFS1 and NDUFV1) is the only known iron-sulfur cluster recipients of Ind1 (42). In human Ind1-deficient cells, the level of the cluster-bound subunits in complex I were decrease in supercomplexes. However, neither direct interaction nor the direct iron-sulfur cluster transfer between Ind1 and the subunits have been reported. Further, effects of the reduced or overexpressed *Dm* Ind1 on complex I have not been determined in *Drosophila* mitochondria. Recently, preliminary 2D-AGE analysis of mtDNA replication intermediates in *Dm* Ind1 overexpressing S2 cells in our

group showed a reduced level of a double Y arc species, representative of a replication stalling (43), indicating an excess of *Dm* Ind1 might prevent stalling and perhaps promote replication fork restart. *Dm* Ind1 might be required for mtDNA replication only under stress conditions such as replication stalling or low glucose (44) by supplying clusters to iron-sulfur cluster-containing mtDNA maintenance proteins. For example, Dna2, which is involved in a nuclear replication fork restarting mechanism (45), is an iron-sulfur cluster nuclease-helicase also found in mitochondria. Thus, to clarify the correlation between *Dm* Ind1 and oxidative phosphorylation or mtDNA replication, I propose an investigation of effects on function and assembly of complex I, and on regulation of mtDNA replication upon knock-down or overexpression of *Dm* Ind1, respectively.

Knock-down and overexpression of *Dm* Ind1 - A *Dm* Ind1 overexpressing stable S2 cell line and an iron-sulfur cluster coordination deficient variant (C214A/ C217A) overexpressing cell line have already been established (data not shown). Because the cell lines are inducible, stressor treatment or expression of a particular protein can be utilized in the cell lines. To knock *Dm* Ind1 down, I recommend designing a construct to produce shRNA (short hairpin RNA). A transfected knock-down cell line is required for large-scale preparations of isolated mitochondria or purified mtDNA for the future experiments such as blue native polyacrylamide gel electrophoresis (BN-PAGE) or 2D-AGE, respectively.

Stress conditions - To test the hypothesis that the overexpressed *Dm* Ind1 promotes mtDNA replication fork restart, rescue experiments by the overexpressed Ind1 will be pursued in mtDNA replication stalling-induced *Drosophila* S2 cells. Overexpression of a catalytically-impaired human mtDNA helicase (K421A) (*Drosophila* homolog, K388A) is a well-documented variant that induces mtDNA replication stalling (43,46,47). Oxidative stress by H_2O_2 or $KBrO_3$

and UV radiation is also able to induce mtDNA replication stalling in cultured cells (48). In addition, short- and long-term glucose stress (44) on Ind1 overexpressing or Ind1 knock-down cell lines will show the effects of the protein level of *Dm* Ind1 on respiratory activity under glucose stress.

Complex I assembly and activity - BN-PAGE and an in-gel activity method ((49) or(50)) can be used to detect complex I and test the activity in supercomplexes of the isolated mitochondria from *Dm* Ind1 knock-down or overexpressing cells under different stresses.

Oxygen consumption rate - The seahorse XF96 analyzer can be used to measure respiratory activity of live cells or isolated mitochondria under different stresses.

2D-AGE - To assess the replication mechanism under different protein levels of Ind1 or different stresses, 2D-AGE will be performed with mtDNA from *Drosophila* S2 cells in different conditions.

Detection of Dna2 and mtDNA helicase - Protein levels of Dna2 and mtDNA helicase will be measured by immunoblots from isolated mitochondria of *Dm* Ind1-overexpressing or knock-down cell line under mtDNA replication stalling or glucose starvation conditions. This will provide useful data to study the mechanism of mtDNA replication fork restart. Subfractionation is necessary because Dna2 is found in both nucleus and mitochondria. Subfractionation will also solve the issue that the endogenous mtDNA helicase has not been detected clearly in the S2 cell lysate by anti-NTD antibody.

2.3. Expected Impact

The rate of mitochondrial DNA replication varies and is affected by oxidative phosphorylation capacity and energy needs (51). The correlation between defects in mtDNA

replication and malfunction of OXPHOS in patient cells is evident, but coordinate regulation of mtDNA replication and oxidative phosphorylation may involve diverse factors. In *Drosophila* mitochondria, *Dm* Ind1 may regulate the processes by controlling delivery of iron-sulfur clusters to subunits in complex I, the mtDNA helicase and possibly Dna2. In addition, the results from *in vitro* experiments proposed in 2.1. will help to understand protein-protein interactions of other iron-sulfur cluster-containing P-loop ATPases such as Nbp35 or Cdf1, which are scaffold proteins in the cytosolic iron-sulfur cluster assembly.

Aim3-New binding partners of Dm mtDNA helicase

3.1. New binding partners of *Dm* mtDNA helicase

Background and Rationale - Identification of new binding partners of *Dm* mtDNA helicase is currently more feasible due to the recent success in production of the full-length *Dm* mtDNA helicase and accumulated knowledge and skills about protein-protein interactions in the helicase. Proteins in regulation of mtDNA replication (3) and mtDNA repair (52-54) are expected as interacting partners. Moreover, iron-sulfur cluster related proteins such as Ind1 (33) and Dna2 (53,55) are also anticipated partner proteins in the *Drosophila* mitochondrial proteome. Identification of interacting partners of *Dm* mtDNA helicase from the isolated mitochondria of cultured *Drosophila* S2 cells under various conditions is important in order to find a key player that regulates mtDNA maintenance or identifies a unique role for the iron-sulfur cluster-containing *Dm* mtDNA helicase.

Modified AP-MS with mitochondrial extracts of S2 cells - An AP-MS approach can be applied with the column crosslinking method (Chapter 2) to stabilize dynamic and weak

interactions of *Dm* mtDNA helicase. An anaerobic chamber or an ATP analog might be needed to stabilize the oxygen-labile iron-sulfur cluster in *Dm* mtDNA helicase or promote possible ATP-mediated binding, respectively. In addition, identification of stress-related proteins in the mitochondrial DNA replisome can be achieved by using a mitochondrial extract from stress-induced *Drosophila* cells (56). Established protocols for *Drosophila* S2 cell culture and protein overexpressing or knock-down S2 cell lines (Chapter 4) will facilitate the generation of mitochondrial extracts enriched in stress-related proteins.

3.2. Expected Impact

The mtDNA helicase is a versatie protein that has numerous enzymatic activities (53); therefore, it is expected to involved in several mtDNA processing mechanisms such as mtDNA repair or mtDNA recombination in addition to mtDNA replication. The proposed screening method in this aim may identify interacting partners that can clarify expanded roles for the mtDNA helicase. Screening using *Dm* mtDNA helicase as a bait may select iron-sulfur cluster proteins that may also explain more explicitly iron-sulfur cluster delivery or DNA-CT. Because this method can be used under several different conditions, its success will bring many new approaches to study the expanded protein network of the mtDNA helicase.

BIBLIOGRAPHY

BIBLIOGRAPHY

1. Stiban, J., Farnum, G. A., Hovde, S. L., and Kaguni, L. S. (2014) The N-terminal domain of the Drosophila mitochondrial replicative DNA helicase contains an iron-sulfur cluster and binds DNA. *The Journal of biological chemistry* **289**, 24032-24042

2. Ciesielski, G. L., Hytonen, V. P., and Kaguni, L. S. (2016) Biolayer Interferometry: A Novel Method to Elucidate Protein-Protein and Protein-DNA Interactions in the Mitochondrial DNA Replisome. *Methods in molecular biology* **1351**, 223-231

3. Kaguni, L. S., and Oliveira, M. T. (2016) Structure, function and evolution of the animal mitochondrial replicative DNA helicase. *Critical reviews in biochemistry and molecular biology* **51**, 53-64

4. Tucker, E. J., Mimaki, M., Compton, A. G., McKenzie, M., Ryan, M. T., and Thorburn, D. R. (2012) Next-generation sequencing in molecular diagnosis: NUBPL mutations highlight the challenges of variant detection and interpretation. *Human mutation* **33**, 411-418

5. Wydro, M. M., and Balk, J. (2013) Insights into the pathogenic character of a common NUBPL branch-site mutation associated with mitochondrial disease and complex I deficiency using a yeast model. *Disease models & mechanisms* **6**, 1279-1284

6. David, D., Almeida, L. S., Maggi, M., Araujo, C., Imreh, S., Valentini, G., Fekete, G., and Haltrich, I. (2015) Clinical Severity of PGK1 Deficiency Due To a Novel p.E120K Substitution Is Exacerbated by Co-inheritance of a Subclinical Translocation t(3;14)(q26.33;q12), Disrupting NUBPL Gene. *JIMD reports* **23**, 55-65

7. Rudolf, J., Makrantoni, V., Ingledew, W. J., Stark, M. J., and White, M. F. (2006) The DNA repair helicases XPD and FancJ have essential iron-sulfur domains. *Molecular cell* **23**, 801-808

8. Wu, Y., Sommers, J. A., Suhasini, A. N., Leonard, T., Deakyne, J. S., Mazin, A. V., Shin-Ya, K., Kitao, H., and Brosh, R. M., Jr. (2010) Fanconi anemia group J mutation abolishes its DNA repair function by uncoupling DNA translocation from helicase activity or disruption of protein-DNA complexes. *Blood* **116**, 3780-3791

9. Ren, B., Duan, X., and Ding, H. (2009) Redox control of the DNA damage-inducible protein DinG helicase activity via its iron-sulfur cluster. *The Journal of biological chemistry* **284**, 4829-4835

10. Pokharel, S., and Campbell, J. L. (2012) Cross talk between the nuclease and helicase activities of Dna2: role of an essential iron-sulfur cluster domain. *Nucleic acids research* **40**, 7821-7830

11. Fan, L., Fuss, J. O., Cheng, Q. J., Arvai, A. S., Hammel, M., Roberts, V. A., Cooper, P. K., and Tainer, J. A. (2008) XPD helicase structures and activities: insights into the cancer and aging phenotypes from XPD mutations. *Cell* **133**, 789-800

12. Matsushima, Y., Farr, C. L., Fan, L., and Kaguni, L. S. (2008) Physiological and biochemical defects in carboxyl-terminal mutants of mitochondrial DNA helicase. *The Journal of biological chemistry* **283**, 23964-23971

13. Matsushima, Y., and Kaguni, L. S. (2009) Functional importance of the conserved N-terminal domain of the mitochondrial replicative DNA helicase. *Biochimica et biophysica acta* **1787**, 290-295

14. Khoroshilova, N., Popescu, C., Munck, E., Beinert, H., and Kiley, P. J. (1997) Iron-sulfur cluster disassembly in the FNR protein of Escherichia coli by O2: [4Fe-4S] to [2Fe-2S] conversion with loss of biological activity. *Proceedings of the National Academy of Sciences of the United States of America* **94**, 6087-6092

15. Popescu, C. V., Bates, D. M., Beinert, H., Munck, E., and Kiley, P. J. (1998) Mossbauer spectroscopy as a tool for the study of activation/inactivation of the transcription regulator FNR in whole cells of Escherichia coli. *Proceedings of the National Academy of Sciences of the United States of America* **95**, 13431-13435

16. Crack, J. C., Green, J., Thomson, A. J., and Le Brun, N. E. (2014) Iron-sulfur clusters as biological sensors: the chemistry of reactions with molecular oxygen and nitric oxide. *Accounts of chemical research* **47**, 3196-3205

17. Ugulava, N. B., Gibney, B. R., and Jarrett, J. T. (2001) Biotin synthase contains two distinct iron-sulfur cluster binding sites: chemical and spectroelectrochemical analysis of iron-sulfur cluster interconversions. *Biochemistry* **40**, 8343-8351

18. Agarwalla, S., Stroud, R. M., and Gaffney, B. J. (2004) Redox reactions of the iron-sulfur cluster in a ribosomal RNA methyltransferase, RumA: optical and EPR studies. *The Journal of biological chemistry* **279**, 34123-34129

19. Netz, D. J., Pierik, A. J., Stumpfig, M., Bill, E., Sharma, A. K., Pallesen, L. J., Walden, W. E., and Lill, R. (2012) A bridging [4Fe-4S] cluster and nucleotide binding are essential for function of the Cfd1-Nbp35 complex as a scaffold in iron-sulfur protein maturation. *The Journal of biological chemistry* **287**, 12365-12378

20. Cheng, Z., Landry, A. P., Wang, Y., and Ding, H. (2017) Binding of nitric oxide in the CDGSH-type [2Fe-2S] clusters of human mitochondrial protein Miner2.

21. Boyd, J. M., Sondelski, J. L., and Downs, D. M. (2009) Bacterial ApbC protein has two biochemical activities that are required for in vivo function. *The Journal of biological chemistry* **284**, 110-118

22. Smith, R. A., Hartley, R. C., and Murphy, M. P. (2011) Mitochondria-targeted small molecule therapeutics and probes. *Antioxidants & redox signaling* **15**, 3021-3038

23. Fidai, I., Wachnowsky, C., and Cowan, J. A. (2016) Glutathione-complexed [2Fe-2S] clusters function in Fe-S cluster storage and trafficking. *Journal of biological inorganic chemistry : JBIC : a publication of the Society of Biological Inorganic Chemistry* **21**, 887-901

24. Johansson, C., Roos, Annette K., Montano, Sergio J., Sengupta, R., Filippakopoulos, P., Guo, K., von Delft, F., Holmgren, A., Oppermann, U., and Kavanagh, Kathryn L. (2011) The crystal structure of human GLRX5: iron–sulfur cluster co-ordination, tetrameric assembly and monomer activity. *Biochemical Journal* **433**, 303-311

25. Wachnowsky, C., Fidai, I., and Cowan, J. A. (2016) Iron-sulfur cluster exchange reactions mediated by the human Nfu protein. *Journal of biological inorganic chemistry : JBIC : a publication of the Society of Biological Inorganic Chemistry* **21**, 825-836

26. Li, J., and Cowan, J. A. (2015) Glutathione-coordinated [2Fe-2S] cluster: a viable physiological substrate for mitochondrial ABCB7 transport. *Chemical communications (Cambridge, England)* **51**, 2253-2255

27. Srinivasan, V., Pierik, A. J., and Lill, R. (2014) Crystal structures of nucleotide-free and glutathione-bound mitochondrial ABC transporter Atm1. *Science* **343**, 1137-1140

28. Lee, J. Y., Yang, J. G., Zhitnitsky, D., Lewinson, O., and Rees, D. C. (2014) Structural basis for heavy metal detoxification by an Atm1-type ABC exporter. *Science* **343**, 1133-1136

29. Li, J., Pearson, S. A., Fenk, K. D., and Cowan, J. A. (2015) Glutathione-coordinated [2Fe-2S] cluster is stabilized by intramolecular salt bridges. *Journal of biological inorganic chemistry : JBIC : a publication of the Society of Biological Inorganic Chemistry* **20**, 1221-1227

30. Qi, W., Li, J., Chain, C. Y., Pasquevich, G. A., Pasquevich, A. F., and Cowan, J. A. (2013) Glutathione-complexed iron-sulfur clusters. Reaction intermediates and evidence for a template effect promoting assembly and stability. *Chemical communications (Cambridge, England)* **49**, 6313-6315

31. Qi, W., Li, J., Chain, C. Y., Pasquevich, G. A., Pasquevich, A. F., and Cowan, J. A. (2012) Glutathione complexed Fe-S centers. *Journal of the American Chemical Society* **134**, 10745-10748

32. Qi, W., and Cowan, J. A. (2011) Mechanism of glutaredoxin-ISU [2Fe-2S] cluster exchange. *Chemical communications (Cambridge, England)* **47**, 4989-4991

33. Guruharsha, K. G., Rual, J. F., Zhai, B., Mintseris, J., Vaidya, P., Vaidya, N., Beekman, C., Wong, C., Rhee, D. Y., Cenaj, O., McKillip, E., Shah, S., Stapleton, M., Wan, K. H., Yu, C., Parsa, B., Carlson, J. W., Chen, X., Kapadia, B., VijayRaghavan, K., Gygi, S. P., Celniker, S. E., Obar, R. A., and Artavanis-Tsakonas, S. (2011) A protein complex network of Drosophila melanogaster. *Cell* **147**, 690-703

34. Mateja, A., Paduch, M., Chang, H. Y., Szydlowska, A., Kossiakoff, A. A., Hegde, R. S., and Keenan, R. J. (2015) Protein targeting. Structure of the Get3 targeting factor in complex with its membrane protein cargo. *Science* **347**, 1152-1155

35. Lutkenhaus, J., and Sundaramoorthy, M. (2003) MinD and role of the deviant Walker A motif, dimerization and membrane binding in oscillation. *Molecular microbiology* **48**, 295-303

36. Schindelin, H., Kisker, C., Schlessman, J. L., Howard, J. B., and Rees, D. C. (1997) Structure of ADP x AlF4(-)-stabilized nitrogenase complex and its implications for signal transduction. *Nature* **387**, 370-376

37. Tezcan, F. A., Kaiser, J. T., Mustafi, D., Walton, M. Y., Howard, J. B., and Rees, D. C. (2005) Nitrogenase complexes: multiple docking sites for a nucleotide switch protein. *Science* **309**, 1377-1380

38. Strycharska, M. S., Arias-Palomo, E., Lyubimov, A. Y., Erzberger, J. P., O'Shea, V. L., Bustamante, C. J., and Berger, J. M. (2013) Nucleotide and partner-protein control of bacterial replicative helicase structure and function. *Molecular cell* **52**, 844-854

39. Maio, N., and Rouault, T. A. (2016) Mammalian Fe-S proteins: definition of a consensus motif recognized by the co-chaperone HSC20. *Metallomics : integrated biometal science* **8**, 1032-1046

40. Uzarska, M. A., Dutkiewicz, R., Freibert, S. A., Lill, R., and Muhlenhoff, U. (2013) The mitochondrial Hsp70 chaperone Ssq1 facilitates Fe/S cluster transfer from Isu1 to Grx5 by complex formation. *Molecular biology of the cell* **24**, 1830-1841

41. Leonard, T. A., Butler, P. J., and Lowe, J. (2005) Bacterial chromosome segregation: structure and DNA binding of the Soj dimer--a conserved biological switch. *The EMBO journal* **24**, 270-282

42. Sheftel, A. D., Stehling, O., Pierik, A. J., Netz, D. J., Kerscher, S., Elsasser, H. P., Wittig, I., Balk, J., Brandt, U., and Lill, R. (2009) Human ind1, an iron-sulfur cluster assembly factor for respiratory complex I. *Molecular and cellular biology* **29**, 6059-6073

43. Goffart, S., Cooper, H. M., Tyynismaa, H., Wanrooij, S., Suomalainen, A., and Spelbrink, J. N. (2009) Twinkle mutations associated with autosomal dominant progressive external ophthalmoplegia lead to impaired helicase function and in vivo mtDNA replication stalling. *Human molecular genetics* **18**, 328-340

44. Williams, E. D., Rogers, S. C., Zhang, X., Azhar, G., and Wei, J. Y. (2015) Elevated oxygen consumption rate in response to acute low-glucose stress: Metformin restores rate to normal level. *Experimental gerontology* **70**, 157-162

45. Thangavel, S., Berti, M., Levikova, M., Pinto, C., Gomathinayagam, S., Vujanovic, M., Zellweger, R., Moore, H., Lee, E. H., Hendrickson, E. A., Cejka, P., Stewart, S., Lopes, M., and Vindigni, A. (2015) DNA2 drives processing and restart of reversed replication forks in human cells. *The Journal of cell biology* **208**, 545-562

46. Pohjoismaki, J. L., Goffart, S., and Spelbrink, J. N. (2011) Replication stalling by catalytically impaired Twinkle induces mitochondrial DNA rearrangements in cultured cells. *Mitochondrion* **11**, 630-634

47. Wanrooij, S., Goffart, S., Pohjoismaki, J. L., Yasukawa, T., and Spelbrink, J. N. (2007) Expression of catalytic mutants of the mtDNA helicase Twinkle and polymerase POLG causes distinct replication stalling phenotypes. *Nucleic acids research* **35**, 3238-3251

48. Torregrosa-Muñumer, R., Goffart, S., Haikonen, J. A., and Pohjoismäki, J. L. O. (2015) Low doses of ultraviolet radiation and oxidative damage induce dramatic accumulation of mitochondrial DNA replication intermediates, fork regression, and replication initiation shift. *Molecular biology of the cell* **26**, 4197-4208

49. Nijtmans, L. G., Henderson, N. S., and Holt, I. J. (2002) Blue Native electrophoresis to study mitochondrial and other protein complexes. *Methods* **26**, 327-334

50. Stehling, O., Sheftel, A. D., and Lill, R. (2009) Chapter 12 Controlled expression of iron-sulfur cluster assembly components for respiratory chain complexes in mammalian cells. *Methods in enzymology* **456**, 209-231

51. Reinecke, F., Smeitink, J. A., and van der Westhuizen, F. H. (2009) OXPHOS gene expression and control in mitochondrial disorders. *Biochimica et biophysica acta* **1792**, 1113-1121

52. Sen, D., Nandakumar, D., Tang, G. Q., and Patel, S. S. (2012) Human mitochondrial DNA helicase TWINKLE is both an unwinding and annealing helicase. *The Journal of biological chemistry* **287**, 14545-14556

53. Khan, I., Crouch, J. D., Bharti, S. K., Sommers, J. A., Carney, S. M., Yakubovskaya, E., Garcia-Diaz, M., Trakselis, M. A., and Brosh, R. M., Jr. (2016) Biochemical Characterization of the Human Mitochondrial Replicative Twinkle Helicase: SUBSTRATE SPECIFICITY, DNA BRANCH MIGRATION, AND ABILITY TO OVERCOME BLOCKADES TO DNA UNWINDING. *The Journal of biological chemistry* **291**, 14324-14339

54. Formstecher, E., Aresta, S., Collura, V., Hamburger, A., Meil, A., Trehin, A., Reverdy, C., Betin, V., Maire, S., Brun, C., Jacq, B., Arpin, M., Bellaiche, Y., Bellusci, S., Benaroch, P., Bornens, M., Chanet, R., Chavrier, P., Delattre, O., Doye, V., Fehon, R., Faye, G., Galli, T., Girault, J. A., Goud, B., de Gunzburg, J., Johannes, L., Junier, M. P., Mirouse, V., Mukherjee, A., Papadopoulo, D., Perez, F., Plessis, A., Rosse, C., Saule, S., Stoppa-Lyonnet, D., Vincent, A., White, M., Legrain, P., Wojcik, J., Camonis, J., and Daviet, L. (2005) Protein interaction mapping: a Drosophila case study. *Genome research* **15**, 376-384

55. Ding, L., and Liu, Y. (2015) Borrowing nuclear DNA helicases to protect mitochondrial DNA. *International journal of molecular sciences* **16**, 10870-10887

56. Achanta, G., Sasaki, R., Feng, L., Carew, J. S., Lu, W., Pelicano, H., Keating, M. J., and Huang, P. (2005) Novel role of p53 in maintaining mitochondrial genetic stability through interaction with DNA Pol gamma. *The EMBO journal* **24**, 3482-3492